Thermal management of atomic and photonic systems

by

Muhammad Tahir Naseem

A Dissertation Submitted to the
Graduate School of Sciences and Engineering
in Partial Fulfillment of the Requirements for
the Degree of

Doctor of Philosophy

in

Physics

KOÇ UNIVERSITY

September 6, 2022

Koç University

Graduate School of Sciences and Engineering

This is to certify that I have examined this copy of a Doctor of Philosophy thesis by

Muhammad Tahir Naseem

and have found that it is complete and satisfactory in all respects,
and that any and all revisions required by the final
examining committee have been made.

Committee Members:

Prof. Dr. Özgür Esat Müstecaplıoğlu (Advisor)

Doç. Dr. Alkan Kabakçıoğlu

Dr. Öğr. Üyesi Mehmet Cengiz Onbaşlı

Dr. Öğr. Üyesi Bariş Çakmak

Dr. Öğr. Üyesi David Gelbwaser-Klimovsky

Date:

To my mother

ABSTRACT

Recent years have seen tremendous progress in developing quantum technologies that rely on the physical systems' quantum features, such as quantum coherence and entanglement. In principle, these quantum systems are not isolated and interact with the environment, which leads to decoherence in which quantum correlations weaken or vanish entirely. The mathematical formulation which describes the system's dynamics in the environment's presence generally requires several approximations. One example is the quantum Markovian master equation based on the perturbative approach in weak system-bath interaction. Typically, a phenomenological approach is adopted in deriving the master equation in which inter-system interactions are ignored, which results in the "local" dissipation terms in the master equation. We show that such an approach is inconsistent with the laws of thermodynamics in the case of nonlinearly coupled resonators. Instead, the master equation derived from the first principles is consistent, usually termed the "global" master equation.

The heat flow put serious restrictions on the miniaturization of quantum-based technologies. One promising direction can be to power these devices with heat rather than considering the heat flow as a noise source. Accordingly, it is desirable to have efficient models of quantum thermal heat managers which can assist in controlling the heat flow. Following this direction, here, we propose an efficient quantum thermal diode and transistor model that can provide perfect rectification and very large tunable heat amplification, respectively. The dynamics of the system are described by the global master equation, which assists in uncovering the underlying mechanism in these thermal devices. In addition, we show that our model of the quantum thermal transistor, based on two coupled qubits, can also be used as a quantum absorption refrigerator, which is in variance with previous proposals of refrigerators that generally

require three-body interaction.

It is often required to cool finite quantum systems rather than classical reservoirs. For instance, cooling mechanical resonators to the ground state is a prerequisite for most applications based on mechanical systems in quantum information and quantum communication. However, cooling multiple resonators to the ground state is challenging using typical laser and feedback cooling schemes. To overcome this challenge, we propose a scheme by which simultaneous cooling of multiple resonators is possible. Unlike previous proposals, external control or work input is not required; instead, incoherent thermal drives can cool the resonators. Finally, we investigate the possibility of generating entanglement between uncoupled mechanical resonators, which are only driven by incoherent thermal baths. We show that it is possible to generate significant entanglement between the resonators by judicious choice of thermal baths spectra. The suppression of undesired dissipation and favoring the desired effective two-mode squeezing-like interactions generated by the incoherent interaction with the baths leads to entanglement between the resonators.

ÖZETÇE

Son yıllarda kuantum eş-uyumluluk ve kuantum dolaşıklık gibi özellikleri barındıran fiziksel sistemlere dayanan çalışmalarda kuantum teknolojilerinde önemli gelişmeler olduğu görülmektedir. Prensip olarak bu sistemler izole olmayan ve çevresiyle etkileşen sistemlerdir. Çevreyle etkileşim, sistemin kuantum korelasyonlarının zayıflamasına veya tamamen yok olmasına karşılık gelen eş-uyumluluk kaybına (decoherence) sebep olmaktadır. Sistemin çevresiyle etkileşiminin dinamiğini tanımlayan matematiksel formülasyon, beraberinde genel olarak pek çok matematiksel yaklaşım gerektirmektedir. Örneğin, bir ısı banyosuyla zayıf etkileşim gösteren sistemin kuantum Markovian master denklemi pertürbasyon yaklaşıma dayanır. Sistemlerin birbiriyle etkileşiminin ihmal edildiği durumda, fenomenolojik bir yaklaşım ile türetilen Master denkleminde, "lokal" dağılım (dissipation) terimlerinin ortaya çıktığı görülür. Biz böyle bir yaklaşımın, aralarında doğrusal olmayan etkileşimler içeren rezonatörler söz konusu olduğunda, termodinamik yasalarıyla tutarsız olduğunu gösteriyoruz. Buna karşılık birinci yasadan türetilen Master denklemi tutarlıdır ve genellikle "global" Master denklemi adını alır.

Kuantum-temelli teknolojilerin minyatürleştirilmesinde, ısı akışının ciddi kısıtlar getirdiğini biliyoruz. Ancak ısı akışını bir gürültü yapısı olarak düşünmek yerine, bu cihazlara ısı ile güç sağlamak umut verici olabilir. Buna göre, ısı akışını kontrol etmede yardımcı olabilecek kuantum termal ısı yöneticilerinin verimli modellerine sahip olmak gerekir. Bu bağlamda, biz, sırasıyla mükemmel düzeltme ve çok büyük ayarlanabilir ısı amplifikasyonu sağlayabilen verimli bir kuantum termal diyot ve kuantum transistör modeli öneriyoruz. Bunlara ek olarak, kuple olmuş iki kübit sisteminden oluşan kuantum termal transistör modelimizin, literatürde daha çok en az üç-kübitlik sistemlerle tasarlanan kuantum soğutucu modellerinin yanında, kuantum absorbsiyon

soğutucusu olarak da kullanılabileceğini gösterdik.

Bu soğutucular, genellikle klasik rezervuarlar yerine, sonlu kuantum sistemlerini soğutmak için gereklidir. Örneğin, kuantum bilgi ve kuantum iletişim alanında tasarlanan mekanik sistemlere dayanan pek çok uygulama için, mekanik rezonatörlerin temel enerji durumuna soğutulması ön koşuldur. Ancak, birden çok rezonatörün temel enerji durumuna soğutulması, tipik lazer ve geri beslemeli soğutma şemalarını kullanarak zordur. Biz de bu zorluğun üstesinden gelmek için, birden çok rezonatörü eş zamanlı olarak soğutmanın mümkün olduğu bir şema öneriyoruz. Daha önce yapılmış çalışmalardan farklı olarak, bir dış kontrol veya iş girdisi gerekmeden, eş-uyumluluk içermeyen termal sürücüler (incoherent thermal drives) yoluyla birden çok rezonatörü eş zamanlı soğutmayı yapabiliyoruz. Son olarak, yalnızca eş-uyumluluk içermeyen ısı banyosu yoluyla sürülen ve birbiriyle kuple olmayan (direk etkileşmeyen) mekanik resonatörler arasında dolaşıklık oluşmasının mümkün olabileceğini keşfettik. Isı banyosunun uygun bir spektrumda seçilmesiyle, resonatörlerin arasında kayda değer bir dolaşıklık oluşumu olabileceğini gösterdik. Eş-uyumluluk içermeyen ısı banyosu, istenmeyen dağılımın (dissipation) bastırılmasını ve gerekli olan iki-mod sıkma-tipi etkileşimlerin üretilmesini sağlayarak, rezonatörler arasında dolaşıklık oluşmasını tetikler.

ACKNOWLEDGMENTS

First of all, I would like to thank my advisor Prof. Özgür E. Müstecaplıoğlu, for giving me the opportunity to work under his supervision during my PhD. In particular, I would like to thank him for his superhuman patience and guidance at every point in academic life and otherwise. It would not be an exaggeration to say I couldn't reach this point without his support. I would also like to thank other faculty members of the Physics department and my thesis committee members for their insightful and fruitful comments. The former and current members of the QuesT group helped me a lot during my PhD. I have enjoyed academic and social discussions with the group members, which will always be a part of my life. I have learned a lot from these fruitful discussions.

I am in great debt to my family, who unconditionally provided their love and support throughout my life. There is no way I can return the love and support I received from my family, particularly my mother. This journey wouldn't be possible without such amazing people, specially, the love of my life–my wife; she has always been very understanding and loving through rough patches of my life.

TABLE OF CONTENTS

LIST OF FIGURES

Chapter 1

INTRODUCTION

Despite its abundance, our ability to control and direct heat flow is surprisingly limited compared to electronic conduction, mainly due to lack of efficient quantum thermal managers. Nevertheless, there is growing interest and significant research endeavors to develop methods and tools for controlling heat transfer in mesoscopic and nanoscale systems. One possible direction to control heat flow is by controlling the system-environment interaction in quantum systems. Recent years have seen tremendous efforts in this direction in which desired dissipative dynamics are obtained by engineering system-bath interaction with external control drives. For instance, suitable dissipative dynamics of the quantum systems can be engineered to cool them to the quantum ground-state [11], or prepare a macroscopic coherent superposition state [12] with the help of external control. In these works, heat is considered a source of noise that needs to be suppressed.

In an alternative approach, heat is considered a friend rather than a foe. For example, entanglement can be generated between two optical cavities using system-environment interaction only [13]. In this thesis, we follow the same direction and investigate different quantum devices powered by heat, such as quantum absorption refrigerators, quantum thermal entanglement machines, and quantum heat managers. The dynamics of these thermal devices are typically described by the Markovian master equations [14]. If the system is composed of interacting subsystems, two different Markovian master equations can be found in the literature to describe the dynamics of the system, namely, the global and the local master equations [15, 16]. Depending on the parameters of the system under consideration, the results of these two equations may diverge from each other [17, 18]. Here, we first investigate the validity of the local and global Markovian master equation for the case of two nonlinearly (optomechanical-like) coupled harmonic oscillators. It is often claimed that the local master equation remains valid in the weak-coupling regime; on the contrary, we show that the local approach is inconsistent with the second law of thermodynamics even in the weak coupling regime for nonlinearly coupled resonators. The nonlinear interaction between the systems is optomechanical-like, which is also referred to as radiation pressure interaction [1]. We show that based on this nonlinear interaction, we can achieve tasks that are otherwise impossible with the linear interaction between the systems. For instance, in chapter 2, we show that heat flow asymmetry can be engineered for resonantly interacting systems, which is in variance with previous proposals on designing heat diodes. Similarly, it has shown that a trilinear interaction is required between three resonators for a quantum absorption refrigerator. However, we show that in chapter 4, considering the optomechanical-like interaction, only two interacting systems are sufficient to design a more efficient quantum absorption refrigerator. The outline of the thesis is as follows:

1.1 Outline of thesis

1.1.1 Chapter 1 (Fundamentals)

In chapter 1, we present the microscopic derivation of the quantum master equation and necessary approximations invoked to obtain the Lindblad (standard) form of the master equation for the case of a damped harmonic oscillator. Secs. 1.2 and 1.3 do not present the original content. We include these sections to fix the notations and briefly describe the set of approximations. In Sec. 1.2, we shortly describe the open quantum system theory. The microscopic derivation of a Markovian master equation for a damped harmonic oscillator is presented in Sec. 1.3. The content in these sections closely follows the material presented in [19, 20]. For more detailed discussions about the invoked approximations and rigorous derivation of the master equation, we refer to more detailed works on the topic [21, 22].

1.1.2 Chapter 2 (Local Vs global master equation)

Chapter 2 is based on our work [23], in which we present a comparison of the local, semi-global, and global master equations for a pair of nonlinearly coupled resonators. The validity of these approaches is investigated through the lens of the laws of thermodynamics. At equilibrium, the global master equation only, accurately describes the Gibbs state of the joint oscillators system. On the contrary, the system does not reach the desired Gibbs thermal state under the local and semi-global description. In the presence of a temperature gradient, both local and semi-global approaches lead to negative entropy production, thus violating the second law of thermodynamics. The global approach remains consistent with the laws of thermodynamics in all parameter regimes, provided the Born-Markov and Secular approximations remain valid.

1.1.3 Chapter 3 (Quantum heat managers)

Chapter 3 discusses the heat flow asymmetry and heat amplification in quantum systems based on two coupled spins and two harmonic oscillators, respectively. This chapter is based on our works on quantum heat diode [24, 25] and quantum thermal transistors [26]. We discuss the essential ingredients which can lead to heat rectification in spin-boson systems. It is shown that heat rectification is possible with two spins coupled via asymmetric interaction in the parameters regime where rectification is otherwise absent. We explain the underlying mechanism of heat rectification by the asymmetry of the energy cycles induced by the thermal baths. Further, we propose a model of a quantum thermal transistor based on a standard optomechanical system. We show that the presence of higher-order photon processes can assist heat amplification in quantum systems.

1.1.4 Chapter 4 (Quantum absorption refrigerator)

In chapter 4, based on our work [27], we propose a model of a quantum absorption refrigerator based on only two coupled qubits. Typically a quantum absorption refrigerator requires tri-linear interaction between the working fluid. Further, for such refrigerators, there exists an upper bound on the efficiency at maximum power, which is although not a fundamental limit enforced by the laws of thermodynamics. On the contrary, we show that our model based on two coupled qubits can surpass this bound. In addition, we investigate the possible relation between the quantum correlations between the qubits and the refrigerator's efficiency. Finally, the effect of heat leaks is discussed in the presence of overlapping bath spectral densities.

1.1.5 Chapter 5 (Cooling mechanical resonators)

Based on the global master equation presented in chapter 2, we proposed a scheme of simultaneous cooling of multiple resonators using a heat bath in chapter 5. The results and discussions in this chapter are adopted from [28]. In typical cooling schemes based on the external coherent drives or feedback control, simultaneous cooling of multiple resonators of nearby frequencies coupled to the same cooling agent is challenging because of the dark mode. By relying on quantum reservoir engineering, we show that it is possible to cool multiple resonators using only incoherent thermal drives. The underlying cooling mechanism is explained by connecting directly with standard laser sideband cooling schemes.

1.1.6 Chapter 6 (Engineering entanglement)

Finally, chapter 6 presents a scheme for engineering entanglement between two uncoupled mechanical resonators using an effective, shared incoherent bath. This chapter is based on the results presented in [29]. Our quantum thermal entanglement generation scheme does not require external control or work input to build quantum correlations between the uncoupled resonators. Unlike previous proposals on entanglement generation via reservoir engineering, we do not require effective, coherent two-mode squeezing interaction between the resonators. Instead, incoherent thermal environments assist in generating entanglement between the resonators.

1.1.7 Chapter 7 (Conclusions)

In the last chapter, we present the summary and review some of the conclusions of this thesis.

1.2 open quantum systems

If we assume that our system of interest is isolated from its environment, then the dynamical evolution of the system state vector $|\psi(t)\rangle$ is given by the Schrödinger equation

$$i\hbar\frac{\partial}{\partial t}|\psi(t)\rangle = \hat{H}|\psi(t)\rangle, \tag{1.1}$$

here $\hat{H}$ is the system Hamiltonian, and it is hermitian. There are two possibilities: (i) if the system Hamiltonian is independent of time, then the solution of the Schrodinger equation can be given by the formal integration of Eq. (1.1)

$$|\psi(t)\rangle = U(t,t_0)|\psi(t_0)\rangle, \tag{1.2}$$

here

$$U(t,t_0) = e^{-\frac{i\hat{H}(t-t_0)}{\hbar}}. \tag{1.3}$$

$|\psi(t_0)\rangle$ describes the state of the system at $t = t_0$. By using the hermeticity of $\hat{H}$

$$U^\dagger(t,t_0) = e^{\frac{i\hat{H}(t-t_0)}{\hbar}} = U^{-1}(t,t_0), \tag{1.4}$$

which employs that U is a unitary operator. (ii) If the Hamiltonian of the system has explicit time dependence, then the Schrodinger equation solution has a time-ordered integral due to the non-commutativity of $\hat{H}$ at different times. The unitary operator in this case changes to

$$U_{t,t_0} = T_{\leftarrow}e^{-i\int_{t_o}^{t} dt'\hat{H}(t')}, \tag{1.5}$$

here $T_{\leftarrow}$ is time-ordering operator.

In case the system under investigation is in a mixed state, the density matrix $\hat{\rho}$ describes the state of the system. The dynamical evolution of the system can be described by the von Neumann equation

$$\frac{d}{dt}\hat{\rho}(t) = -\frac{i}{\hbar}[\hat{H}(t), \hat{\rho}(t)]. \tag{1.6}$$

In analogy with the Liouville equation, the von Neumann equation can be written as

$$\frac{d}{dt}\hat{\rho}(t) = \mathcal{L}(t)\hat{\rho}(t), \tag{1.7}$$

here, the Liouvillian is given by

$$\mathcal{L}(t)\hat{O} = -\frac{i}{\hbar}[\hat{H}(t), \hat{O}], \tag{1.8}$$

where $\hat{O}$ is a generic operator in the Hilbert space of the system. If the Hamiltonian $\hat{H}$ of the system has no explicit time dependence, the solution of the von Neumann equation is given by

$$\hat{\rho}(t) = e^{\mathcal{L}t}\hat{\rho}(0). \tag{1.9}$$

Here $\hat{\rho}(0)$ describes the initial state of the system. In the case of explicit time dependence in the system Hamiltonian, the formal solution of the von Neumann equation is given by

$$\hat{\rho}(t) = T_{\leftarrow} e^{\int_0^t dt' \mathcal{L}(t')}\hat{\rho}(0). \tag{1.10}$$

Most of the time, the assumption that a quantum system is well isolated from its environment is incorrect. The environment interacts with the system unavoidably, and the question is: how to obtain the system's dynamics? Let's assume that the system+reservoir Hamiltonian is given as

$$\hat{H} = \hat{H}_{\mathrm{S}} + \hat{H}_{\mathrm{R}} + \hat{H}_{\mathrm{SR}} \tag{1.11}$$

here, system, reservoir and system-reservoir Hamiltonians are described by $\hat{H}_{\mathrm{S}}$, $\hat{H}_{\mathrm{R}}$, and $\hat{H}_{\mathrm{SR}}$, respectively. We can consider total system and reservoir as closed system and still use the von Neumann equation

$$\frac{d}{dt}\hat{\rho}_{\mathrm{SR}}(t) = -\frac{i}{\hbar}[\hat{H}(t), \hat{\rho}_{\mathrm{SR}}(t)], \tag{1.12}$$

here $\hat{\rho}_{\mathrm{SR}}(t)$ represents the joint density matrix of system and reservoir. However, generally, the reservoir has a very large number of degrees of freedom which makes the evolution under the von Neumann equation intractable. Most of the time, we do not have control or influence on the dynamics of the environment, and it causes irreversibility and decoherence in the system. We are only interested in the system's evolution, which is interacting with its surroundings. Specifically, this situation may be relevant in quantum information processing [30], and in general, applications based on the quantum systems in the open quantum system settings [31]. A quantum master equation can be used to model an open quantum system arrangement in which the central system of interest interacts with its environment. In this approach, the starting point is the von Neumann equation, and by expanding it to the second order in the system-environment interaction, a partial trace is taken over the environment. It may be convenient to derive the master equation in the interaction picture, for this purpose, we write the von Neumann equation in interaction picture

$$\frac{d}{dt}\bar{\rho}_{\mathrm{SR}}(t) = -\frac{i}{\hbar}[\bar{H}(t), \bar{\rho}_{\mathrm{SR}}(t)], \tag{1.13}$$

where we have defined

$$\bar{H}_{\mathrm{SR}}(t) \equiv e^{\frac{i}{\hbar}(\hat{H}_{\mathrm{S}}+\hat{H}_{R})t}\hat{H}_{\mathrm{SR}}e^{-\frac{i}{\hbar}(\hat{H}_{\mathrm{S}}+\hat{H}_{R})t}, \tag{1.14}$$

$$\bar{\rho}_{\mathrm{SR}}(t) \equiv e^{\frac{i}{\hbar}(\hat{H}_{\mathrm{S}}+\hat{H}_{R})t}\hat{\rho}_{\mathrm{SR}}e^{-\frac{i}{\hbar}(\hat{H}_{\mathrm{S}}+\hat{H}_{R})t}. \tag{1.15}$$

The formal integration of Eq. (1.13) results

$$\bar{\rho}_{\mathrm{SR}}(t) = \bar{\rho}_{\mathrm{SR}}(0) - \frac{i}{\hbar}\int_0^t dt'\big[\bar{H}_{\mathrm{SR}}(t'), \bar{\rho}_{\mathrm{SR}}(t')\big]. \tag{1.16}$$

The substitution of $\bar{\rho}(t)$ in Eq. (1.13) gives

$$\frac{d}{dt}\bar{\rho}_{\mathrm{SR}}(t) = \frac{1}{i\hbar}[\bar{H}_{\mathrm{SR}}(t), \bar{\rho}_{\mathrm{SR}}(0)] - \frac{1}{\hbar^2}\int_0^t dt'\big[\bar{H}_{\mathrm{SR}}(t), \big[\bar{H}_{\mathrm{SR}}(t'), \bar{\rho}_{\mathrm{SR}}(t')\big]. \tag{1.17}$$

We note this equation is exact; no approximation is made to obtain this equation. For the microscopic derivation of the master equation, we need specific interaction between the system and the environment. In the next section, we present the derivation of the Markovian master equation for a damped harmonic oscillator. This derivation closely follows the content presented in [32].

1.3 Master equation

Here, first, we discuss the major approximations in the derivation of the Markovian master equation. Afterward, we give a textbook example derivation of the master equation for a damped harmonic oscillator.

1.3.1 Born approximation

We assume that no correlations are present between the system and reservoir at $t = 0$, and the initial joint state of the system and environment is given by

$$\hat{\rho}_{\mathrm{SR}}(0) = \hat{\rho}(0)\hat{\chi}_0, \tag{1.18}$$

here $\hat{\chi}_0$ is the initial state of the reservoir. We are only interested in the evolution of the system; therefore, taking a partial trace over the reservoir in Eq. (1.17)

$$\frac{d}{dt}\bar{\rho}(t) = -\frac{1}{\hbar^2}\int_0^t dt' \mathrm{tr}_{\mathrm{R}}\big\{\big[\bar{H}_{\mathrm{SR}}(t), \big[\bar{H}_{\mathrm{SR}}(t'), \bar{\rho}_{\mathrm{SR}}(t')\big]\big\}. \tag{1.19}$$

For simplicity, we have ignored the first term in Eq. (1.17), and the assumption behind this is

$$\mathrm{tr}_{\mathrm{R}}\big\{[\bar{H}_{\mathrm{SR}}(t), \bar{\rho}_{\mathrm{R}}(0)]\big\} = 0. \tag{1.20}$$

This simplification is justified if the coupling of the reservoir operator to the system has zero mean in the state $\bar{\rho}_{\mathrm{R}}$, which can always be arranged.

We have assumed that there are no correlations between the system and reservoir; therefore, the initial joint state of the system and reservoir can be written in a product state. However, during the evolution of the joint system, correlations may build up due to the coupling between the system and the reservoir. If we assume the coupling between the system and reservoir is very weak, then the assumption of the uncorrelated state of the system and reservoir show deviation of the order $\hat{H}_{\mathrm{SR}}$, and we can write

$$\bar{\rho}_{\mathrm{SR}}(t) = \bar{\rho}(t)\chi_0 + \mathcal{O}(\hat{H}_{\mathrm{SR}}), \tag{1.21}$$

here we have changed the hat sign to the bar sign over the reservoir state, as $\hat{\chi}_0 = \bar{\chi}_0$. By keeping the second order terms in $\hat{H}_{\mathrm{SR}}$ and neglecting higher order terms, Eq. (1.19) takes the form

$$\frac{d}{dt}\bar{\rho}(t) = -\frac{1}{\hbar^2}\int_0^t dt' \mathrm{tr}_{\mathrm{R}}\big\{\big[\bar{H}_{\mathrm{SR}}(t), \big[\bar{H}_{\mathrm{SR}}(t'), \bar{\rho}(t')\chi_0\big]\big\}. \tag{1.22}$$

This is the first major approximation, namely, the *Born approximation*, in which all terms higher than second order in system reservoir interaction are ignored based on a weak system-bath coupling assumption.

1.3.2 Markov approximation

The master equation given in Eq. (1.22) is not time local, as the state of the system $\bar{\rho}(t)$ depends on the previous time t'. Due to the coupling between the system and reservoir, the state of the system changes, and this interaction also affects the state of the reservoir. The information of this interaction is imprinted on the reservoir's state, and the system's future evolution depends on the *memory* of the reservoir. In general, the environment is very large compared to the system, and the interaction between the system and the reservoir does not significantly affect the state of the reservoir. On the contrary, the system's state changes considerably due to this interaction. In this case, there exist two different time scales: (i) the reservoir correlation time τ_{R} and (ii) the time scale τ_{s} over which the state of the system changes significantly. If $\tau_{\mathrm{R}} \ll \tau_{\mathrm{s}}$, then t' can be replaced by t in Eq. (1.19)

$$\bar{\rho}(t) = -\frac{1}{\hbar^2}\int_0^t dt' \mathrm{tr}_{\mathrm{R}}\big\{\big[\bar{H}_{\mathrm{SR}}(t), \big[\bar{H}_{\mathrm{SR}}(t'), \bar{\rho}(t)\chi_0\big]\big\}. \tag{1.23}$$

This is commonly known as *Markov approximation*.

We assume a specific interaction between the system and environment of the form

$$\hat{H}_{\rm SR} = \hbar \sum_i \hat{s}_i \hat{B}_i, \tag{1.24}$$

here $\hat{s}_i$ and $\hat{B}_i$ are the operators in the Hilbert spaces of the system and reservoir, respectively. By using this interaction, the master equation (1.22) with Born approximation takes the form

$$\begin{aligned} \frac{d}{dt}\bar{\rho}(t) &= -\sum_{i,j}\int_0^t dt' \Big\{ \big[\bar{s}_i(t)\bar{s}_j(t')\bar{\rho}(t') - \bar{s}_j(t')\bar{\rho}(t')\bar{s}_i(t)\big]\langle \bar{B}_i(t)\bar{B}_j(t')\rangle_{\rm R} \\ &+ \big[\bar{\rho}(t')\bar{s}_j(t')\bar{s}_i(t) - \bar{s}_i(t)\bar{\rho}(t')\bar{s}_j(t')\big]\langle \bar{B}_j(t')\bar{B}_i(t)\rangle_{\rm R} \Big\}, \end{aligned} \tag{1.25}$$

here

$$\begin{aligned} \langle \bar{B}_i(t)\bar{B}_j(t')\rangle_{\rm R} &= {\rm tr}_{\rm R}\big\{\bar{\chi}_0 \bar{B}_i(t)\bar{B}_j(t')\big\}, \\ \langle \bar{B}_j(t')\bar{B}_i(t)\rangle_{\rm R} &= {\rm tr}_{\rm R}\big\{\bar{\chi}_0 \bar{B}_j(t')\bar{B}_i(t)\big\}. \end{aligned} \tag{1.26}$$

The Markovian approximation can only be justified if two distinct time scales exist, meaning the bath correlations must rapidly vanish on a time scale on which the system changes significantly. In addition, weak system-bath coupling is also required for the validity of the Markov approximation. Ideally, the bath correlations should follow

$$\langle \bar{B}_i(t)\bar{B}_j(t')\rangle_{\rm R} \propto \delta(t-t'), \tag{1.27}$$

then we can replace $\bar{\rho}(t')$ with $\bar{\rho}(t)$ in Eq. (1.25)

$$\begin{aligned} \frac{d}{dt}\bar{\rho}(t) &= -\sum_{i,j}\int_0^t dt' \Big\{ \big[\bar{s}_i(t)\bar{s}_j(t')\bar{\rho}(t) - \bar{s}_j(t')\bar{\rho}(t)\bar{s}_i(t)\big]\langle \bar{B}_i(t)\bar{B}_j(t')\rangle_{\rm R} \\ &+ \big[\bar{\rho}(t)\bar{s}_j(t')\bar{s}_i(t) - \bar{s}_i(t)\bar{\rho}(t)\bar{s}_j(t')\big]\langle \bar{B}_j(t')\bar{B}_i(t)\rangle_{\rm R} \Big\}. \end{aligned} \tag{1.28}$$

This is the central equation obtained after the Born-Markov approximation. This will be our starting point in deriving the master equations in subsequent sections.

1.4 Master equation for damped harmonic oscillator

We consider a harmonic oscillator of frequency ω_a, coupled to a reservoir maintained at thermal equilibrium at temperature T. The full Hamiltonian of the system and reservoir is given by

$$\hat{H}_{\mathrm{s}} = \omega_a \hat{a}^\dagger \hat{a}, \tag{1.29}$$

$$\hat{H}_{\mathrm{R}} = \sum_k \omega_k \hat{b}_k^\dagger \hat{b}_k, \tag{1.30}$$

$$\hat{H}_{\mathrm{sR}} = \sum_k \eta_k (\hat{a}\hat{b}_k^\dagger + \hat{a}^\dagger \hat{b}_k). \tag{1.31}$$

Here, $\hat{a}$ and $\hat{a}^\dagger$ represent the system annihilation and creation operators, respectively. The annihilation and creation operators of the k-th mode of the bath are denoted by $\hat{b}_k$ and $\hat{b}_k^\dagger$, respectively. The coupling between the system and k-th mode of the bath is described by η_k. The index k in the sum is taken over the infinite number of bath modes. We assume that the environment is maintained at a thermal state of temperature T and given by

$$\hat{\chi}_0 = \bar{\chi}_0 = \prod_j e^{-\hbar\omega_k \hat{b}_k^\dagger \hat{b}_k / k_{\mathrm{B}} T}(1 - e^{-\hbar\omega_k / k_{\mathrm{B}} T}), \tag{1.32}$$

k_B is the Boltzmann's constant.

1.4.1 Lindblad master equation

First, we need to identify the *jump* operators in the Hilbert space of the system, and then transform these jump operators into the interaction picture and replace these in the master equation with Born approximation (1.25). The jump operators for harmonic oscillator coupled to a thermal bath via interaction (1.29) are given by

$$\hat{s}_1 = \hat{a} \qquad \hat{B}_1 = \hat{b}_j^\dagger, \tag{1.33}$$

$$\hat{s}_2 = \hat{a}^\dagger \qquad \hat{B}_2 = \hat{b}_j. \tag{1.34}$$

In the interaction picture, these operators take the form

$$\bar{s}_1(t) = \bar{a}(t) = \hat{a}e^{-i\omega_a t}, \tag{1.35}$$

$$\bar{s}_2(t) = \bar{a}^\dagger(t) = \hat{a}^\dagger e^{i\omega_a t}, \tag{1.36}$$

$$\bar{B}_1(t) = \bar{b}_j^\dagger(t) = \hat{b}_j^\dagger e^{i\omega_j t}, \tag{1.37}$$

$$\bar{B}_2(t) = \bar{b}_j(t) = \hat{b}_j e^{-i\omega_j t}. \tag{1.38}$$

Note that the sum in Eq. (1.25) now has $i = 1, 2$ and $j = 1, 2$ accordingly there are sixteen terms in the integrand and Eq. (1.25) evaluate to

$$\begin{aligned} \frac{d}{dt}\bar{\rho}(t) = -\int_0^t dt' \quad & \Big\{ \big[\hat{a}\hat{a}\bar{\rho}(t') - \hat{a}\bar{\rho}(t')\hat{a}\big] e^{-i\omega_a(t+t')} \langle \bar{\Gamma}^\dagger(t)\bar{\Gamma}^\dagger(t')\rangle_{\mathrm{R}} + \mathrm{h.c.} \\ + \quad & \big[\hat{a}^\dagger\hat{a}^\dagger\bar{\rho}(t') - \hat{a}^\dagger\bar{\rho}(t')\hat{a}^\dagger\big] e^{i\omega_a(t+t')} \langle \bar{\Gamma}(t)\bar{\Gamma}(t')\rangle_{\mathrm{R}} + \mathrm{h.c.} \\ + \quad & \big[\hat{a}\hat{a}^\dagger\bar{\rho}(t') - \hat{a}^\dagger\bar{\rho}(t')\hat{a}\big] e^{-i\omega_a(t-t')} \langle \bar{\Gamma}^\dagger(t)\bar{\Gamma}(t')\rangle_{\mathrm{R}} + \mathrm{h.c.} \\ + \quad & \big[\hat{a}^\dagger\hat{a}\bar{\rho}(t') - \hat{a}\bar{\rho}(t')\hat{a}^\dagger\big] e^{i\omega_a(t-t')} \langle \bar{\Gamma}(t)\bar{\Gamma}^\dagger(t')\rangle_{\mathrm{R}} + \mathrm{h.c.} \Big\}, \end{aligned} \tag{1.39}$$

here we have defined

$$\bar{\Gamma}(t) \equiv \sum_k \eta_k \hat{b}_k e^{-i\omega_k t}. \tag{1.40}$$

By using the fact that reservoir is maintained at a thermal state (Eq. (1.32)), only the terms with following bath correlations survive in Eq. (1.39)

$$\langle \bar{\Gamma}^\dagger(t)\bar{\Gamma}(t')\rangle_{\mathrm{R}} = \sum_k |\eta_k|^2 e^{i\omega_k(t-t')}\bar{n}(\omega_k), \tag{1.41}$$

$$\langle \bar{\Gamma}(t)\bar{\Gamma}^\dagger(t')\rangle_{\mathrm{R}} = \sum_k |\eta_k|^2 e^{-i\omega_k(t-t')}\big(\bar{n}(\omega_k) + 1\big), \tag{1.42}$$

here $\bar{n}(\omega)$ is the Bose-Einstein distribution of the excitations in the bath, which is given by

$$\bar{n}(\omega) = \frac{1}{e^{\hbar\omega/k_{\mathrm{B}}T} - 1}. \tag{1.43}$$

The nonzero correlation functions of the bath have summation, which we change to integration by using the density of states $g(\omega)$ and change of variables $\tau = t - t'$ in

Eq. (1.39) yields

$$\frac{d}{dt}\bar{\rho}(t) = -\int_0^t d\tau \Big\{ \big[\hat{a}\hat{a}^\dagger\bar{\rho}(t-\tau) - \hat{a}^\dagger\bar{\rho}(t-\tau)\hat{a}\big] e^{-i\omega_a\tau} \langle \bar{\Gamma}^\dagger(t)\bar{\Gamma}(t-\tau)\rangle_{\mathrm{R}} + \text{h.c.}$$

$$+ \big[\hat{a}^\dagger\hat{a}\bar{\rho}(t-\tau) - \hat{a}\bar{\rho}(t-\tau)\hat{a}^\dagger\big] e^{i\omega_a\tau} \langle \bar{\Gamma}(t)\bar{\Gamma}^\dagger(t-\tau)\rangle_{\mathrm{R}} + \text{h.c.} \Big\}, \tag{1.44}$$

where

$$\langle \bar{\Gamma}^\dagger(t)\bar{\Gamma}(t-\tau)\rangle_{\mathrm{R}} = \int_0^\infty d\omega e^{i\omega_k\tau} g(\omega)|\eta|^2 \bar{n}(\omega_k), \tag{1.45}$$

$$\langle \bar{\Gamma}(t)\bar{\Gamma}^\dagger(t-\tau)\rangle_{\mathrm{R}} = \int_0^\infty d\omega e^{-i\omega_k\tau} g(\omega)|\eta|^2 \big(\bar{n}(\omega_k)+1\big). \tag{1.46}$$

If we assume, there exists two different time scales, τ_s and τ_R for system evolution and bath correlations such that τ_s is much larger than τ_R, then we can invoke the Markov approximation, which allows us to replace $\bar{\rho}(t-\tau)$ with $\bar{\rho}(t)$. Consequentally the master equation (1.44) becomes

$$\frac{d}{dt}\bar{\rho}(t) = \phi_1(\hat{a}\bar{\rho}\hat{a}^\dagger - \hat{a}^\dagger\hat{a}\bar{\rho}) + \phi_2(\hat{a}\bar{\rho}\hat{a}^\dagger + \hat{a}^\dagger\bar{\rho}\hat{a} - \hat{a}^\dagger\hat{a}\bar{\rho} - \bar{\rho}\hat{a}\hat{a}^\dagger), \tag{1.47}$$

here

$$\phi_1 \equiv \int_0^t d\tau \int_0^\infty d\omega e^{-i(\omega-\omega_a)\tau} g(\omega)|\eta|^2, \tag{1.48}$$

$$\phi_2 \equiv \int_0^t d\tau \int_0^\infty d\omega e^{-i(\omega-\omega_a)\tau} g(\omega)|\eta|^2 \bar{n}(\omega). \tag{1.49}$$

The integration in Eqs. (1.48) are dominated by time scale τ_{R} which is much shorter than τ_{s}, and t is in similar order of τ_{s}, therefore, integration upper limit can be changed from t to ∞. After performing the integration and rearranging the terms, the master equation can be written in the Lindblad form in the interaction picture

$$\frac{d}{dt}\bar{\rho} = -i\Delta[\hat{a}^\dagger\hat{a}, \bar{\rho}] + \frac{\gamma}{2}(2\hat{a}\bar{\rho}\hat{a}^\dagger - \hat{a}^\dagger\hat{a}\bar{\rho} - \bar{\rho}\hat{a}^\dagger\hat{a}) + \gamma\bar{n}(\hat{a}\bar{\rho}\hat{a}^\dagger + \hat{a}^\dagger\bar{\rho}\hat{a} - \hat{a}^\dagger\hat{a}\bar{\rho} - \bar{\rho}\hat{a}\hat{a}^\dagger), \tag{1.50}$$

here

$$\Delta \equiv P\int_0^\infty d\omega \frac{g(\omega)|\eta|^2}{\omega_a - \omega}, \tag{1.51}$$

$$\gamma \equiv 2\pi g(\omega_a)|\eta|^2, \tag{1.52}$$

where P is the Cauchy principal value. In Eq. (1.50), the density matrix $\bar{\rho}$ is in the interaction picture. The master equation in the Schrödinger picture can be written after some rearrangements of the terms as

$$\frac{d}{dt}\hat{\rho} = -i\omega'_a[\hat{a}^\dagger\hat{a}, \hat{\rho}] + \frac{\gamma}{2}(\bar{n}+1)(2\hat{a}\hat{\rho}\hat{a}^\dagger - \hat{a}^\dagger\hat{a}\hat{\rho} - \bar{\rho}\hat{a}^\dagger\hat{a}) + \frac{\gamma}{2}\bar{n}(2\hat{a}\hat{\rho}\hat{a}^\dagger - \hat{a}\hat{a}^\dagger\bar{\rho} - \hat{\rho}\hat{a}\hat{a}^\dagger), \tag{1.53}$$

here $\omega'_a = \omega_a + \Delta$. The master equation (1.53) can be written in a compact form

$$\frac{d}{dt}\hat{\rho} = -i\omega'_a[\hat{a}^\dagger\hat{a}, \hat{\rho}] + \gamma(\bar{n}+1)D[\hat{a}]\hat{\rho} + \gamma\bar{n}D[\hat{a}^\dagger]\hat{\rho}, \tag{1.54}$$

here the Lindblad dissipator operator is given by

$$D[\hat{o}]\hat{\rho} = \frac{1}{2}[2\hat{o}\hat{\rho}\hat{o}^\dagger - \hat{o}^\dagger\hat{o}\hat{\rho} - \hat{\rho}\hat{o}^\dagger\hat{o}]. \tag{1.55}$$

Chapter 2

GLOBAL MASTER EQUATION FOR NONLINEARLY COUPLED OSCILLATORS

In Sec. 2.1, we present the microscopic model of a typical optomechanical system in which two harmonic oscillators are nonlinearly coupled via so-called *energy-field* interaction. In addition, three different master equations for the system are presented, and we derive the Lindblad-Gorini-Kossakowski-Sudarshan (LGKS) master equation for this system in the energy basis of the system. The validity of these master equations is compared through the lens of thermodynamics in Sec. 2.2. Finally, we present concluding remarks in Sec. 2.3.

2.1 *Master equation of nonlinearly coupled oscillators*

This section is based on the published work [23], in which we derive the so-called the *global* master equation for two harmonic oscillators interacting via the nonlinear optomechanical interaction. We compare the thermodynamical consistency of the derived master equation with widely used *local* master equation.

2.1.1 *Introduction: The optomechanical system*

A typical optomechanical system consists of an optical resonator coupled to a mechanical resonator via the *energy-field* interaction [1]. In the last two decades, extensive theoretical and experimental works have tested the fundamental laws of quantum mechanics using macroscopic optomechanical systems and preparing macroscopic nonclassical states [1, 33, 34, 35, 36, 37, 38, 39, 40, 41, 42, 43, 44, 45, 46]. In optomechanical systems, the interaction of light with mechanical motion, such as oscillations of a micromirror, has been used for various applications such as state transfer be-

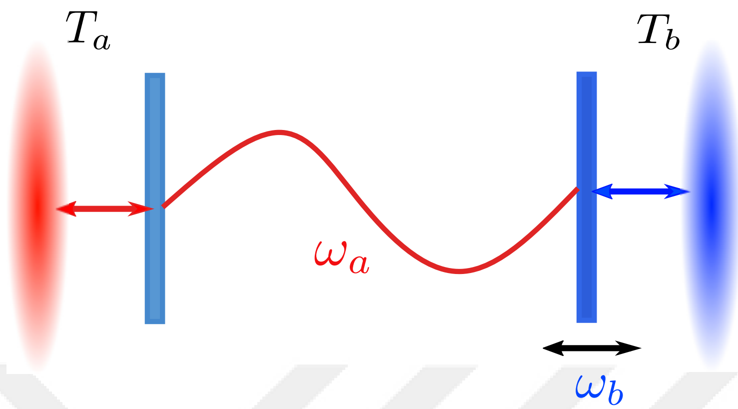

Figure 2.1: A schematic depiction of a typical optomechanical system. It consists of an optical cavity mode of frequency ω_a which is coupled to a mechanical resonator of frequency ω_b via the energy-field (optomechanical) interaction. This system is representative of a vast class of systems; for instance, the optomechanical-like coupling can be realized in circuit QED, cold atoms, electro-mechanical systems, and cavity QED [1]. The optical and mechanical resonators are coupled to independent thermal baths maintained at non-negative temperatures T_a, and T_b, respectively.

tween the mechanical excitations and optical pulses [47], quantum communication [48], quantum information processing [49, 50].

Recently, much attention has been paid to developing the thermodynamical applications of optomechanical systems [51, 52, 53, 54, 55, 56, 57, 58], such as quantum heat engines [59, 60, 61, 62], heat flow through optomechanical arrays [63], and optomechanical heat managers [26]. Recent years have seen tremendous experimental progress in the strong light-matter interaction regime [64]. The single-photon strong optomechanical coupling has been reported in several setups, including circuit QED [65, 66]. Therefore, it is crucial to have a thermodynamical consistent open system description of the optomechanical system in both weak and strong coupling regimes.

We consider a typical optomechanical system that consists of an optical cavity mode of frequency ω_a coupled to a mechanical resonator of frequency ω_b via optomechanical coupling g. In addition, the cavity and mechanical resonators are coupled to an independent thermal bath maintained at temperatures T_a and T_b, respectively. The Hamiltonian of the isolated optomechanical system excluding thermal baths is given by (for simplicity, we take $\hbar = 1$)

$$\hat{H}_{\mathrm{s}} = \omega_a \hat{a}^\dagger \hat{a} + \omega_b \hat{b}^\dagger \hat{b} - g\hat{a}^\dagger \hat{a}(\hat{b} + \hat{b}^\dagger), \tag{2.1}$$

here, $\hat{a}$ ($\hat{b}$) and $\hat{a}^\dagger$ ($\hat{b}^\dagger$) are the annihilation and creation operators of the optical (mechanical) resonator, respectively, and g denotes the single-photon coupling strength between the optical and mechanical resonators. The Hamiltonian of the two thermal baths is given by

$$\hat{H}_{jB} = \sum_{j,k} \omega_{j,k} \hat{b}^\dagger_{j,k} \hat{b}_{j,k}, \tag{2.2}$$

here $\hat{b}_{j,k}$ and $\hat{b}^\dagger_{j,k}$ are the annihilation and creation operators of the k-th mode of the thermal bath, in addition, $j = a, b$ indicates the optical and mechanical resonator's bath, respectively. The interaction between the isolated optomechanical system and the thermal baths has the form

$$\hat{H}_{sB} = \sum_k \left[g_{a,k}(\hat{a}\hat{b}^\dagger_{a,k} + \hat{a}^\dagger \hat{b}_{a,k}) + g_{b,k}(\hat{b}\hat{b}^\dagger_{b,k} + \hat{b}^\dagger \hat{b}_{b,k}) \right]. \tag{2.3}$$

The first term describes the interaction between the optical resonator and bath modes, where $g_{a,k}$ represents the interaction strength of the bath mode indexed by k. Similarly, the second term is associated with interaction between the mechanical resonator and thermal bath of temperature T_b, where the sum is taken over infinite bath modes indexed by k.

2.1.2 The local master equation (LME)

A standard method of deriving the Markovian master equation involves Born-Markov approximations, and to obtain GKLS form; the rotating wave approximation is invoked (see Sec. 1.3 for details). In the so-called *local* approach, the master equation is derived by ignoring the interaction term between the subsystem, in our case, dropping the optomechanical coupling in the derivation. In such a case, the *jump* operators are associated only with the individual oscillators; therefore, these are dubbed as local jump operators, and the master equation is referred to as the local master equation. The first step in the derivation requires identification of the jump operators, in the local approach, the jump operators are given by (see Sec. 1.3)

$$\hat{s}_1 = \hat{a} \qquad \hat{B}_1 = \hat{b}^{\dagger}_{a,k}, \tag{2.4}$$
$$\hat{s}_2 = \hat{a}^{\dagger} \qquad \hat{B}_2 = \hat{b}_{a,k}, \tag{2.5}$$
$$\hat{s}_3 = \hat{b} \qquad \hat{B}_3 = \hat{b}^{\dagger}_{b,k}, \tag{2.6}$$
$$\hat{s}_4 = \hat{b}^{\dagger} \qquad \hat{B}_4 = \hat{b}_{b,k}. \tag{2.7}$$

Following the derivation detailed in Sec. 1.3, the local master equation for the optomechanical system has the form

$$\frac{d}{dt}\hat{\rho} = -[\hat{H}_{\mathrm{s}}, \hat{\rho}] + \mathcal{L}_a^{(l)}\hat{\rho} + \mathcal{L}_b^{(l)}\hat{\rho} \tag{2.8}$$

where

$$\mathcal{L}_a^{(l)}\hat{\rho} = G_a(\omega_a)D[\hat{a}]\hat{\rho} + G_a(-\omega_a)D[\hat{a}^{\dagger}]\hat{\rho}, \tag{2.9}$$
$$\mathcal{L}_b^{(l)}\hat{\rho} = G_b(\omega_b)D[\hat{b}]\hat{\rho} + G_b(-\omega_b)D[\hat{b}^{\dagger}]\hat{\rho} \tag{2.10}$$

here $\mathcal{L}_a^{(l)}\hat{\rho}$, and $\mathcal{L}_b^{(l)}\hat{\rho}$ are the Liouville superoperators of the optical and mechanial resonators, respectively. In the rest of this thesis, we consider Ohmic spectral densities of the baths unless otherwise mentioned, which is given by

$$G_j(\omega) = \omega\kappa_j(1 + \bar{n}_j(\omega)), \tag{2.11}$$
$$G_j(-\omega) = \omega\kappa_j\bar{n}_j(\omega). \tag{2.12}$$

Here, κ_j is the coupling strength between the system and baths.

2.1.3 The dressed-state master equation (DSME)

Unlike the local master equation, in the dressed state master equation, some of the jump operators are nonlocal. In the first step, the optomechanical Hamiltonian is diagonalized using the polaron transformation

$$\hat{S} = e^{-\alpha \hat{a}^\dagger \hat{a}(\hat{b}^\dagger - \hat{b})}, \tag{2.13}$$

following which the Hamiltonian takes the form

$$\tilde{H}_s = \omega_a \tilde{a}^\dagger \tilde{a} + \omega_b \tilde{b}^\dagger \tilde{b} - \frac{g^2}{\omega_b}(\tilde{a}^\dagger \tilde{a})^2. \tag{2.14}$$

The operators are transformed to

$$\tilde{a} = \hat{a} e^{-\alpha(\hat{b}^\dagger - \hat{b})} \quad \text{and} \qquad \tilde{b} = \hat{b} - \alpha \hat{a}^\dagger \hat{a}. \tag{2.15}$$

Here, the jump operators are different then in the local approach, and the jump operators are given by

$$\hat{s}_1 = \tilde{a} = \hat{a} \qquad \hat{B}_1 = \hat{b}^\dagger_{a,k}, \tag{2.16}$$

$$\hat{s}_2 = \tilde{a}^\dagger = \hat{a}^\dagger \qquad \hat{B}_2 = \hat{b}_{a,k}, \tag{2.17}$$

$$\hat{s}_3 = \tilde{b} = \hat{b} - \alpha \hat{a}^\dagger \hat{a} \qquad \hat{B}_3 = \hat{b}^\dagger_{b,k}, \tag{2.18}$$

$$\hat{s}_4 = \tilde{b}^\dagger = \hat{b} - \alpha \hat{a}^\dagger \hat{a} \qquad \hat{B}_4 = \hat{b}_{b,k}. \tag{2.19}$$

The jump operators $\hat{s}_1$ and $\hat{s}_2$ are still local because of dropping all α dependent terms in these operators, here $\alpha = g/\omega_b$. We note that the derivation of dressed state master equation is presented in [67], in which authors argue to drop α-dependent terms from cavity transformed operator $\tilde{a}$ by assuming flat spectral density for the optical bath. However, this approximation leads to an inconsistent master equation, and alpha-dependent terms can not be ignored for thermodynamic consistency (see Figs. 2.2 and 2.3). We will discuss this in the next section while deriving the global master equation. By dropping α-dependent terms, the optical bath can now only access the optical mode, and on the other hand, the mechanical bath has access to both mechanical and optical resonators. Accordingly, this derivation can be regarded as *semi-global* approach. Following this, the system operators in Eq. (2.3) evaluate to

$$\hat{a}(t) = \tilde{a} e^{-i\omega_{\mathrm{a}} t} \quad \text{and} \qquad \hat{b}(t) = \tilde{b} e^{-i\omega_{\mathrm{b}} t} + \alpha \tilde{a}^\dagger \tilde{a}. \tag{2.20}$$

labelch2:eq:DSMEint In Ref. [67], a detailed derivation of the DSME is given, which has the form

$$\frac{d}{dt}\hat{\rho} = -i[\hat{H}_{\mathrm{s}}, \hat{\rho}] + \mathcal{L}_{\mathrm{a}}^{(\mathrm{d})}\hat{\rho} + \mathcal{L}_{\mathrm{b}}^{(\mathrm{d})}\hat{\rho} + \mathcal{L}_{\mathrm{b,d}}^{(\mathrm{d})}\hat{\rho}, \tag{2.21}$$

where

$$\mathcal{L}_{\mathrm{a}}^{(\mathrm{d})}\hat{\rho} = G_{\mathrm{a}}(\omega_{\mathrm{a}})D[\hat{a}]\hat{\rho} + G_{\mathrm{a}}(-\omega_{\mathrm{a}})D[\hat{a}^\dagger]\hat{\rho}, \tag{2.22}$$

$$\mathcal{L}_{\mathrm{b}}^{(\mathrm{d})}\hat{\rho} = G_{\mathrm{b}}(\omega_{\mathrm{b}})D[\hat{b} - \alpha\hat{n}_{\mathrm{a}}]\hat{\rho} + G_{\mathrm{b}}(-\omega_{\mathrm{b}})D[\hat{b}^\dagger - \alpha\hat{n}_{\mathrm{a}}]\hat{\rho}, \text{ and} \tag{2.23}$$

$$\mathcal{L}_{\mathrm{b,d}}^{(\mathrm{d})}\hat{\rho} = 4(\kappa_{\mathrm{b}}T_{\mathrm{b}}/\omega_{\mathrm{b}})\alpha^2 D[\hat{n}_{\mathrm{a}}]\hat{\rho}. \tag{2.24}$$

Here, the first two terms describe the optical and mechanical dissipation, respectively, and the last term represents the optical resonator's pure decoherence (dephasing). In addition, $\alpha = g/\omega_b$, and $\hat{n}_a = \hat{a}^\dagger\hat{a}$. It may be worth noting that this equation reduces to the LME in the limit $g \to 0$.

2.1.4 The global master equation (GME)

Similar to the derivation of the DSME, in the global approach, first the Hamiltonian is diagonalized, then the jump operators are obtained in the diagonal basis, which are of the form

$$\hat{s}_1 = \tilde{a} = \hat{a}e^{-\alpha(\hat{b}^\dagger - \hat{b})} \qquad \hat{B}_1 = \hat{b}_{a,k}^\dagger, \tag{2.25}$$

$$\hat{s}_2 = \tilde{a}^\dagger = \hat{a}^\dagger e^{\alpha(\hat{b}^\dagger - \hat{b})} \qquad \hat{B}_2 = \hat{b}_{a,k}, \tag{2.26}$$

$$\hat{s}_3 = \tilde{b} = \hat{b} - \alpha\hat{a}^\dagger\hat{a} \qquad \hat{B}_3 = \hat{b}_{b,k}^\dagger, \tag{2.27}$$

$$\hat{s}_4 = \tilde{b}^\dagger = \hat{b}^\dagger - \alpha\hat{a}^\dagger\hat{a} \qquad \hat{B}_4 = \hat{b}_{b,k}. \tag{2.28}$$

Note in this case, all jump operators are nonlocal. The system operators then transformed into the interaction picture and given by

$$\hat{a}(t) = \tilde{a}e^{-i\omega_{\mathrm{a}}t}\sum_{n=0}^{\infty}\alpha^n(\tilde{b}e^{-i\omega_{\mathrm{b}}t} - \tilde{b}^\dagger e^{i\omega_{\mathrm{b}}t})^n \quad \text{and} \qquad \hat{b}(t) = \tilde{b}e^{-i\omega_{\mathrm{b}}t} + \alpha\tilde{a}^\dagger\tilde{a}. \tag{2.29}$$

In Eq. (2.1.4), there are infinite terms in the sum which makes the derivation of the master equation intractable. In addition, it is sufficient to consider first few terms for weak optomechanical coupling $\alpha \ll 1$. Here, we drop all terms of order higher than α^2, and follow the standard derivation of the master equation by making the Born-Markov and Secular approximations. The GME is given as

$$\frac{d}{dt}\tilde{\rho} = \mathcal{L}_{\mathrm{a}}^{(\mathrm{g})}\tilde{\rho} + \mathcal{L}_{\mathrm{b}}^{(\mathrm{g})}\tilde{\rho} + \mathcal{L}_{\mathrm{b,d}}^{(\mathrm{g})}\tilde{\rho}, \tag{2.30}$$

where the dissipation and pure decoherence terms are given by

$$\begin{aligned}
\mathcal{L}_{\mathrm{a}}^{(\mathrm{g})}\tilde{\rho} = G_{\mathrm{a}}(\omega_{\mathrm{a}})\big\{D[\tilde{a}] + \alpha^2 D[\tilde{a}\tilde{b}^\dagger\tilde{b}]\big\}\tilde{\rho} + G_{\mathrm{c}}(-\omega_{\mathrm{a}})\big\{D[\tilde{a}^\dagger] + \alpha^2\big(+D[\tilde{a}^\dagger\tilde{b}^\dagger\tilde{b}]\big)\big\}\tilde{\rho}& \\
+ \sum_{n=1,2}\Big\{\alpha^n G_{\mathrm{c}}(\omega_{\mathrm{a}} + n\omega_{\mathrm{b}})D[\tilde{a}\tilde{b}^n]\tilde{\rho}& \\
+ \alpha^n G_{\mathrm{a}}(-\omega_{\mathrm{a}} - n\omega_{\mathrm{b}})D[\tilde{a}^\dagger\tilde{b}^{\dagger n}]\tilde{\rho} + \alpha^n G_{\mathrm{a}}(\omega_{\mathrm{a}} - n\omega_{\mathrm{b}})D[\tilde{a}\tilde{b}^{\dagger n}]\tilde{\rho}& \\
+ \alpha^n G_{\mathrm{a}}(-\omega_{\mathrm{a}} + n\omega_{\mathrm{b}})D[\tilde{a}^\dagger\tilde{b}^n]\tilde{\rho}\Big\},& \qquad (2.31)
\end{aligned}$$

$$\mathcal{L}_{\mathrm{b}}^{(\mathrm{g})}\tilde{\rho} = G_{\mathrm{b}}(\omega_{\mathrm{b}})D[\tilde{b} - \alpha\hat{n}_{\mathrm{a}}]\tilde{\rho} + G_{\mathrm{b}}(-\omega_{\mathrm{b}})D[\tilde{b}^\dagger - \alpha\hat{n}_{\mathrm{a}}]\tilde{\rho}, \text{ and} \tag{2.32}$$

$$\mathcal{L}_{\mathrm{b,d}}^{(\mathrm{g})}\tilde{\rho} = G_{\mathrm{b}}(0)\alpha^2 D[\hat{n}_{\mathrm{a}}]\tilde{\rho}. \tag{2.33}$$

Note that in Eq. (2.30) is given in the interaction picture and in the polaron basis. Upon transformation to the local basis, the jump operators remain nonlocal both for the optical and mechanical resonators. In addition, in the limit $g \to 0$, this equation reduces to the local master equation as required. The sum over n in Eq. (2.30) describes the contributions from the phonon sidebands, for instance, $n = 1$ indicates first-order phonon sideband.

2.2 Thermodynamical consistency ananlysis

We will now proceed to the analysis of the thermodynamical consistency of the three master equations described earlier. In our results, we use system parameters representative of a circuit QED optomechanical system [65, 66]. $\omega_{\mathrm{a}} = 2\pi \times 10\,\mathrm{GHz}$, as well as $\omega_{\mathrm{b}} = 2\pi \times 600\,\mathrm{MHz}$, $\kappa_{\mathrm{a}} = 2\pi \times 200\,\mathrm{MHz}$, and $\kappa_{\mathrm{b}} = 2\pi \times 50\,\mathrm{MHz}$. We have scaled all system parameters by the frequency ω_a, and thus all parameters are dimensionless in the numerical results.

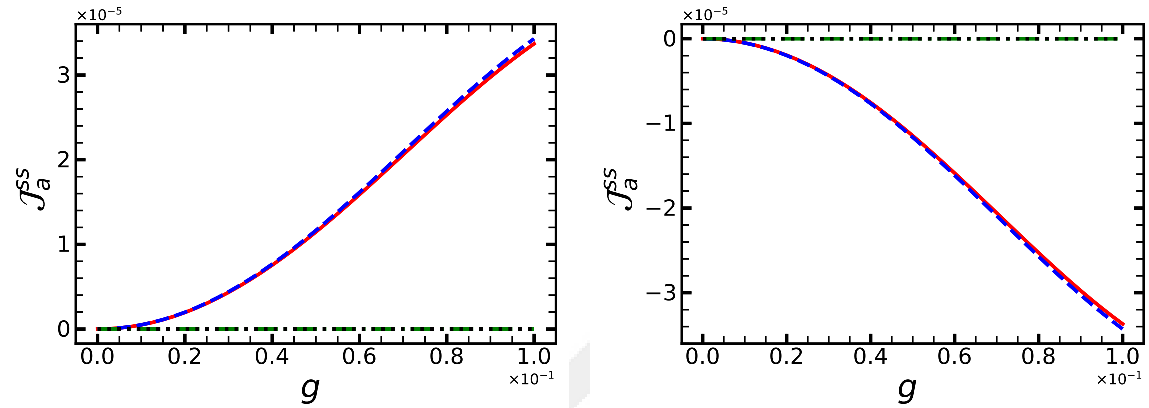

a b

Figure 2.2: **(a-b)** The steady-state heat currents $\mathcal{J}_a^{\mathrm{ss}}$, and $\mathcal{J}_b^{\mathrm{ss}}$ as a function of the single-photon optomechanical coupling strength g. There is no temperature bias $T_a = T_b = 0.210$ K. Solid, dashed, dot-dashed, and dotted lines represent the heat currents for the LME, DSME, GME2, and GME4, respectively. Where GME2, and GME4 indicated the global master equation with two and four phonon sidebands, respectively. Without a temperature gradient, the heat flow must be zero through the coupled resonators. However, LME and DSME predict non-zero heat flow, violating the second law of thermodynamics. Deriving the master equation (GME) in the energy basis of the system recovers the second law of thermodynamics.

2.2.1 The first law: Energy conservation

The first law of thermodynamics is about energy conservation, according to which the energy of an isolated system is conserved and can be broken into work and heat [68]. In our model, there is no source of work; thus, the first law dictates that at steady-state the sum of heat flow through the system must be zero

$$\mathcal{J}_a + \mathcal{J}_b = 0 \tag{2.34}$$

here, $\mathcal{J}_a$ and $\mathcal{J}_b$ represent the heat flow from the optical and mechanical resonator's bath, respectively, which is given as [68]

$$\mathcal{J}_j = \mathrm{Tr}\{(\mathcal{L}_j^{(\zeta)}\hat{\rho})\hat{H}_{\mathrm{s}}\}. \tag{2.35}$$

Here, $(\mathcal{L}_j^{(\zeta)}\hat{\rho}$ describes the Liouville superoperators for the LME ($\zeta = l$), the DSME ($\zeta = d$), or the GME ($\zeta = g$). We have adopted the sign convention of heat flowing out of (into) the negative (positive) system. At steady-state, the heat currents can be calculated analytically for the cases of the LME and DSME, and it is given in Appendix .1. The equations in Appendix .2 show that irrespective of the parameters regime, the first law of thermodynamics is always satisfied by the LME and DSME. For the GME, due to nonlocal dissipators, the heat flows have to be calculated numerically. The GME also predicts energy conservation; consequently, all three master equations are consistent with the first law of thermodynamics.

2.2.2 The second law: Non-negative entropy production

According to the second law of thermodynamics, an isolated system's entropy production remains nonnegative. In the case of a quantum system, the dynamics version of the second law is given by [68]

$$\xi := \frac{dS}{dt} - \sum_j \frac{\mathcal{J}_j}{T_j} \geq 0. \tag{2.36}$$

here S being the von Neumann entropy, given by $S(\hat{\rho}) = -\mathrm{Tr}(\hat{\rho}\log\hat{\rho})$; the second term $\mathcal{J}_j$ describes the heat flow from the j-th thermal bath. We discuss the validity of the master equations in three different parameters regimes.

(i) *Equal temperatures* $T_a = T_b$: In the absence of any temperature gradient, the second law of thermodynamics dictates that no heat should flow through the system, which means the steady-state heat currents should be zero in our case $\mathcal{J}_a^{\mathrm{ss}} = \mathcal{J}_b^{\mathrm{ss}} = 0$. However, suppose the LME or DSME describes the dynamics of the optomechanical system. In that case, these predict a nonzero heat flow through the system, as shown in Fig. 2.2. This violates the second law of thermodynamics, as stated above. We

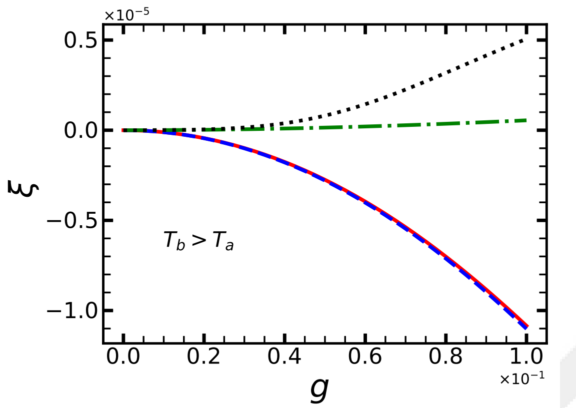

a

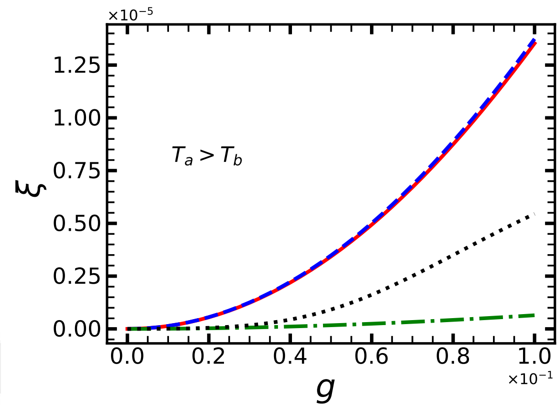

b

Figure 2.3: **(a-b)** The steady-state entropy production rate ξ, as a function of the single-photon optomechanical coupling strength g. (a) For $T_a = 0.210$, and $T_b = 0.220$ K, and for (b) $T_a = 0.220$, and $T_b = 0.210$ K. Solid, dashed, dot-dashed, and dotted lines represent the heat currents for the LME, DSME, GME2, and GME4, respectively. Where GME2, and GME4 indicated the global master equation with two and four phonon sidebands, respectively.

report that these non-physical heat flows becomes zero in the case of GME, and we recover the second law by adding phonon sidebands in the master equation. Thus the global approach captures the correct dynamics compared to the local approach in the absence of any thermal gradient.

(ii) *Higher temperature mechanical bath* $T_a < T_b$: In the case of the mechanical bath at a higher temperature than the optical bath, the entropy production rate becomes negative for the LME and DSME. This violation of the second law can be explained by analytically calculating the entropy production rate for the LME and DSME. We solve the rate equations in Appendix .2, and using these find the steady-state entropy production rate as

$$\xi^{\rm ss} = g\kappa_{\rm a}\left(\frac{2g\omega_{\rm b} + \alpha\kappa_{\rm b}\kappa}{\omega_{\rm b}^2 + \kappa^2}\right)\bar{n}_{\rm a}(\bar{n}_{\rm a}+1)\left(\frac{1}{T_{\rm b}} - \frac{1}{T_{\rm a}}\right), \tag{2.37}$$

where $\kappa = \kappa_{\mathrm{a}} + \frac{\kappa_{\mathrm{b}}}{2}$ and $\bar{n}_a := \bar{n}_a(\omega_a)$. In this equation, all the factor are non-negative except the last one. Therefore the sign of ξ^{ss} is determined by the relative magnitudes of the temperatures T_{a} and T_{b}. It is clear from this equation that if $T_b > T_a$, the entropy production rate remains negative irrespective of the other system parameters, which is against the second law of thermodynamics. This violation of the second law of thermodynamics can be removed by consider the GME in which phonon sideband helps to recover the second law as shown in Fig. 2.3a. In the case of GME, we are not aware of any exact concise expression for the steady-state entropy production.

(ii) *Higher temperature optical bath $T_a > T_b$*: For this case, all three master equations are consistent with both the first and second law of thermodynamics, this is confirmed in Fig. 2.3b. However, the heat flows are different both quantitatively and qualitatively.

2.3 Summary

We have investigated a typical optomechanical system in which the optical and the mechanical resonators are each coupled to a thermal bath. We focused our analysis on the thermodynamic consistency of the master equations in the local and global approaches. At thermal equilibrium, the local and semi-global master equations predicted nonzero heat current through the system, violating the second law of thermodynamics. Upon describing the system dynamics with the global master equation, in which the jump operators become nonlocal, the heat currents vanish at thermal equilibrium, per the laws of thermodynamics. Hence, the global approach predicts the dynamics accurately compared to the local description of the system. In addition, in the presence of temperature bias, the local approaches predict heat flow from the cold to the hot bath, violating the second law of thermodynamics. The addition of the phonon sideband in the global master equation corrects the direction of heat flow and recovers the validity of the second law in this regime. Our results show that the global approach is superior and consistent with the laws of thermodynamics in predicting the evolution of the optomechanical system in both weak and strong coupling regimes.

Our analysis shows that the widely used assumption of the validity of the local master equation in the weak optomechanical coupling is incorrect. Significant qualitative and quantitative differences in the local and global approaches to predicting the heat current in both weak and strong coupling can facilitate testing our predictions in the current optomechanical systems.

Chapter 3

QUANTUM HEAT DIODE AND HEAT TRANSISTOR

In the recent past, there have been extensive theoretical and experimental efforts related to heat management in quantum systems, in particular, rectification and amplification of heat flow [69, 70, 71, 72, 73, 74, 75, 76, 77, 78, 79, 24, 80, 81, 82, 83, 84, 85, 8]. The primary motivation behind this upsurge of interest in heat management is its potential applications in quantum technologies; however, these studies can also help give insight into the fundamental principles of these devices. The lack of general principles and fundamental mechanisms has led to a plethora of microscopic models of quantum heat diodes and transistors. The general principles of heat management can help optimal designs for thermal rectifiers and transistors. In addition, these principles can also give insight into a deeper understanding of quantum thermodynamics. In this chapter, we discuss the fundamental sources of asymmetry in the heat flow and minimal design for the quantum heat diode and transistor.

3.1 Intoduction: Quantum heat diode

In analogy to an electronic diode, a heat diode enforces an asymmetrical heat flow between two thermal baths under the change of temperature gradient. A quantum heat diode consists of a quantum system sandwiched between two thermal baths of different temperatures T_L, and T_R as shown in Fig. 3.1. T_L, and T_R are the temperatures of the left and right baths, respectively. An ideal thermal diode allows the heat flow only in one direction, say, from a heat bath on the right side to the heat bath on the left side. On reversal of the temperature bias, there should not be any heat flow from the left to the right bath.

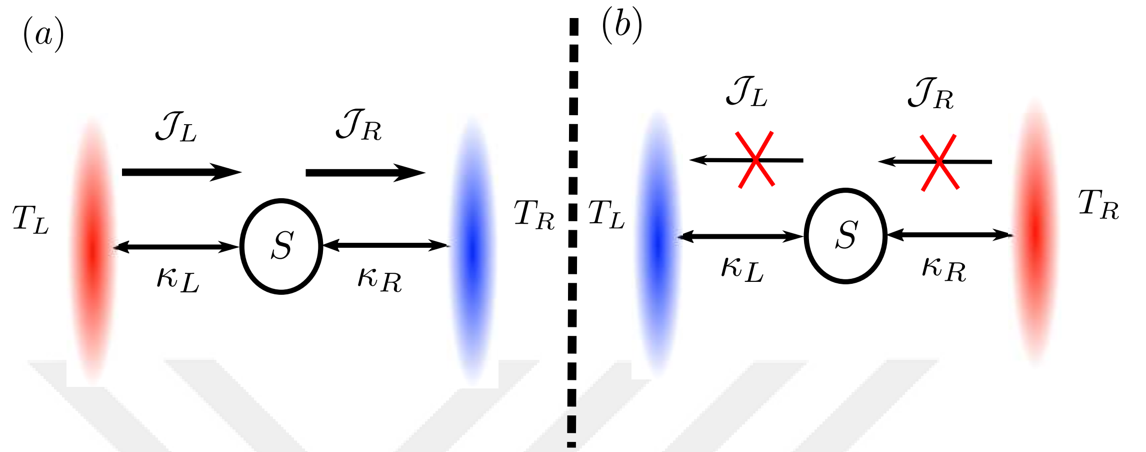

Figure 3.1: A schematic depiction of a generic quantum heat diode. A quantum system S with discrete energy levels is sandwiched between two thermal baths of temperatures T_L and T_R, indicating the left and right baths, respectively. In addition, κ_L and κ_R are the coupling strengths of the left and right bath, respectively. **(a)** In the case of $T_L > T_R$, the left bath heat current $\mathcal{J}_L$ is positive, and the right bath heat current $\mathcal{J}_R$ is negative. **(b)** $T_R > T_L$ the heat currents change their sign following the second law of thermodynamics. For the diode operation, the heat flow should be asymmetric under the temperature gradient change, represented by the width of the heat current arrows in this figure.

3.1.1 Rectification figure of merit

A figure of merit is needed for heat rectification to quantify the quality of a heat diode. For this purpose, we define rectification factor $\mathcal{R}$

$$\mathcal{R} = \frac{|\mathcal{J}_\mathrm{R}(T_\mathrm{R},T_\mathrm{L}) + \mathcal{J}_\mathrm{R}(T_\mathrm{L},T_\mathrm{R})|}{\mathrm{Max}(|\mathcal{J}_\mathrm{R}(T_\mathrm{R},T_\mathrm{L})|\,,|\mathcal{J}_\mathrm{R}(T_\mathrm{L},T_\mathrm{R}))|}, \tag{3.1}$$

here $\mathcal{J}_L$ and $\mathcal{J}_R$ being the left and right bath heat currents, respectively. The heat currents can be calculated using

$$\mathcal{J}_\alpha = \mathrm{Tr}[(\mathcal{L}_\alpha\hat{\rho})\hat{H}_\mathrm{s}], \tag{3.2}$$

here $\alpha = L, R$, and $\mathcal{L}_\alpha\hat{\rho}$ is the Liouville superoperator which describe the dissipation process, and $\hat{H}_\mathrm{s}$ is the system Hamiltonian. The rectification factor $\mathcal{R}$ can take a value between zero and one. For an ideal heat diode, $\mathcal{R}$ becomes one, and for no asymmetry in the heat flow, the rectification factor $\mathcal{R}$ goes to zero.

3.2 Possible sources of asymmetry in heat flow

This section describes the possible sources of asymmetry present in the quantum system that may lead to heat rectification. We explain the underlying physical mechanism that is model-independent and provides sufficient conditions for designing a heat diode.

3.2.1 Asymmetric system-bath coupling

The first proposal of a quantum heat diode based on a spin-boson coupled system was presented by Segal et al. [69]. The system consists of a single two-level system coupled to two bosonic thermal baths via spin-boson interaction. The schematic of this system is the same as shown in Fig. 3.1 by replacing system S with a two-level system. In this system, the right bath heat current is given by [69]

$$\mathcal{J}_R = \omega_s \frac{\kappa_L \kappa_R}{\kappa_L(1+2\bar{n}_L)+\kappa_R(1+2\bar{n}_R)}(\bar{n}_L-\bar{n}_R), \tag{3.3}$$

here, ω_s is the frequency of the two-level system, and κ_α is the system-bath coupling strength. In addition $\bar{n}_\alpha = (e^{\omega_s/T_\alpha}-1)^{-1}$ is the average excitation number of $\alpha = L, R$ baths. According to the first law of thermodynamics, in this model, at steady-state the two heat flow through the system must be zero $\mathcal{J}_L + \mathcal{J}_R = 0$, which means the left bath heat current can be obtained by placing a minus sign in Eq. (3.3). Note that Eq. (3.3) is not symmetric under the exchange of L and R, however, if $\kappa_L = \kappa_R$, this asymmetry vanishes. This expression of heat current shows that asymmetric system-bath coupling in a spin-boson model can lead to heat rectification.

3.2.2 Off-resonant coupled qubits

In a spin-boson heat diode consisting of a single two-level system, heat rectification is only possible if the system-baths couplings are unequal. If the system-baths

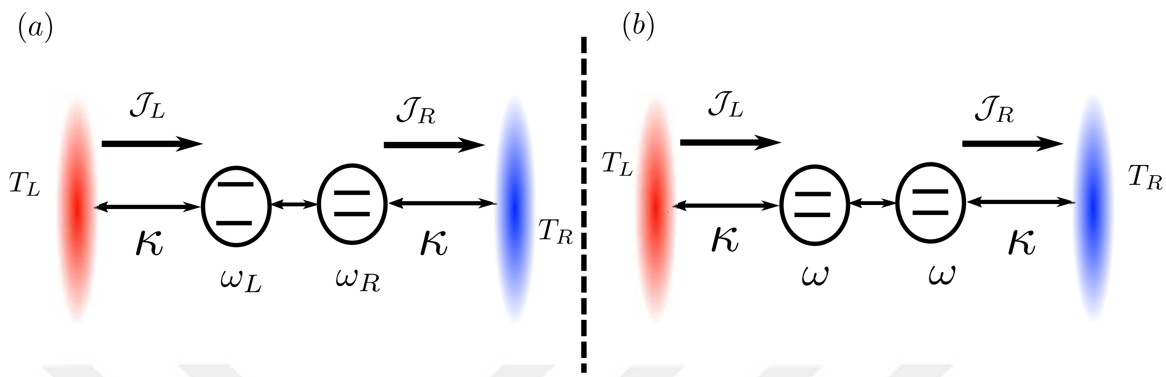

Figure 3.2: **(a)** A schematic representation of a heat diode based on two coupled qubits of different frequencies $\omega_L \neq \omega_R$. The interaction between the qubits is symmetric under the change of L and R labels; for instance, $\hat{\sigma}_L^z\hat{\sigma}_R^z$, and $\hat{\sigma}_L^x\hat{\sigma}_R^x$. The system-bath couplings κ are identical. The asymmetry of heat flow under the exchange of temperature gradient originates due to the different frequencies of the qubits. **(b)** A quantum heat diode based on two coupled qubits via anisotropic exchange interaction $\hat{\sigma}_L^z\hat{\sigma}_R^x$. Both the dissipation rates induced by baths and the frequencies of the qubits are considered identical. The anisotropic coupling, which is asymmetric under the exchange of L and R labels, leads to heat current rectification.

interactions are the same, heat rectification is not possible. This condition of asymmetric bath couplings can be relaxed if a multipartite spin system is considered. For instance, it has been shown that if two interacting qubits ($\hat{\sigma}_L^z\hat{\sigma}_R^z$ interaction) of different frequencies are considered, heat rectification becomes possible even for equal bath dissipation rates [77].

The emergence of heat rectification can be explained by writing the master equation for a generic quantum system coupled to two different thermal baths

$$\frac{d}{dt}\hat{\rho} = \mathcal{L}_L\hat{\rho} + \mathcal{L}_R\hat{\rho}, \tag{3.4}$$

the Liouville superoperators have the form

$$\mathcal{L}_\alpha \hat{\rho} = \sum_k [G_\alpha(\omega_k) D[\hat{A}_{\omega_k}] + G_\alpha(-\omega_k) D[\hat{A}^\dagger_{\omega_k}]] \tag{3.5}$$

here $G_\alpha(\omega_k)$ being the system-bath coupling spectra, the explicit expression depends on the choice of bath spectrum, and we consider Ohmic spectral densities of the baths Eq. (2.11). The $\hat{A}_{\omega_k}$ are the jump operators of the system, and the Lindblad dissipator is given by

$$D[\hat{o}]\hat{\rho} = \frac{1}{2}[2\hat{o}\hat{\rho}\hat{o}^\dagger - \hat{o}^\dagger \hat{o}\hat{\rho} - \hat{\rho}\hat{o}^\dagger \hat{o}] \tag{3.6}$$

It is clear from Eq. (3.5) that under the exchange of temperature bias, the Liouville superoperators differ only in temperature; hence the respective heat currents are interchangeable. Consequently, there is no heat rectification without unequal system-bath coupling. To have asymmetrical heat flow, we must have asymmetry in the $\mathcal{L}_L$ and $\mathcal{L}_R$, irrespective of the temperature bias. One way to make Liouville superoperators asymmetrical is by considering a multipartite spin system in which the jump operators are global and assuming the subsystems are off-resonant. The off-resonant qubits lead to asymmetrical heat flow, reported in many different works by considering different microscopic models [73, 86, 75, 77].

3.2.3 Asymmetric qubit-qubit interaction

As discussed above, heat rectification in spin-boson system-bath interaction is possible either by considering unequal baths dissipation rates or by considering more than one coupled two-level system, for instance, coupled qubits, which should be off-resonant. For resonantly coupled qubits with identical system-bath coupling, rectification is impossible in spin-boson-based systems. It is desirable that a good thermal diode should be able to conduct high heat currents along with rectification close to unity. However, this is impossible by considering asymmetric bath coupling or off-resonant qubits. The goal of simultaneous higher rectification and larger heat currents can be achieved using asymmetric inter-qubit coupling. For example, it is not possible to have rectification for resonantly $\hat{\sigma}_L^x\hat{\sigma}_R^x$ coupled qubits, however, if we consider $\hat{\sigma}_L^z\hat{\sigma}_R^x$, then rectification becomes possible for resonant qubits [24]. In the next section, we will discuss the case of a heat diode based on asymmetrically coupled qubits.

3.3 Two-atom heat diode

3.3.1 The model

We consider two qubits of transitions frequencies ω_L and ω_R as shown in Fig. 3.2. The Hamiltonian of the isolated system is given by

$$\hat{H} = \frac{\omega_{\rm L}}{2}\hat{\sigma}_{\rm L}^z + \frac{\omega_{\rm R}}{2}\hat{\sigma}_{\rm R}^z + g\hat{\sigma}_{\rm L}^z\hat{\sigma}_{\rm R}^x, \tag{3.7}$$

here, $\hat{\sigma_j}$ $(j = x, y, z)$ are the Pauli matrices and g is the coupling strength between the qubits. Each qubit in the system is coupled to a thermal bath of temperature T_α, with $\alpha = L, R$ indication the left and right qubit baths. To investigate the heat flow through the system, we first derive the master equation for the setup shown in Fig. 3.2.

3.3.2 The Master equation

To derive the global master equation, we first diagonalize the system Hamiltonian using the unitary transformation

$$S = e^{-i\frac{\theta}{2}\hat{\sigma}_{\rm L}^z\hat{\sigma}_{\rm R}^y}, \tag{3.8}$$

here θ is given by

$$\sin\theta = \frac{2g}{\Omega}, \qquad \cos\theta = \frac{\omega_{\rm R}}{\Omega}, \qquad \tan\theta = \frac{2g}{\omega_{\rm R}}, \tag{3.9}$$

and $\Omega = \sqrt{\omega_{\rm R}^2 + 4g^2}$. The system operators are transformed and evaluate to

$$\tilde{\sigma}_{\rm L}^x = \cos\theta\hat{\sigma}_{\rm L}^x + \sin\theta\hat{\sigma}_{\rm L}^y\hat{\sigma}_{\rm R}^y, \qquad \tilde{\sigma}_{\rm L}^y = \cos\theta\hat{\sigma}_{\rm L}^y - \sin\theta\hat{\sigma}_{\rm L}^x\hat{\sigma}_{\rm R}^y, \qquad \tilde{\sigma}_{\rm L}^z = \hat{\sigma}_{\rm L}^z, \tag{3.10}$$

and

$$\tilde{\sigma}_{\rm R}^x = \cos\theta\hat{\sigma}_{\rm R}^x - \sin\theta\hat{\sigma}_{\rm L}^z\hat{\sigma}_{\rm R}^z, \qquad \tilde{\sigma}_{\rm R}^y = \hat{\sigma}_{\rm R}^y, \qquad \tilde{\sigma}_{\rm R}^z = \cos\theta\hat{\sigma}_{\rm R}^z - \sin\theta\hat{\sigma}_{\rm L}^z\hat{\sigma}_{\rm R}^x. \tag{3.11}$$

The Hamiltonian in Eq. (3.7) is diagonalized with the transformation given in Eq. (3.8)

$$\tilde{H} = \frac{\omega_{\mathrm{L}}}{2}\tilde{\sigma}^z_{\mathrm{L}} + \frac{\Omega}{2}\tilde{\sigma}^z_{\mathrm{R}}. \tag{3.12}$$

Eigenstates of the diagonalized Hamiltonian in the indvidual basis of the qubits are given by

$$|1\rangle = \cos\tfrac{\theta}{2}\,|{+}{+}\rangle - \sin\tfrac{\theta}{2}\,|{+}{-}\rangle\,, \qquad |2\rangle = \sin\tfrac{\theta}{2}\,|{+}{+}\rangle + \cos\tfrac{\theta}{2}\,|{+}{-}\rangle\,, \tag{3.13}$$

$$|3\rangle = \cos\tfrac{\theta}{2}\,|{-}{+}\rangle + \sin\tfrac{\theta}{2}\,|{-}{-}\rangle\,, \qquad |4\rangle = \cos\tfrac{\theta}{2}\,|{-}{-}\rangle - \sin\tfrac{\theta}{2}\,|{-}{+}\rangle\,, \tag{3.14}$$

and the associated eigenvalues are $\omega_1 = \frac{1}{2}(\omega_{\mathrm{L}}+\Omega)$, $\omega_2 = \frac{1}{2}(\omega_{\mathrm{L}}-\Omega)$, $\omega_3 = \frac{1}{2}(-\omega_{\mathrm{L}}+\Omega)$, and $\omega_4 = \frac{1}{2}(-\omega_{\mathrm{L}}-\Omega)$, respectively. Each qubit is coupled to a single thermal bath maintained at temperature T_α and has the Hamiltonian

$$\hat{H}^{\alpha j}_{SB} = \hat{\sigma}^x_\alpha \otimes \sum_k g^\alpha_k(\hat{a}^\alpha_k + \hat{a}^{\alpha\dagger}_k), \tag{3.15}$$

here g^α_k is the coupling strength of α qubit with the k-th mode of the bath, and the corresponding annihilation (creation) operator is indicated by $\hat{a}^\alpha_k$ ($\hat{a}^{\alpha\dagger}_k$). The Hamiltonian of the baths is given by

$$\hat{H}_\alpha = \sum_k \omega_k \hat{a}^{\alpha\dagger}_k \hat{a}^\alpha_k. \tag{3.16}$$

To derive the master equation, we transform the system operators into the interaction picture

$$\begin{aligned}
\hat{\sigma}^x_{\mathrm{L}}(t) &= \cos\theta\tilde{\sigma}^-_{\mathrm{L}}e^{-i\omega_{\mathrm{L}}t} - \sin\theta\tilde{\sigma}^+_{\mathrm{L}}\tilde{\sigma}^-_{\mathrm{R}}e^{-i(\Omega-\omega_{\mathrm{L}})t} + \sin\theta\tilde{\sigma}^-_{\mathrm{L}}\tilde{\sigma}^-_{\mathrm{R}}e^{-i(\Omega+\omega_{\mathrm{L}})t} + \mathrm{H.c.} \\
\hat{\sigma}^x_{\mathrm{R}}(t) &= \cos\theta\tilde{\sigma}^-_{\mathrm{R}}e^{-i\Omega t} + \frac{1}{2}\sin\theta\tilde{\sigma}^z_{\mathrm{L}}\tilde{\sigma}^z_{\mathrm{R}} + \mathrm{H.c.}
\end{aligned} \tag{3.17}$$

here the transformed operators are given by

$$\begin{aligned}
\tilde{\sigma}^-_{\mathrm{L}} &= \frac{1}{2}\big(\cos\theta(\hat{\sigma}^x_{\mathrm{L}} - i\hat{\sigma}^y_{\mathrm{L}}) + \sin\theta\hat{\sigma}^y_{\mathrm{R}}(\hat{\sigma}^y_{\mathrm{L}} + i\hat{\sigma}^x_{\mathrm{L}})\big), \\
\tilde{\sigma}^-_{\mathrm{R}} &= \frac{1}{2}\big((\cos\theta\hat{\sigma}^x_{\mathrm{R}} - \sin\theta\hat{\sigma}^z_{\mathrm{L}}\hat{\sigma}^z_{\mathrm{R}}) - i\hat{\sigma}^y_{\mathrm{R}}\big).
\end{aligned} \tag{3.18}$$

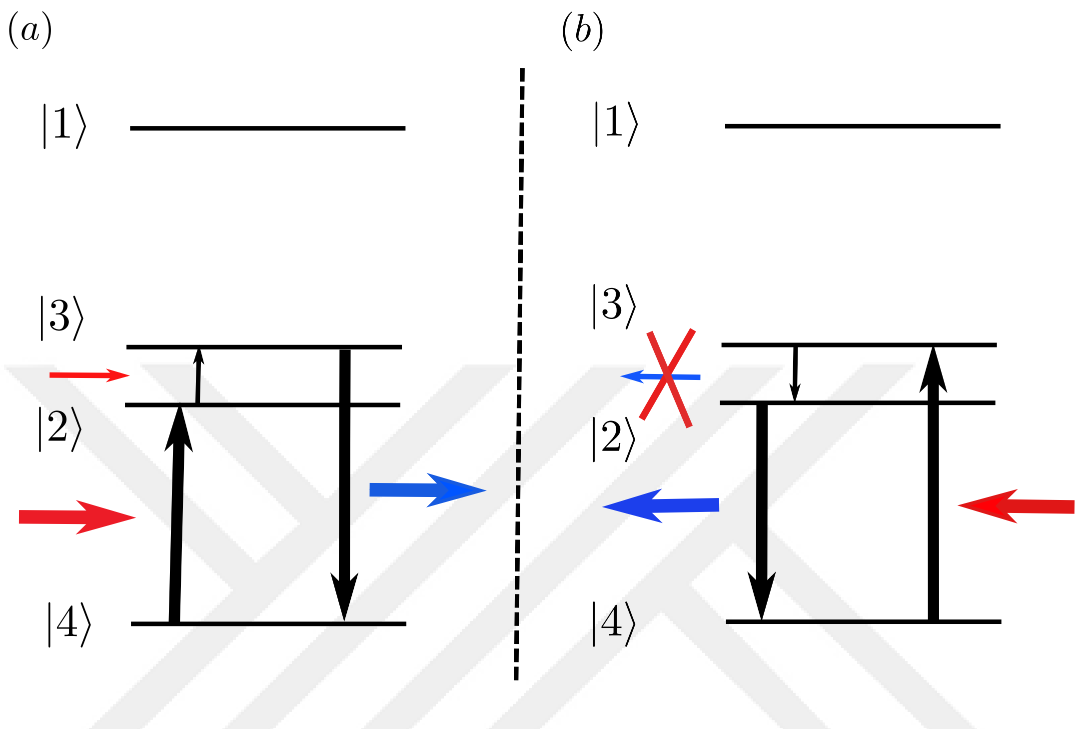

Figure 3.3: Physical mechanism behind heat current rectification in case of resonant qubits. Examples of the dissipative energy cycles induced by heat baths which lead to heat rectification. **(a)** and **(b)** represent heat flow from left to right and right to left, respectively. The weight of the arrows indicates the coupling rate between two energy levels; for instance, $|2\rangle \rightarrow |3\rangle$ transition is the weakest, which is represented by low weight arrow. A left hot reservoir can induce this weak $|2\rangle \rightarrow |3\rangle$ transition (a); however, this transition does not occur if the right cold bath is coupled to $|3\rangle \rightarrow |2\rangle$ energy levels (b). Consequently, our system rectifies heat from right to left even when the qubits are resonant. We note heat rectification for resonant qubits is not possible with previously proposed models of heat diodes.

Following the standard derivation of the master equation outlined in Sec. 1.3, the master equation for coupled qubits has the form

$$\frac{d}{dt}\tilde{\rho} = \mathcal{L}_{\mathrm{L}}\tilde{\rho} + \mathcal{L}_{\mathrm{R}}\tilde{\rho}, \tag{3.19}$$

here $\mathcal{L}_\mathrm{L}\tilde{\rho}$ and $\mathcal{L}_\mathrm{R}\tilde{\rho}$ being the Liouville superoperators which describe the energy exchange of the qubits with the baths, and have the form

$$\begin{aligned} \mathcal{L}_\mathrm{L} &= G_\mathrm{L}(\omega_\mathrm{L})\cos^2\theta D[\tilde{\sigma}_\mathrm{L}^-] + G_\mathrm{L}(-\omega_\mathrm{L})\cos^2\theta D[\tilde{\sigma}_\mathrm{L}^+] \\ &+ G_\mathrm{L}(\omega_-)\sin^2\theta D[\tilde{\sigma}_\mathrm{L}^-\tilde{\sigma}_\mathrm{R}^+] + G_\mathrm{L}(-\omega_-)\sin^2\theta D[\tilde{\sigma}_\mathrm{L}^+\tilde{\sigma}_\mathrm{R}^-] \\ &+ G_\mathrm{L}(\omega_+)\sin^2\theta D[\tilde{\sigma}_\mathrm{L}^-\tilde{\sigma}_\mathrm{R}^-] + G_\mathrm{L}(-\omega_+)\sin^2\theta D[\tilde{\sigma}_\mathrm{L}^+\tilde{\sigma}_\mathrm{R}^+], \end{aligned} \tag{3.20}$$

$$\mathcal{L}_\mathrm{R} = G_\mathrm{R}(\Omega)\cos^2\theta D[\tilde{\sigma}_\mathrm{R}^-] + G_\mathrm{R}(-\Omega)\cos^2\theta D[\tilde{\sigma}_\mathrm{R}^+]. \tag{3.21}$$

Here, $G_\alpha(\omega)$ being the spectral densities of the baths, and we consider Ohmic spectral densities in our results (see Eq. (2.11)). We define the transition frequencies as $\omega_\pm = \omega_\mathrm{L} \pm \Omega$, in addition, $D[\hat{A}]$ being the Lindblad dissipators which is given by Eq. (3.6).

3.4 Results and discussion

3.4.1 Physical mechanism behind rectification

The master equation (3.19) describes the dynamics of two uncoupled qubits which exchange excitations via the *global* channels of heat transport. In Eq. (3.19) the first two dissipators in $\mathcal{L}_\mathrm{L}$ and $\mathcal{L}_\mathrm{R}$ describe the local exchange of energy between the qubits with their respective baths. The heat flow between two thermal baths through the system qubits is described by the last four terms in the $\mathcal{L}_\mathrm{L}$. From the structure of these dissipators, the underlying physical mechanism of heat rectification can be explained in our system. The local dissipators in Eq. (3.19) do not contribute to the heat flow asymmetry, these only describe the energy exchange between the qubits and their respective baths. There are different channels for heat transport which are identified by frequencies $\omega_{24} = \omega_{13} = \omega_L$, $\omega_+ = \omega_{14} = \omega_\mathrm{L} + \Omega$, $\omega_- = \omega_{23} = \omega_\mathrm{L} - \Omega$, and $\omega_{34} = \omega_{12} = \Omega$. The frequency $\omega_- = \omega_{23} = \omega_\mathrm{L} - \Omega$ channel is responsible for exchange of single-excitation, and $\omega_+ = \omega_{14} = \omega_\mathrm{L} + \Omega$ describes a process which transfer the heat through the qubits via two-quanta process. A sufficiently high temperature of the baths is required, which can open one or both the global channels of heat transport. If the temperature of the cold bath is not very high, some of these global channels

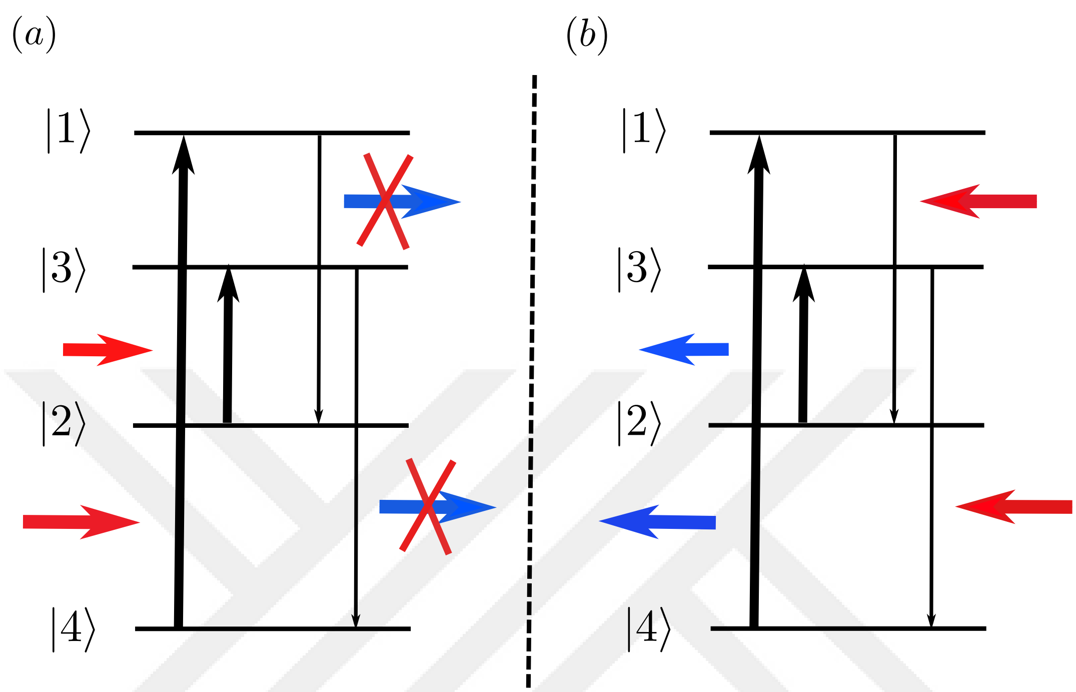

Figure 3.4: The physical mechanism behind heat current rectification in case of resonant qubits. An example of four-wave mixing cycles induced by heat baths leads to heat rectification. **(a)** and **(b)** represent heat flow from left to right and right to left, respectively. The weight of the arrows indicates the coupling rate between two energy levels. For large values of g, the coupling between $|1\rangle \leftrightarrow |2\rangle$ and $|3\rangle \leftrightarrow |4\rangle$ is weak compared to the transition rates $|1\rangle \leftrightarrow |4\rangle$ and $|2\rangle \leftrightarrow |3\rangle$. In the case of the cold right bath (a), the transitions $|1\rangle \rightarrow |2\rangle$ and $|3\rangle \rightarrow |4\rangle$ are inhibited; on the contrary, the hot right bath may be able to induce these transitions. Consequently, our system rectifies heat from left to right in the strong coupling regime, which is opposite to the direction in the weak coupling regime.

of heat transport are entirely or partially inhibited. However, the same channels can be opened by the sufficiently high-temperature hot bath on the reversal of the temperature bias. As a result, the heat flow becomes asymmetric, and diode action can be achieved by controlling the system parameters.

More specifically, the heat rectification in our system can be explained by considering the possible energy cycles induced by thermal baths and responsible for transferring heat through the qubits. The master equation shows that, in general, three Raman cycles are possible (4234), (3213), (4214), and the inverse of these cycles are also possible. Here, (4234) describes the $|4\rangle \rightarrow |2\rangle \rightarrow |3\rangle \rightarrow |4\rangle$ transitions. Further, in principle, three four-wave mixing cycles (43124), (41234), and (41324) can be possible along with their inverses. In these four-wave mixing cycles, (41234) is the cycle that can transfer heat from the cold to the hot bath; the other two cycles do not describe the heat transfer as they do not change the energies of the baths. The master equation shows that the transition rates between the energy levels depend on the angle θ. Some of these coupling strengths can become very small compared to the others depending on the mixing angle θ. The weakest transition in the cycle may become a bottleneck, and only a sufficiently high-temperature thermal bath can complete the cycle.

We analyze some examples of the energy cycles induced by thermal baths in the case of resonant qubits $\omega_L = \omega_R = \omega$ in Figs. 3.3-3.4. If we consider weakly coupled qubits $g \ll \omega$ (Fig. 3), the $2 \leftrightarrow 3$ energy transition becomes the weakest in the cycle (4234). For the case of the left hot bath (Fig. 3.3(a)), this bottleneck transition does not obstruct the cycle. However, the right cold bath may not be able to induce this transition, and the cycle (4234) is completely obstructed (Fig. 3.3(b)). As a result, our system rectifies heat from left to right in the weak coupling regime. On the contrary, if the qubits are strongly coupled $g \sim \omega_R$, the four-wave mixing cycle (41234) includes $|3\rangle \leftrightarrow |4\rangle$ and $|1\rangle \leftrightarrow |2\rangle$ transitions which are the weakest. The heat diode based on coupled qubits rectifies heat from right to left in this case (Fig. 3.4). Our analysis shows that heat rectification is possible in our scheme without the need for asymmetric system-bath coupling and off-resonant qubits. This is in contrast to previous proposals of heat diodes, which required either unequal dissipation rates of the baths or the frequency difference between the coupled system. Our advantageous scheme of heat diode allows a large heat flow without compromising the rectification quality of the diode. In the previous models, large heat currents are associated with

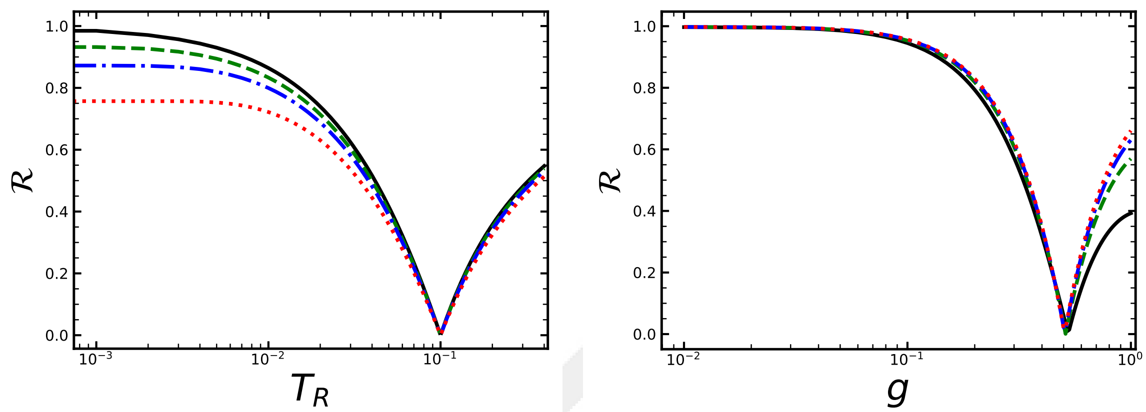

a b

Figure 3.5: **(a-b)** The steady-state rectification factor $\mathcal{R}$ as a function of the right bath temperature T_{R}, and the coupling strength g, respectively. (a) The solid, dashed, dot-dashed, and dotted lines are for the coupling strength $g = 0.01, 0.05, 0.07$ and 0.1, respectively. The left bath temperature is $T_{\mathrm{L}} = 0.1$. (b) The solid, dashed, dot-dashed, and dotted lines are for the right bath temperature $T_{\mathrm{R}} = 2.5, 5.5, 8.5$ and 11.5, respectively. The right bath temperature is $T_{\mathrm{R}} = 0.1$. The dissipation rates $\kappa_{\mathrm{L}} = \kappa_{\mathrm{R}} = \kappa = 0.01$ and the qubits frequencies $\omega_{\mathrm{L}} = \omega_{\mathrm{R}} = \omega = 1$ is same in both panels. All the system parameters are scaled by the left qubit frequency $\omega_{\mathrm{L}}/2\pi = 10$ GHz. We note that in the limit $g \to 0$, the rectification vanishes because the heat flow becomes zero, and in the figures, we have not shown this limit.

low rectification rates, which are undesirable.

3.4.2 Rectification quality

Heat diode operation with the perfect rectification can be achieved for a wide range of system parameters in the case of off-resonant qubits. Here we investigate the asymmetry in heat flow for resonant qubits only, as, in previous models of heat diodes, the heat flow becomes symmetric for all system parameters [73, 86, 75, 77]. In what follows, we consider resonat qubits with symmetric dissipation rates of the thermal baths.

We plot the rectification factor $\mathcal{R}$ as a function of the right bath temperature T_{R} for different values of the coupling strength g in Fig. 3.5a. For $T_{\mathrm{L}} > T_{\mathrm{R}}$, the heat rectification is smaller compared to the case of reversed temperature gradient. The rectification vanishes at $T_{\mathrm{L}} = T_{\mathrm{R}}$ because the heat flow becomes zero at equal temperatures in accordance with the second law of thermodynamics. The larger rectification factors are associated with a large temperature gradient. The rectification shows a nonmonotonic behavior as a function of the coupling strength g in Fig. 3.5b. The rectification is large for a weak coupling regime compared to the strong coupling regime for the same system parameters. Our diode rectifies heat from left to right in the weak coupling regime and right to left in the strong coupling regime. The change in the direction of the heat rectification is explained in Figs. 3.4-3.4 via different energy cycles induced by the thermal baths. Between the weak and strong coupling regime, the rectification shows a sharp dip which is associated with the point where the global channel of the transition frequency ω_- vanishes. At this point, due to the value of coupling strength g, the transition frequency $\omega_L - \Omega \approx 0$. Due to the collapse of this transition, the energy levels $|2\rangle$ and $|3\rangle$ becomes degenerate, and majority of the global cycles responsible for heat transfer and rectification disappear. Accordingly, the heat rectification becomes zero at this particular point.

3.5 Possible implementations of the model

Our proposal for the thermal diode employs asymmetric interaction between the qubits, i.e., $\hat{\sigma}^z_{\mathrm{L}}\hat{\sigma}^x_{\mathrm{R}}$, such coupling between the two-level systems can be found in ferromagnetic systems [87], or magnetic molecules placed in a nuclear spin environment [88]. In this section, we propose different physical model systems for the possible realization of asymmetric interaction between the two-level systems.

3.5.1 Optomechanical coupling based realization

In a typical optomechanical system, an optical cavity mode of frequency ω_a interacts with a mechanical resonator of frequency ω_b via the Hamiltonian [1]

$$\hat{H} = \omega_a \hat{a}^\dagger \hat{a} + \omega_b \hat{b}^\dagger \hat{b} - g\omega_a \hat{a}^\dagger \hat{a}(\hat{b} + \hat{b}^\dagger), \tag{3.22}$$

here g being the single-photon optomechanical coupling strength. The annihilation (creation) operator of the optical and mechanical modes is identified by $\hat{a}$ ($\hat{a}^\dagger$), and $\hat{b}$ ($\hat{b}^\dagger$), respectively. By applying Holstein Primakoff transformation to convert bosonic operators to spin operators [89]

$$\hat{a}^\dagger \hat{a} \;=\; \hat{J}\mathbb{1} + \hat{J}_z, \quad \hat{a} = \frac{1}{\sqrt{\hat{J}\mathbb{1} + \hat{J}_z}}\hat{J}_-, \quad \hat{a}^\dagger = \hat{J}_+\frac{1}{\sqrt{\hat{J}\mathbb{1} + \hat{J}_z}}, \tag{3.23}$$

here $\hat{J}$ being the total spin and $\hat{J}_z$, $\hat{J}_\pm$ follow the SU(2) algebra. If we assume spins are weakly excited ($\langle \hat{J}_x \rangle \ll \hat{J}$), and apply this transformation to bosonic operators, the asymmetric spin-spin $\hat{\sigma}_L^z \hat{\sigma}_R^x$ coupling can be obtained from the optomechanical model. This replacement of bosonic operators with the spin-(1/2) operators is valid if we assume the bosonic modes are weakly excited $\hat{a}^\dagger \hat{a} \ll 1$. In this limit of low excitations, the lowest two energy levels of bosonic modes can be accessible [89].

3.5.2 Circuit QED based realization

We assume a superconducting qubit interacts with a superconducting resonator by the Hamiltonian [90]

$$\hat{H} = \omega_a \hat{a}^\dagger \hat{a} + \frac{\Omega}{2} + g(\cos\theta \hat{\sigma}_z + \sin\theta \hat{\sigma}_x)(\hat{a} + \hat{a}^\dagger), \tag{3.24}$$

here, the creation and annihilation operators of the superconducting resonators are denoted by $\hat{a}$, and $\hat{a}^\dagger$, respectively. In addition, ω_a, and Ω are the frequencies of the superconducting resonator and the qubit, respectively. The interaction strength g between the resonator and the qubit, and θ depends on the properties of the Josephson-Junction. The system parameters can be adjusted to $\theta = 0$ to obtain the phase-gate term [91]. In the weak excitation limit of the resonator $\langle \hat{a}^\dagger \hat{a} \rangle \ll 1$, the interaction reduces to the required coupling $\hat{\sigma}_L^z \hat{\sigma}_R^x$.

3.5.3 Trapped ions based realization

Trapped ions can simulate the quantum walk on a circle in which the phase space is used to describe the steps of the walker. The generator of the single step is given by [92]

$$\hat{U} = \mathrm{e}^{i\hat{p}\hat{\sigma}_z} H, \tag{3.25}$$

here H represents the Hadamard gate operator, and $\hat{p}$ being the momentum operator which generates the step depending on the outcome of the coin toss operation. Raman beam pulses are proposed to implement these steps [92]. If we assume the weak vibrational excitation limit in which the excitations are much less than 1, the desired asymmetric spin-spin $\hat{\sigma}_L^z\hat{\sigma}_R^x$ interaction can be obtained from the effective Hamiltonian.

3.5.4 Coupled Raman model based realization

We asuume a three-level atom is placed in a single mode cavity, the Hamiltonian of this system is given by

$$\begin{aligned} \hat{H} &= \omega_a\hat{a}^\dagger\hat{a} + \omega_r|r\rangle\langle r| + \omega_e|e\rangle\langle e| + \omega_g|g\rangle\langle g| + \\ &+ \lambda(\hat{a}^\dagger(|g\rangle\langle r| + |e\rangle\langle r|) + \text{H.c.}, \end{aligned} \tag{3.26}$$

here ω_i $(i = g, e, r)$ is associated with lower, middle and upper energy levels of the three-level atom described the states $|g\rangle, |e\rangle, |r\rangle$, respectively. In addition, the coupling between the atom and cavity mode is denoted by λ. We assume the lower two energy levels are quasi-degenerate ($\omega_g \approx \omega_e$), and the detuning $\Delta = \omega_r - \omega_a - \omega_e$ greater than the coupling strength g, we can eliminate the upper level from the dynamics of the system. In this case, the effective Hamiltonian is given by the Raman coupled model [93]

$$\hat{H} = \omega_a a^\dagger a + \epsilon\hat{\sigma}_z - \frac{g^2}{\Delta}\hat{a}^\dagger\hat{a}\hat{\sigma}_x. \tag{3.27}$$

Here we define $\epsilon = \omega_e - \omega_g$, and $\hat{\sigma}_x = |e\rangle\langle g| + |g\rangle\langle e|$, $\hat{\sigma}_z = |e\rangle\langle e| - |g\rangle\langle g|$. Similar to the previously discussed optomechanical-based realization of the asymmetric spin-spin

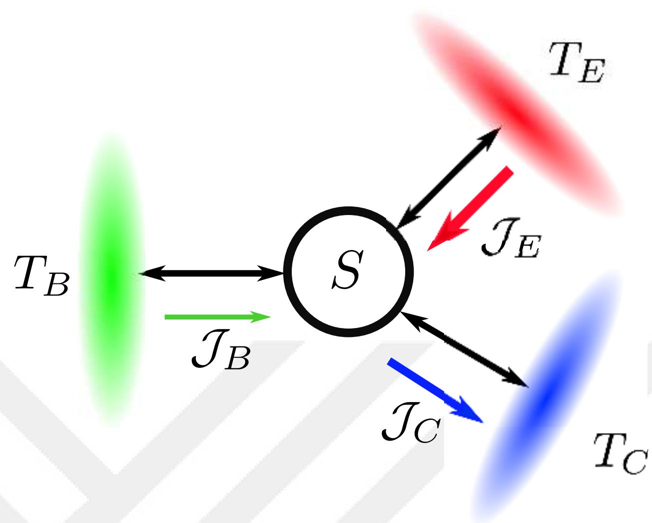

Figure 3.6: A schematic depiction of a quantum thermal transistor. S being the quantum system that has an anharmonic energy spectrum. By analogy with the electronic transistor, the quantum system S is coupled with the three independent thermal baths of temperatures T_B, T_E, T_C, mimicking the base, emitter, and collector terminals of the electronic transistor, respectively. The base temperature is the control parameter that acts as a control signal and modulates the heat flow between the other two terminals of the transistor. The direction and magnitude of the heat currents $\mathcal{J}_B, \mathcal{J}_E$, and $\mathcal{J}_C$ depend on the temperature and other system paramteres.

interaction, if we consider the weak excitation limit of the cavity mode in this model, the bosonic mode of the cavity can be replaced by corresponding spin operators, and the effective asymmetric spin-spin $\hat{\sigma}_L^z \hat{\sigma}_R^x$ interaction can describe the system dynamics.

3.6 Quantum heat transistor: Introduction

The ability to control signals is of paramount importance in logical computational devices—for instance, classical integrated circuits based on electronic transistors can control the electronic current flow depending on the control voltage. In a typical bipolar junction transistor, the voltage at the base terminal can control the electronic current between the emitter and collector terminals. By exploiting this ability to control the electronic current, the electronic transistor can be used to implement the switch operation, or the current amplifier can be designed in which a slight change in the control signal results in a large electronic current at the output terminals.

By analogy to the electronic transistor, a quantum thermal transistor is a device that, in principle, can control the heat flow between two independent thermal baths. In a quantum thermal transistor (see Fig. 3.6), a quantum system S is coupled to three different thermal baths of temperature T_E, T_C, and T_B mimicking the emitter, collector, and base terminals of a transistor.

3.6.1 Amplification factor

A three terminal device in which a slight change of the temperature on one terminal results in a large increase in the heat flow through the other two terminals is called thermal amplifier. With the analogy of typical bipolar junction transistor (BJT) we consider thermal baths of temperatures T_E, T_B, and T_C as emitter, base, and collector, respectively. For amplification, we assume that emitter bath is hotter than the other two and the temperature of the base is varied. The amplification factor can be defined as

$$\alpha_{\mathrm{E,C}} = \frac{\partial \mathcal{J}_{\mathrm{E,C}}}{\partial \mathcal{J}_{\mathrm{M}}}, \tag{3.28}$$

this definition implies that in order to have transistor effect we must have $|\alpha_{\mathrm{E,C}}|>1$. Using the energy conservation relation in our system along with definition of α in Eq. (3.28) the amplification α can also be written as

$$\alpha_E = \frac{\partial(\mathcal{J}_{\mathrm{E}})}{\partial(\mathcal{J}_{\mathrm{E}} + \mathcal{J}_{\mathrm{C}})} = \frac{R_{\mathrm{E}}}{R_{\mathrm{E}} + R_{\mathrm{C}}}. \tag{3.29}$$

Here $R_{\mathrm{E}} = (\partial\mathcal{J}_{\mathrm{E}}/\partial\mathcal{J}_{\mathrm{B}})^{-1}_{T_{\mathrm{E=const}}}$ and $R_{\mathrm{C}} = -(\partial\mathcal{J}_{\mathrm{C}}/\partial\mathcal{J}_{\mathrm{B}})^{-1}_{T_{\mathrm{C=const}}}$ are differential thermal resistances, similar relations can also be written for α_{C}. From Eq. (3.29) it is clear that in order to have amplification $|\alpha_{\mathrm{L,R}}|>1$, one of the differential thermal resistance needs to be negative; $R_{\mathrm{E}} \times R_{\mathrm{C}} < 0$. Thus we must have a negative differential thermal

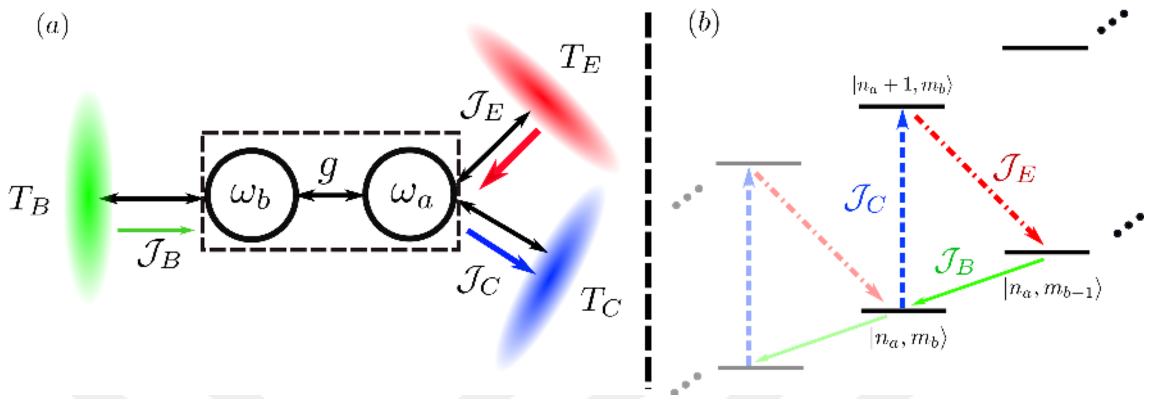

Figure 3.7: **(a)** A schematic depiction of a quantum thermal transistor based on the optomechanical system. Here, ω_a, and ω_b are the frequencies of the optical and mechanical resonator, respectively, and g is the coupling strength. The optical resonator is coupled with two thermal baths of temperatures T_E and T_C and the mechanical mode is coupled with one control thermal bath of temperature T_B. The small changes in the temperature of the mechanical bath control the heat flow between the baths of the optical mode. **(b)** An example of the processes which are responsible for the heat transfer between the thermal baths. The dressed energy levels of the optomechanical system denoted by $|n_a, m_b\rangle$, where $n_a = 0, 1, 2, ...$ is the photon number and m_b shows the phonon number of the mechanical resonator. The dashed, dot-dashed and solid lines show the transitions induced by the collector, emitter, and base thermal baths, respectively. The base current is associated with the smallest energy transition in the system.

resistance (NDTR). In a two terminal device, if the increase in thermal gradient results in a decrease of heat flow between the two baths then such behavior is termed as NDTR [81, 82].

3.7 Microscopic model of the transistor

We consider a standard optomechanical setup containing localized electromagnetic field mode at frequency ω_a coupled to a mechanical oscillator at frequency ω_b. The optical resonator is coupled with two independent thermals baths at temperatures $T_{\rm E}$ and $T_{\rm C}$, while the mechanical resonator is coupled to a third thermal bath kept at temperature $T_{\rm B}$. The Hamiltonian of the isolated optomechanical system consisting of the cavity and mechanical modes is

$$\hat{H}_{\rm S} = \omega_a \hat{a}^\dagger \hat{a} + \omega_b \hat{b}^\dagger \hat{b} - g\hat{a}^\dagger \hat{a}(\hat{b} + \hat{b}^\dagger). \tag{3.30}$$

Here, the first term is the energy of the cavity mode and the second term represents the energy of the mechanical resonator. The last term in Hamiltonian denotes the optomechanical interaction with single-photon coupling strength g. The annihilation (creation) operator for the mechanical mode is represented by $\hat{b}$ ($\hat{b}^\dagger$) and of the cavity mode by $\hat{a}$ ($\hat{a}^\dagger$). The Hamiltonian describing the full system including heat baths is

$$\hat{H}_{\rm tot} = \hat{H}_{\rm S} + \hat{H}_{\rm B} + \hat{H}_{\rm SB}, \tag{3.31}$$

where

$$\hat{H}_{\rm B} = \sum_{\lambda,k} \omega_{\lambda,k} \hat{a}^\dagger_{\lambda,k} \hat{a}_{\lambda,k}, \tag{3.32}$$

$\lambda = {\rm C, B, E}$ represent the collector, base and emitter baths, respectively. The sums in Eq. (3.32) runs over the infinite number of bath modes, indexed by k for the optical and mechanical baths. ω_C ($\omega_{\rm E}$) being the frequency of the collector (emitter) optical bath mode and $\omega_{\rm B}$ is the frequency of mechanical bath mode indexed by k. In addition, $\hat{a}^\dagger_{\lambda,k}$ ($\hat{a}_{\lambda,k}$) is the creation (annihilation) operators of the baths modes. The interaction Hamiltonian between the system and baths is

$$\hat{H}_{\rm SB} = \sum_k g_{f,k}(\hat{a} + \hat{a}^\dagger)(\hat{a}_{f,k} + \hat{a}^\dagger_{f,k}) + \sum_k g_{{\rm m},k}(\hat{b} + \hat{b}^\dagger)(\hat{a}_{{\rm B},k} + \hat{a}^\dagger_{{\rm B},k}), \tag{3.33}$$

$f = {\rm E, C}$. The first term represents the interaction between the left and right baths with the optical resonator, where the interaction with the bath mode indexed by α is governed by a strength $g_{f,k}$. The second term is analogous to the first one, but describes the mechanical bath modes and their interaction with the mechanical resonator. The optical and mechanical baths are assumed to be at thermal equilibrium at temperatures $T_{\rm E}$, $T_{\rm C}$ and $T_{\rm B}$, respectively.

3.7.1 The master equation

The Hamiltonian $\hat{H}_{\mathrm{S}}$, can be diagonalized using the transformation

$$\hat{S} = e^{-\alpha\hat{a}^\dagger\hat{a}(\hat{b}^\dagger-\hat{b})}, \tag{3.34}$$

with $\alpha = g/\omega_{\mathrm{b}}$, and takes the form

$$\tilde{H}_{\mathrm{S}} = \omega_a\tilde{a}^\dagger\tilde{a} + \omega_b\tilde{b}^\dagger\tilde{b} - \frac{g^2}{\omega_b}(\tilde{a}^\dagger\tilde{a})^2. \tag{3.35}$$

The eigenstates of the optomechanical system, without baths, can be written as

$$|n, l^n\rangle = |n\rangle_{\mathrm{a}}\, e^{n\alpha(\hat{b}^\dagger-\hat{b})}\, |l\rangle_b\,, \tag{3.36}$$

and the associated eigen energies is given by $E_{n,m} = \omega_a n + \omega_b m + g^2/\omega_b n^2$.

The dynamics of the reduced system of interest can be described by following Markovian master equation [26]

$$\frac{d}{dt}\tilde{\rho} = \mathcal{L}_{\mathrm{a}}^{\mathrm{E}}\tilde{\rho} + \mathcal{L}_{\mathrm{a}}^{\mathrm{C}}\tilde{\rho} + \mathcal{L}_{\mathrm{b}}^{\mathrm{B}}\tilde{\rho}, \tag{3.37}$$

where the dissipative terms are given by

$$\begin{aligned}
\mathcal{L}_{\mathrm{a}}^{(\mathrm{f})}\tilde{\rho} = {} & G_{\mathrm{a}}^{(f)}(\omega_{\mathrm{a}})\big\{D[\tilde{a}] + \alpha^2 D[\tilde{a}\tilde{b}^\dagger\tilde{b}]\big\}\tilde{\rho} + G_{\mathrm{a}}^{(f)}(-\omega_{\mathrm{a}})\big\{D[\tilde{a}^\dagger] + \alpha^2\big(+D[\tilde{a}^\dagger\tilde{b}^\dagger\tilde{b}]\big)\big\}\tilde{\rho} \\
& + \sum_{n=1,2}\Big\{\alpha^n G_{\mathrm{a}}^{(f)}(\omega_{\mathrm{a}} + n\omega_{\mathrm{b}})D[\tilde{a}\tilde{b}^n]\tilde{\rho} \\
& + \alpha^n G_{\mathrm{a}}^{(f)}(-\omega_{\mathrm{a}} - n\omega_{\mathrm{b}})D[\tilde{a}^\dagger\tilde{b}^{\dagger n}]\tilde{\rho} + \alpha^n G_{\mathrm{a}}^{(f)}(\omega_{\mathrm{a}} - n\omega_{\mathrm{b}})D[\tilde{a}\tilde{b}^{\dagger n}]\tilde{\rho} \\
& + \alpha^n G_{\mathrm{a}}^{(f)}(-\omega_{\mathrm{a}} + n\omega_{\mathrm{b}})D[\tilde{a}^\dagger\tilde{b}^n]\tilde{\rho}\Big\},
\end{aligned} \tag{3.38}$$

$$\mathcal{L}_{\mathrm{b}}\tilde{\rho} = G_{\mathrm{b}}(\omega_{\mathrm{b}})D[\tilde{b} - \alpha\tilde{n}_{\mathrm{a}}]\tilde{\rho} + G_{\mathrm{b}}(-\omega_{\mathrm{b}})D[\tilde{b}^\dagger - \alpha\tilde{n}_{\mathrm{a}}]\tilde{\rho}. \tag{3.39}$$

Here, $G(\omega)$ being the spectral densities of the baths, and we consider Ohmic spectral densities in our results (see Eq. (2.11)). In addition, $D[\hat{A}]$ being the Lindblad dissipators and given by Eq. (3.6).

3.8 Results: Heat amplification

In Fig. 3.8 we show all three heat currents associated with three independent thermal baths in our device as a function of control bath temperature T_{B}, the inset of the figure

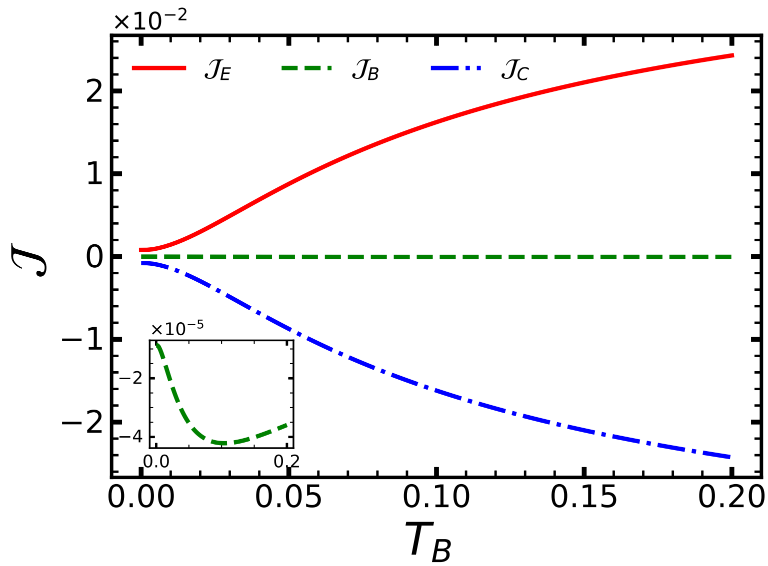

Figure 3.8: The heat current $\mathcal{J}$ as a function of the control bath base temperature T_B. The solid, dashed, and dot-dashed lines are for emitter $\mathcal{J}_E$, base $\mathcal{J}_B$, and collector $\mathcal{J}_c$ currents, respectively. The inset shows the zoomed-in curve of the base heat current $\mathcal{J}_B$ as a function of the base temperature. The minima in the base current at a critical value of T_B indicates the presence of the negative differential thermal resistance, which is a sufficient condition for the heat current amplification. Parameters: $\omega_a = 1$, $\omega_b = 0.01$, $g = 0.1\omega_b$, $\kappa_E = \kappa_C = \kappa_B = 0.001$, $T_E = 1.4$, and $T_R = 0.1$. All the system parameters are scaled with $\omega_a/2\pi = 10$ GHz.

shows the heat current $\mathcal{J}_{\mathrm{B}}$. If the temperature T_{B} is non-zero, all three heat currents are non-zero; this is because we have a non-equilibrium steady state in the presence of three independent baths held at different temperatures. A small change in the temperature of the control bath T_{B} results in a minute change in the associated heat current $\mathcal{J}_{\mathrm{B}}$, on contrary, the collector and emitter heat currents $\mathcal{J}_{\mathrm{C}}$ and $\mathcal{J}_{\mathrm{E}}$ increase dramatically, as shown in Fig. 3.8. To emphasize this we plot amplification factors α_{E} and α_{C} in Fig. 3.9, and the inset of the figure shows R_{E} and R_{C}. A sufficient condition for amplifying heat current is the system is negative differential thermal

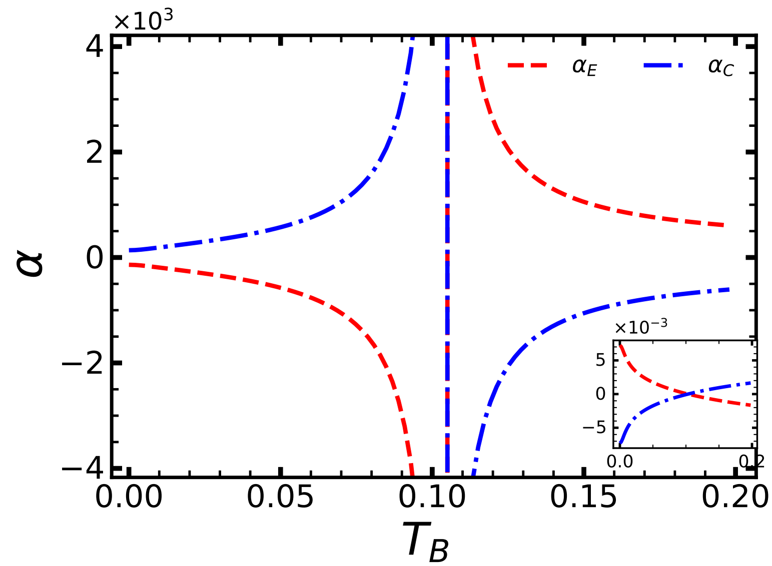

Figure 3.9: The heat amplification factor α as a function of the base temperature T_B. The dashed and dot-dashed lines are for the amplification factor α_E and α_R, respectively. The inset shows the thermal differential resistance R as a function of the base temperature T_B. The dashed and dot-dashed lines are for R_E, and R_C, respectively. Parameters: $\omega_a = 1$, $\omega_b = 0.01$, $g = 0.1\omega_b$, $\kappa_E = \kappa_C = \kappa_B = 0.001$, $T_E = 1.4$, and $T_R = 0.1$. All the system parameters are scaled with $\omega_a/2\pi = 10$ GHz.

resistance (DTR). As one of the DTR remains negative for all the considered range of the system parameters in Fig. 3.9, this ensures that we have amplification greater than one for an extensive range of the base bath temperatures.

At $T_{\mathrm{B}} \approx 0.15$, the amplification factors α_{E} and α_{C} diverges. This is because the heat current $\mathcal{J}_{\mathrm{B}}$ has a local minimum at this temperature, shown in the inset of Fig. 3.8. In addition, this can also be explained from the inset of Fig. 3.9, at this temperature $T_{\mathrm{B}} \approx 0.15$ both DTR becomes zero consequently the denominator in the Eq. (3.29) becomes zero and the amplification diverges. For small temperatures $T_{\mathrm{B}} < 0.03$, we have a plateau in the amplification with $\alpha_{\mathrm{E}} = \alpha_{\mathrm{C}} \approx 50$, this can be considered as stable region of amplification of our device. For temperatures $0.04 <$

$T_{\mathrm{B}} < 0.16$, we have sensitive region of amplification in which a small change in the T_{B} results in a very large change in the output heat currents $\mathcal{J}_{\mathrm{E}}$ and $\mathcal{J}_{\mathrm{C}}$. This is the best region for the amplification of the collector and emitter heat currents in our quantum thermal transistor. For temperatures $T_{\mathrm{B}} > 0.16$, we again have a flat line in the amplification, and it is still greater than one; consequently, our device can also work as an amplifier at higher baths temperatures. We note that the amplification factors α_{E} and α_{C} increase monotonically with the optomechanical coupling g for a given set of system parameters. We can have higher amplification factors in the stable amplification regime than the other existing transistor proposals [76]. This can be achieved in the single-photon ultra-strong coupling regime of optomechanics.

3.9 Summary

We investigated the thermal management between independent thermal baths based on either two coupled qubits or two nonlinearly coupled harmonic oscillators. In particular, it was shown that two qubits coupled via asymmetric spin-spin interaction support the heat flow asymmetry between two thermal baths. In previous proposals, the heat rectification based on spins required either unequal bath dissipation rates or frequency difference of the coupled spins. In the case of equal dissipation and resonant spins, it was not possible to have thermal diode operation in the previous schemes. We showed that by considering asymmetric spin-spin interaction, a high-quality diode could be designed with equal dissipation rates with the baths and the same frequencies of the spins. Our advantageous proposal of the heat diode, contrary to the previous proposals, showed no trade-off between the heat flow and rectification factor. We explained the rectification by the preferential direction of the energy cycles induced by the thermal baths between the dressed states of the qubits. Some of the heat transport channels between the qubits were obstructed due to the asymmetry of the coupling strengths between the energy levels under the exchange of the temperature gradient.

We showed that it is possible to construct a quantum thermal transistor based on two nonlinearly coupled harmonic oscillators. The control of the base bath temperature showed the modulation of the heat current between the collector and emitter baths. It is possible to obtain substantial amplification factors by tuning either the coupling strength between the resonators or the relative magnitude of the frequencies of the resonators. The origin of the heat amplification is explained by the negative differential resistance, which appeared in our system due to the presence of the anharmonicity induced by the nonlinear coupling between the resonators. The control base heat current was associated with the lowest energy transition in the system, and the output heat currents were associated with the most significant energy transition. Accordingly, a slight change in the base heat current could control the large magnitudes of the collector and emitter heat currents.

Chapter 4

TWO-BODY QUANTUM ABSORPTION REFRIGERATOR

4.1 Intoduction: Qauntum absorption refrigerator (QAR)

In the recent past, much attention has been paid to thermal machines based on quantum systems; some of the examples are quantum heat engines [94, 95, 60, 61], quantum thermal refrigerators [96, 97]. In particular, a promising direction can be the quantum thermal machines which do not require external control or work resource. Implementing quantum technologies on compact and energetically viable schemes demands autonomous cooling schemes based on quantum systems. To achieve this goal of cheap autonomous cooling, many schemes of quantum absorption refrigerators (QARs) [98, 99, 100, 101, 102, 103, 104, 105, 106, 107, 108, 109, 110, 111, 112, 113, 114, 115, 116, 117, 118, 119, 120, 121] have been put forward, and an experimental demonstration has been reported in a three-ion system [122]. Typically, a quantum absorption refrigerator requires a three-body interaction between the harmonic oscillators [101] or two-level systems [123].

It is possible to achieve Carnot bound at the cost of vanishing cooling power in the ideal quantum absorption refrigerators [123]. However, efficiency at maximum cooling power can be more practical bound for the quantum absorption refrigerators. In the QARs, which have three-level masers as the building blocks, the efficiency at maximum cooling power has an upper bound in these models. The existing proposals on QARs obey this bound, which is much smaller than the Carnot bound. Here we consider a quantum absorption refrigerator based on coupled qubits with an asymmetric interaction. We show that our QAR based on only two qubits can surpass

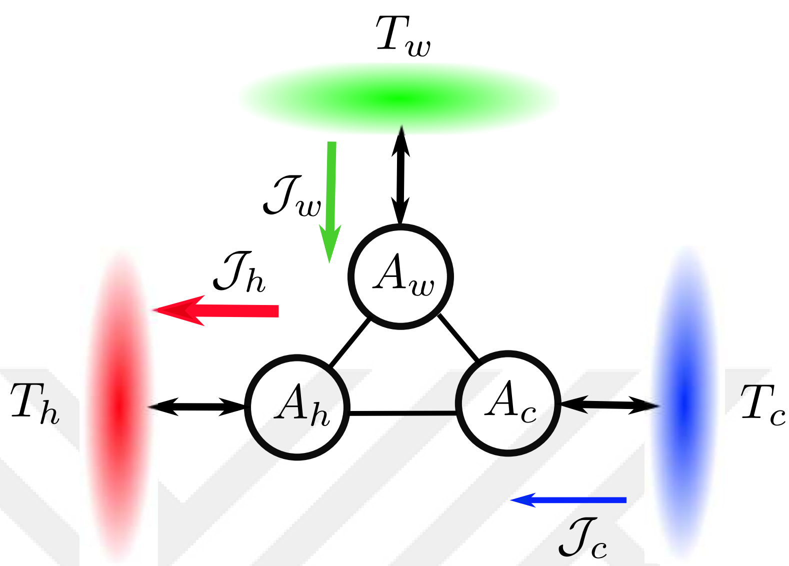

Figure 4.1: Schematic description of a quantum absorption refrigerator based on three-body interaction. The working medium consists of three harmonic oscillators or three qubits; each coupled to an independent thermal bath. The temperatures of the cold, hot and work-like thermal baths are T_c, T_h, and T_w, respectively. For the refrigeration, the temperatures of the baths are considered in the limit $T_c < T_h \ll T_w$. For the cooling process, the heat current $\mathcal{J}_c$ direction must be from the cold bath to the system; accordingly, from the first and second law of thermodynamics, the other two heat currents should be $\mathcal{J}_w > 0$, $\mathcal{J}_h < 0$.

the established bound on the efficiency at maximum cooling power. In the strong coupling regime of the qubits, the efficiency at maximum power reaches close to the Carnot limit at the cost of vanishing cooling power as required by the second law of thermodynamics. In addition, we investigate the effect of the size of the Hilbert space and correlations between the working medium on the cooling power and efficiency of the QAR. In the non-ideal case where heat leaks are present—one transition between the dressed states of the system may be induced by more than one thermal bath—is also discussed.

4.2 Ideal quantum absorption refrigerator

4.2.1 Tree-body quantum absorption refrigerator

The minimal model of a typical quantum absorption refrigerator is based on three body-interaction working mediums, which can be three harmonic oscillators or three qubits [123]. Each of which is coupled to an independent thermal bath as shown in Fig. 4.1. The interaction between the harmonic oscillators of the working medium is given by [100]

$$\hat{H}_{\text{int}} = g(\hat{A}_h\hat{A}_c^\dagger\hat{A}_w^\dagger + \hat{A}_h^\dagger\hat{A}_c\hat{A}_w), \tag{4.1}$$

here, A_α and $A_\alpha^\dagger(\alpha = h, c, w)$ is the annihilation and creation operator of the harmonic oscillator coupled to the hot, cold, and work-like baths, respectively. In addition, ω_α is the frequency of the α-th harmonic oscillator. We assume the constraint on the frequencies of the resonators the so-called *resonance* condition

$$\omega_w = \omega_h - \omega_c, \tag{4.2}$$

this enables the heat transfer between the thermal baths via working medium. The interaction given in Eq. (4.1), enforces the annihilation of one quantum of energy from the cold bath and dumps it into the hot bath by spending quanta of energy from the work-like bath. We note that the interaction between the resonators is a three-body interaction, which is non-quadratic, and it has shown that a tri-linear interaction is required to realize a quantum absorption refrigerator [124]. In the limit of the temperatures $T_c < T_h \ll T_w$, and appropriate system parameters, the cold bath heat current $\mathcal{J}_c$ can become positive, resulting in the refrigeration process.

4.2.2 The cooling window

We analyze the quantum absorption refrigerator at steady-state, and the heat currents from the α-th bath is given by

$$\mathcal{J}_\alpha = \text{Tr}[\mathcal{L}_\alpha\tilde{\rho}\tilde{H}] \tag{4.3}$$

here $\mathcal{L}_b^{(l)}\hat{\rho}$ being the Liouville superoperator and $\tilde{H}$ is the system Hamiltonian. We adopt the convention that heat flow is positive from the thermal bath to the system. The first and second laws of thermodynamics in the absence of any external control (see Fig. 4.1) is given by

$$\sum_\alpha \mathcal{J}_\alpha = 0, \tag{4.4}$$

$$\sigma = \frac{d}{dt}S(\tilde{\rho}) - \sum_\alpha \frac{\mathcal{J}_\alpha}{T_\alpha} \geq 0, \tag{4.5}$$

here $S(\tilde{\rho}) = -\mathrm{Tr}[\tilde{\rho}\ln\tilde{\rho}]$ being the von Neumann entropy, and σ is the total entropy production of the system and the baths.

The efficiency of a quantum absorption refrigerator is obtained by taking a ratio of the heat removed from the cold bath to heat pumped by the work-like reservoir. As a result, the efficiency, which is termed the coefficient of performance (COP) for a refrigerator is defined as

$$\epsilon \equiv \frac{\mathcal{J}_c}{\mathcal{J}_w}. \tag{4.6}$$

Unlike the efficiency of a heat engine, the COP of the quantum absorption refrigerator can be greater than one. For the cooling process to occur, the work, cold, and hot heat currents must satisfy $\mathcal{J}_w > 0$, $\mathcal{J}_c > 0$, and $\mathcal{J}_h < 0$, respectively. From the first and second law of thermodynamics, we have

$$\epsilon = \frac{\mathcal{J}_c}{\mathcal{J}_w} \leq \frac{(T_w - T_h)T_c}{(T_h - T_c)T_w} \equiv \epsilon_c, \tag{4.7}$$

here, ϵ_c is the Carnot efficiency for the heat-driven quantum absorption refrigerator for three independent thermal baths, and it gives an upper bound on the COP of a quantum absorption refrigerator.

For the trilinear interaction between the quantum systems of a working-medium, if the resonance condition given in Eq. (4.2) holds, the ratio of heat currents satisfy the relation

$$\frac{\mathcal{J}_\alpha}{\mathcal{J}_\beta} = \frac{\omega_\alpha}{\omega_\beta}. \tag{4.8}$$

Using this and Eq. (4.7), we can write

$$\omega_c \leq \omega_{c,\max} \equiv \frac{(T_w - T_h)T_c}{(T_h - T_c)T_w}\omega_w, \tag{4.9}$$

which is the "cooling window". The quantum absorption refrigerator achieves maximum COP if $\omega_c \to \omega_{c,\max}$, at this point, the entropy production $\sigma \to 0$ as required by the second law of the thermodynamics.

4.3 QAR based on two qubits

4.3.1 Microscopic model

We propose a model of a quantum absorption refrigerator based on only two qubits, as shown in the figure. The two qubits are coupled via asymmetric spin-spin interaction. In addition, the qubit A is coupled to two independent thermal baths of temperatures T_h, and T_w which plays the role of the hot and work-like reservoir in our scheme. The qubit B is placed in a cold thermal bath of temperature T_c. All three thermal baths are independent and can attain any non-negative temperature within the limit $T_c < T_h \ll T_w$.

The Hamiltonian of the coupled qubits (A + B) is given by [24]

$$\hat{H} = \frac{\omega_{\mathrm{A}}}{2}\hat{\sigma}^z_{\mathrm{A}} + \frac{\omega_{\mathrm{B}}}{2}\hat{\sigma}^z_{\mathrm{R}} + g\hat{\sigma}^z_{\mathrm{A}}\hat{\sigma}^x_{\mathrm{B}}, \tag{4.10}$$

g being the coupling strength between the qubits, ω_A and ω_B are the frequencies of the left and right qubits, respectively.

The Hamiltonian of the independent thermal baths is given by

$$\hat{H}_{B\alpha} = \sum_{\mu,\alpha} \omega_\mu \hat{a}^\dagger_{\mu,\alpha}\hat{a}_{\mu,\alpha}, \tag{4.11}$$

the annihilation and creation operators of the bath modes are represented by $\hat{a}_{\mu,\alpha}$, and $\hat{a}^\dagger_{\mu,\alpha}$, respectively, and the sum is taken over infinite number of bath modes, indexed by μ, and $k = w, h$. The interaction of the qubits with the baths are defined as

$$\hat{H}_{SB} = \sum_{\mu} g_{k,\mu}\hat{\sigma}^x_{\mathrm{A}} \otimes (\hat{a}_{k,\mu} + \hat{a}^\dagger_{k,\mu}) + \sum_{\mu} g_{c,\mu}\hat{\sigma}^x_{\mathrm{B}} \otimes (\hat{a}_{c,\mu} + \hat{a}^\dagger_{c,\mu}). \tag{4.12}$$

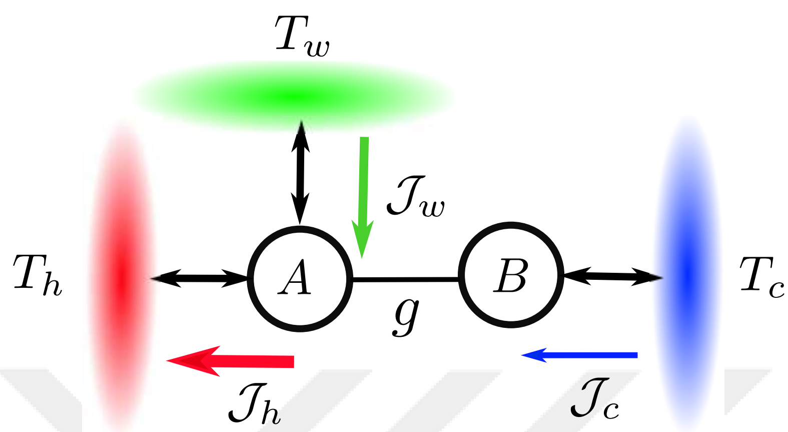

Figure 4.2: Schematic illustration of a quantum absorption refrigerator based on two coupled two-level systems, for example, two qubits. The qubits are coupled via asymmetric interaction $\hat{\sigma}_A^z\hat{\sigma}_B^x$ of strength g. The work-like and the hot thermal baths of temperatures T_w, and T_h, respectively, are coupled to the left qubit, and the cold bath of temperature T_c is in connection with the right qubit. For the cooling process, the heat current $\mathcal{J}_c$ direction must be from the cold bath to the system; accordingly, from the first and second law of thermodynamics, the other two heat currents should be $\mathcal{J}_w > 0$, $\mathcal{J}_h < 0$.

4.3.2 The master equation

Following the standard derivation of the master equation outlined in Sec. 1.3, the master equation for coupled qubits is given by

$$\frac{d}{dt}\tilde{\rho} = \mathcal{L}_w\tilde{\rho} + \mathcal{L}_h\tilde{\rho} + \mathcal{L}_c\tilde{\rho}, \tag{4.13}$$

here $\mathcal{L}_w\tilde{\rho}$, $\mathcal{L}_h\tilde{\rho}$, and $\mathcal{L}_w\tilde{\rho}$ being the Liouville superoperators of the work-like, hot and cold baths, respectively, which describe the energy exchange of the qubits with the baths, and have the form

$$\begin{aligned} \mathcal{L}_k &= G_k(\omega_{\rm A})\cos^2\theta D[\tilde{\sigma}_{\rm A}^-] + G_k(-\omega_{\rm A})\cos^2\theta D[\tilde{\sigma}_{\rm A}^+] \\ &+ G_k(\omega_-)\sin^2\theta D[\tilde{\sigma}_{\rm L}^-\tilde{\sigma}_{\rm R}^+] + G_k(-\omega_-)\sin^2\theta D[\tilde{\sigma}_{\rm A}^+\tilde{\sigma}_{\rm B}^-] \\ &+ G_k(\omega_+)\sin^2\theta D[\tilde{\sigma}_{\rm A}^-\tilde{\sigma}_{\rm B}^-] + G_k(-\omega_+)\sin^2\theta D[\tilde{\sigma}_{\rm A}^+\tilde{\sigma}_{\rm B}^+], \end{aligned} \tag{4.14}$$

$$\mathcal{L}_c = G_c(\Omega)\cos^2\theta D[\tilde{\sigma}_{\rm B}^-] + G_c(-\Omega)\cos^2\theta D[\tilde{\sigma}_{\rm B}^+]. \tag{4.15}$$

Here, $G_\alpha(\omega)$ being the spectral densities of the baths, and we consider Ohmic spectral densities in our results (see Eq. (2.11)). We define the transition frequencies as $\omega_\pm = \omega_A \pm \Omega$, and $\Omega = \sqrt{\omega_{\rm B}^2 + 4g^2}$. In addition, $D[\hat{A}]$ being the Lindblad dissipators and given by Eq. (3.6).

4.4 Cooling mechanism

This section investigates the cooling mechanism in our proposed quantum absorption refrigerator. First, we describe the critical step toward our cooling scheme. To this end, we employ the quantum reservoir engineering scheme, namely, *bath spectrum filtering*.

4.4.1 Bath spectrum filtering

The critical step to obtaining the refrigeration process in the quantum systems requires selective energy transport [125]. Various methods can be used to implement selective energy transport; here, we are interested in the quantum reservoir engineering schemes. In particular, we employ so-called bath spectrum filtering in which undesired channels of heat transport are removed or suppressed by using thermal band-pass filters [126]. Kurizki and co-workers pioneer bath spectrum filtering [126], and it has been shown to implement different thermal functions such as heat management [26], autonomous cooling of the mechanical resonators [28], and antibunching of the phonon field [127].

In bath spectrum filtering, additional harmonic oscillators are coupled with the left qubit. In this approach, the resonators coupled between the left qubit and thermal baths are included in the environment. The left qubit sees a structured environment composed of a thermal bath and an additional resonator. As a result, the effective spectral density of the hot and cold thermal bath is given by [126, 128]

$$G_k^f(\omega) = \frac{\kappa_f}{\pi} \frac{(\pi G_k(\omega))^2}{[\omega - \left(\omega_k^f + \Delta_k(\omega)\right)^2] + (\pi G_k(\omega))^2}, \tag{4.16}$$

here $G_k(\omega)$ being the unfiltered coupling spectrum, and

$$\Delta_k(\omega) = P\left[\int_o^{\infty} d\omega' \frac{G_k(\omega')}{\omega - \omega'}\right], \tag{4.17}$$

where P is the principal value. We employ bath spectrum filtering to suppress the unwanted transitions induced by the thermal baths and avoid overlapping the hot and cold baths. The overlapping spectra of the thermal baths in the quantum absorption refrigerator decrease performance due to the direct energy transfer between the baths referred to as "heat leaks", and the details of which are given in Sec. 4.5.4.

4.4.2 Cooling cycles

We assume the work-like and hot thermal baths spectra are filtered and follow $G_w(\omega_-) \gg G_h(\omega_-)$, $G_w(\omega_+) \ll G_h(\omega_+)$, and $G_h(\omega_A) \approx G_w(\omega_B) \approx 0$. These spectral functions can be obtained by selecting the resonance frequencies of the work-like and thermal baths filtered as $\omega_w^f = \omega_-$ and $\omega_h^f = \omega_+$, respectively, in Eq. (4.16). We note that the cold bath spectrum is unchanged. The selection of nonoverlapping filtered spectra of the baths guarantees the absence of direct energy transfer between the thermal baths; consequently, the ideal refrigeration at the Carnot limit becomes possible in our model.

The selection of filtered bath spectra suppresses the unwanted overlapped energy transitions between the dressed states of the coupled qubits. The master equation for the filtered bath spectra is given by

$$\begin{aligned}
\mathcal{L}_w &= \tilde{G}_w(\omega_w) \sin^2\theta D[\tilde{\sigma}_{\mathrm{L}}^- \tilde{\sigma}_{\mathrm{R}}^+] + \tilde{G}_h(-\omega_w) \sin^2\theta D[\tilde{\sigma}_{\mathrm{A}}^+ \tilde{\sigma}_{\mathrm{B}}^-] \\
\mathcal{L}_h &= \tilde{G}_h(\omega_h) \sin^2\theta D[\tilde{\sigma}_{\mathrm{A}}^- \tilde{\sigma}_{\mathrm{B}}^-] + \tilde{G}_h(-\omega_h) \sin^2\theta D[\tilde{\sigma}_{\mathrm{A}}^+ \tilde{\sigma}_{\mathrm{B}}^+], \\
\mathcal{L}_c &= G_c(\omega_c) \cos^2\theta D[\tilde{\sigma}_{\mathrm{B}}^-] + G_c(-\omega_c) \cos^2\theta D[\tilde{\sigma}_{\mathrm{B}}^+],
\end{aligned} \tag{4.18}$$

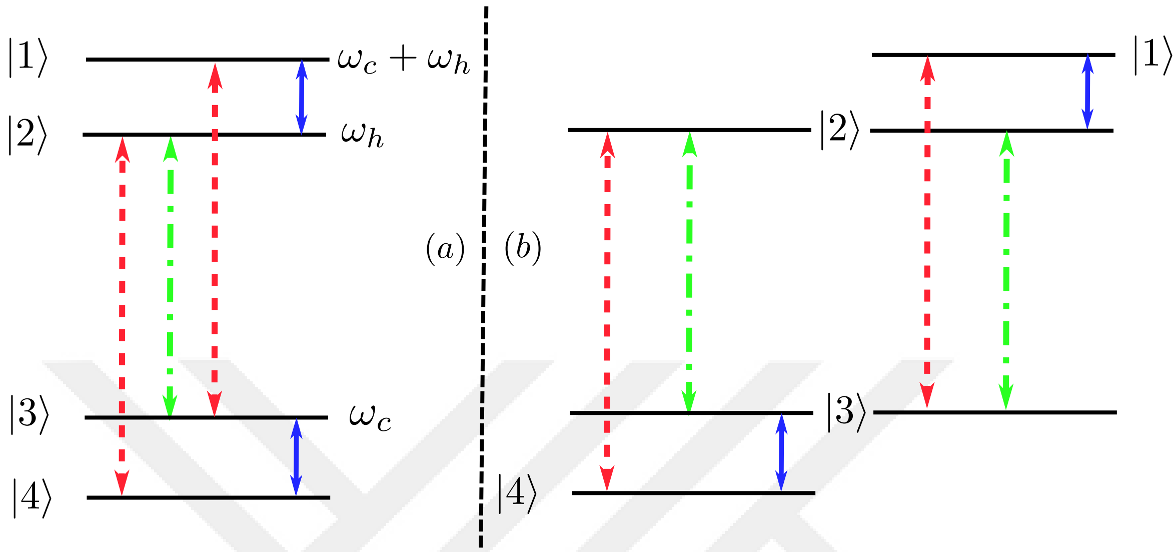

Figure 4.3: **(a)** All the possible energy transitions induced by the thermal baths with filtered spectra. **(b)** Our model of the quantum absorption refrigerator based on two-coupled qubits can be broken into two three-level refrigerators working simultaneously with a common transition induced by the work-like reservoir. The solid, dashed, and dot-dashed lines in both panels indicate the transitions induced by the cold, hot, and work-like thermal baths.

here we have defined $\omega_w = \omega_-$, $\omega_h = \omega_+$, and $\omega_c = \Omega$.

The possible transitions induced by the thermal baths under bath filtering are shown in Fig. 4.3, which shows that our model of QAR based on two coupled qubits can be broken down into two three-level subsystems. As a result, our QAR model can be understood as two three-level refrigerators working simultaneously by sharing a common transition induced by the work-like reservoir. There are no overlapping energy transitions due to bath spectrum filtering; in addition, we assume the resonance condition (see Eq. (4.2)), therefore the ratio of the heat currents is given by the ratio of the associated energy transition frequencies as given in Eq. (4.8). The steady-state heat current can be calculated numerically by solving the master equation (4.18). However, in the high temperature limit of the work-like reservoir, the

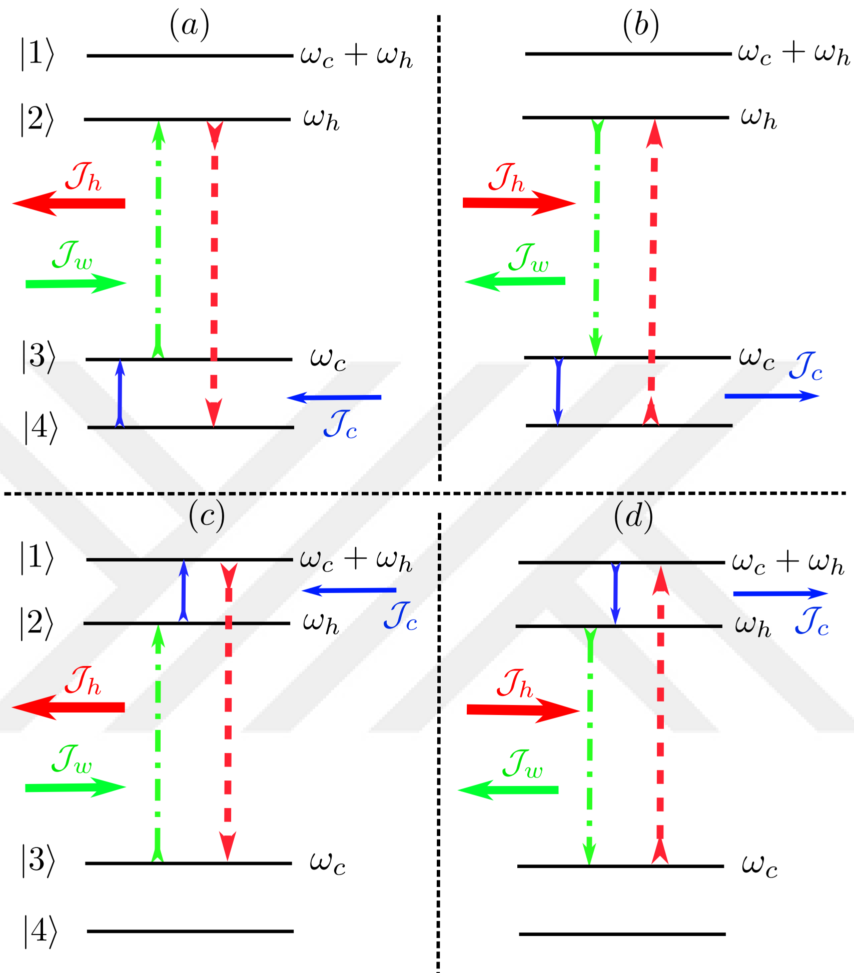

Figure 4.4: The possible cycles induced by thermal baths assist the heat transfer. (a) and (c) show the cooling cycles (4324) and (3213), which are responsible for refrigeration. Panels (b) and (d) show the associated inverse heating cycles, which, if dominant, lead to the heating process. If the parameters are selected within the cooling window (Eq. (4.9)), the cooling cycles are favored, and the heating cycles are forbidden, following the second law of thermodynamics. The solid, dashed, and dot-dashed lines indicate the transitions induced by the cold, hot and dot-dashed thermal baths.

analytical expressions for the heat currents is given by (see Appendix for details)

$$\mathcal{J}_\alpha = C\omega_\alpha. \tag{4.19}$$

For the filtered spectra of the work-like and hot baths, there are only two possible Raman cycles [(4324) and (3213)] and their inverses that can transfer the heat between the thermal baths, shown in Fig. 4.4. Here the cycle (4324) indicates the sequence of the energy transitions $|4\rangle \to |3\rangle \to |2\rangle \to |4\rangle$. If the Raman cycles shown in Figs. 4.4a and 4.4c are completed, these lead to the refrigeration process, and we termed these cycles "cooling cycles". However, if the inverse of these cycles is more favorable, then the heat is dumped into the cold bath, and we refer to these cycles as "heating cycles". To determine which of these cycles are allowed by the second law of thermodynamics, we need to calculate the entropy production. For instance, according to the second law of thermodynamics, the entropy production for the cooling cycle (4324) is given by

$$\sigma = \frac{\omega_h}{T_h} - \frac{\omega_c}{T_c} - \frac{\omega_w}{T_w}. \tag{4.20}$$

If the system parameters are selected within the cooling window, the entropy production of this Raman cycle remains positive. On the contrary, for the same set of parameters, the entropy production of the heating cycles shown in Figs. 4.4b and 4.4d becomes negative, thus not allowed by the second law of thermodynamics. As a result, the cooling cycles dominate the heat transfer, and the refrigeration process occurs. If the system parameters lie outside the cooling window, the heating cycles become more favorable and obstruct the cooling process.

The choice to couple qubit A with work-like and hot thermal baths and qubit B with cold baths is motivated by resonance condition given in Eq. (4.2). To explain this, we recall $\omega_w = \omega_A - \Omega$, $\omega_h = \omega_A + \Omega$, and $\omega_c = \Omega$ (Fig. 4.3). By looking at different possible allowed transitions, it can be seen that to follow the resonance condition (Eq. (4.2)), one possibility is to couple the work-like and hot bath with $2 \leftrightarrow 3$ and $2 \leftrightarrow 4$ ($1 \leftrightarrow 3$) transitions, respectively, and the remaining possible transitions $1 \leftrightarrow 2$ ($3 \leftrightarrow 4$) are coupled with the cold bath. These transitions indicate that one possible arrangement to make a refrigerator based on our system is that the work-like and hot baths couple to qubit A and the cold bath to qubit B. However, this is not the only possible arrangement of the three baths in our model. For example, the other possibility can be to couple the hot and cold baths with qubit A and the work-like bath with qubit B. In this arrangement, we need to design bath filters such that hot and cold baths induce $\omega_A + \Omega$ ($2 \leftrightarrow 4$, $1 \leftrightarrow 3$) and ω_A ($2 \leftrightarrow 3$) transitions, respectively; and the work-like reservoir needs to be coupled with Ω ($1 \leftrightarrow 2$, $3 \leftrightarrow 4$) transitions to satisfy the resonance condition. Accordingly, the choice to couple the hot and work-like reservoir with qubit A and the cold bath with qubit B is not unique.

4.5 Results

4.5.1 Cooling power

Figs. 4.5(a) and 4.5(b) show the cooling power and scaled efficiency as a function of the right qubit frequency ω_c for different values of the coupling strength g. The efficiency curves for different values of coupling strength are not very distinct because the efficiency is given by the ratio of the frequencies of the cold to work bath induced transitions $\epsilon = \omega_c/\omega_w$. As a result, the performance coefficient can be arbitrarily close to the Carnot bound by tuning the effective frequency of the right qubit ω_c. At the Carnot limit $\epsilon \rightarrow \epsilon_c$, the entropy production approaches to zero $\sigma \rightarrow 0$, consequently, the cooling power $\mathcal{J}_c$ of QAR vanishes as shown in Figs. 4.5. For both $\omega_c = 0$ and $\omega_c = \omega_{c,max}$, the cooling power vanishes $\mathcal{J}_c = 0$, therefore, for given system parameters, the cooling power is maximum for an optimum value of ω_c. The existence of an optimum ω_c can be explained by the cooling cycles shown in Fig. 4.4. For the optimal cooling, two conditions must be satisfied (i) the work-like reservoir must be hot enough ($T_w \gg \omega_h - \tilde{\omega}_c$) to induce $|3\rangle \rightarrow |2\rangle$ transition, (ii) the cold bath must able to induce ω_c energy transition $T_c > \omega_c$. For a given set of system parameters with small values of ω_c, condition (i) may not hold, and for the higher values of ω_c, (ii) may not be satisfied. Accordingly, the optimal value of ω_c can satisfy both of these conditions simultaneously, resulting in optimal cooling.

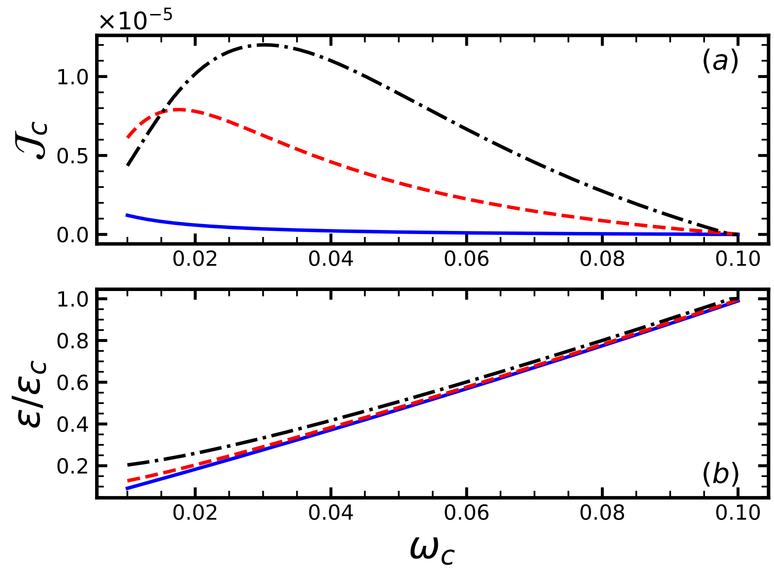

Figure 4.5: The possible cycles induced by thermal baths assist the heat transfer. (a) and (c) show the cooling cycles (4324) and (3213), which are responsible for refrigeration. Panels (b) and (d) show the associated inverse heating cycles, which, if dominant, lead to the heating process. If the parameters are selected within the cooling window (Eq. (4.9)), the cooling cycles are favored, and the heating cycles are forbidden, following the second law of thermodynamics. The solid, dashed, and dot-dashed lines indicate the transitions induced by the cold, hot and dot-dashed thermal baths.

4.5.2 Quantum correlations and cooling power

Here we investigate the possible relation between the performance of our proposed quantum absorption refrigerator and the quantum correlations. For the considered system parameters, we observe no entanglement between the coupled qubits of the system. The absence of the entanglement between the qubits can be explained by

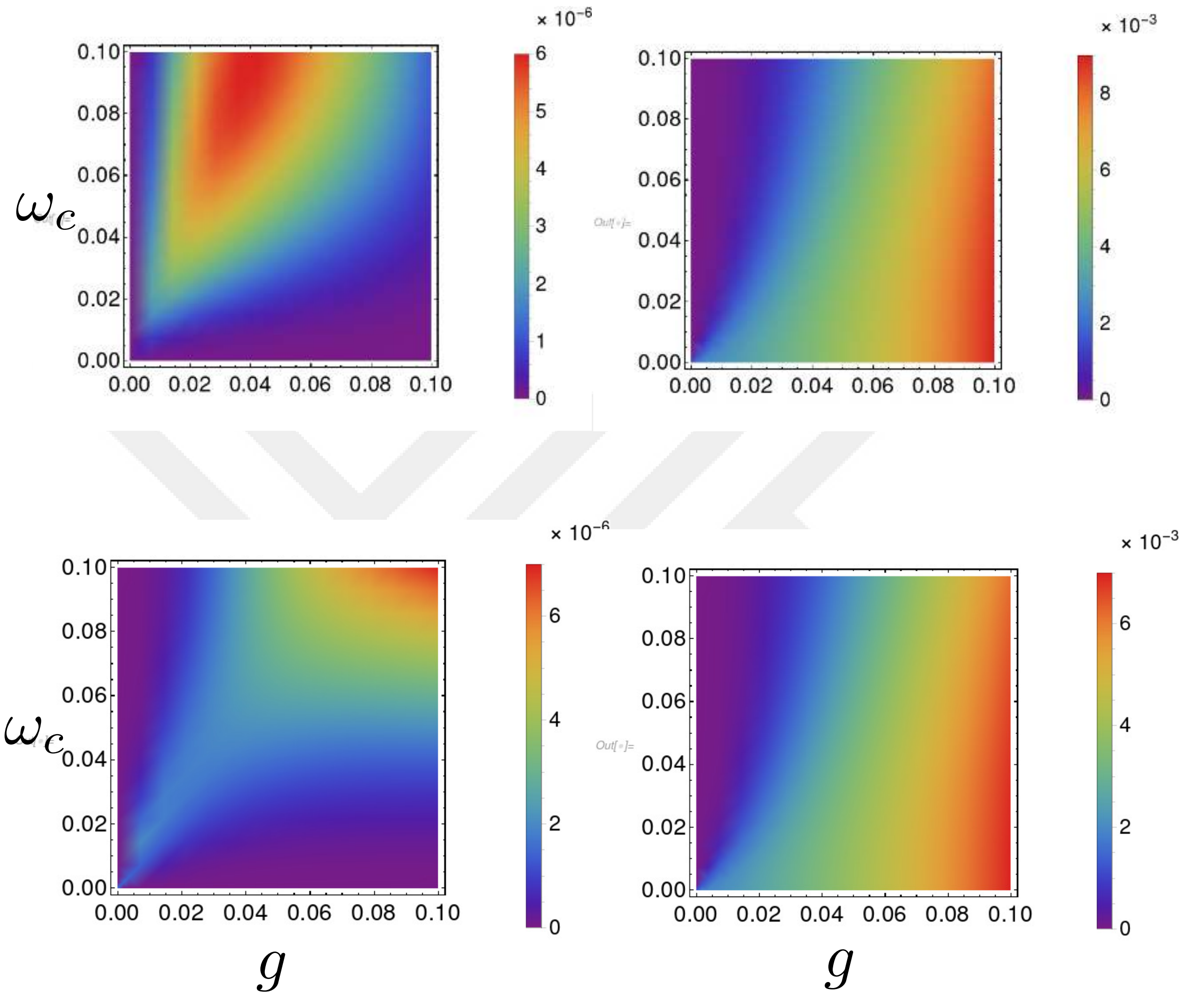

Figure 4.6: (a) The cold bath heat current $\mathcal{J}_c$ (b) total correlations $\mathcal{I}(\hat{\rho}_{AB})$ (c) quantum correlations $D(\hat{\rho}_{AB})$ (d) classical correlations $\mathcal{I}(\sigma_{AB})$ between the coupled qubits as a function of the coupling strength g, and the cold bath qubit frequency ω_c. System parameters: $\omega_h = 1$, $\kappa_c = \kappa_w = \kappa_h = 0.005$, $T_h = 2$, $T_w = 3$, and $T_c = 1$.

writing the density matrix of the coupled qubits in the local basis of the qubits as

$$\hat{\rho}_{AB} = \begin{pmatrix} r_{11} & c_{12} & 0 & 0 \\ c_{12} & r_{22} & 0 & 0 \\ 0 & 0 & r_{33} & c_{34} \\ 0 & 0 & c_{34} & r_{44} \end{pmatrix}. \tag{4.21}$$

The least eigenvalue of the of the partial-transpose of the density matrix $\tilde{\rho}_{AB}$ is positive for the considered system parameters; $r_{11} + r_{22} - ((r_{11} - r_{22})^2 + 4c_{12}^2)^{1/2} > 0$. According to the positivity-of-the-partial-transpose separability criterion [129], the two qubits are not entangled in our system. To go beyond the entanglement-separability criterion and quantify the quantum correlations between the coupled qubits, we employ quantum discord, which is given by [130, 131]

$$D(\hat{\rho}_{AB}) = \mathcal{I}(\hat{\rho}_{AB}) - \mathcal{I}(\sigma_{AB}). \tag{4.22}$$

here, $\mathcal{I}(\rho_{AB})$ being the quantum mutual information which describes the total correlations between the qubits, and it is given by

$$\mathcal{I}(\hat{\rho}_{AB}) = S_{\hat{\rho}_A} + S_{\hat{\rho}_B} - S_{\hat{\rho}_{AB}}. \tag{4.23}$$

$S_{\hat{\rho}_i} = -\mathrm{Tr}[\rho_i \log \rho_i]$ denotes the von Neumann entropy of the density matrix $\hat{\rho}_i$ of the subsystem i. The classical correlations between the qubits are described by $\mathcal{I}(\sigma_{AB})$ in Eq. (4.22), here σ_{AB} denotes the state obtained by the minimally disturbing projective measurement on qubit B [130, 131]. We look for the possible connection between the cooling power and quantum correlations by plotting the total correlations $\mathcal{I}(\hat{\rho}_{AB})$, classical correlations $\mathcal{I}(\sigma_{AB})$, quantum correlations $D(\rho_{AB})$ and the cooling power $\mathcal{J}_c$ in Fig. 4.6. The results show that the classical correlations are much stronger than the quantum correlations, and we find no overlap between the maximum cooling power and correlations between the qubits. As a result, in our model, the quantum or classical correlations between the working fluid qubits play no role in the refrigerator's performance.

4.5.3 Efficiency at maximum cooling power

Following the second law of thermodynamics, at the Carnot limit, a quantum absorption refrigerator's efficiency becomes unity and becomes an ideal refrigerator at the cost of vanishing cooling power. Consequently, a more relevant bound for practical absorption refrigerators can be the efficiency at maximum cooling power ϵ_*. It has

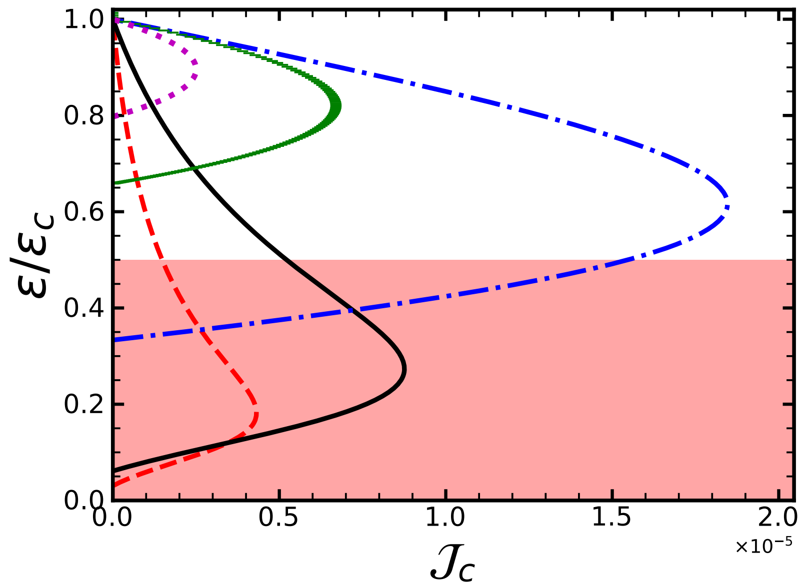

Figure 4.7: Parametric plot of cooling power $\mathcal{J}_c$ as a function of the normalized coefficient of performance ϵ/ϵ_c for different values of the coupling strength g. Dashed, solid, dash-dotted, horizontal dashed and dotted lines are for $g = 0.005, 0.01, 0.05, 0.09, and\ 0.11$, respectively. The shaded region shows the ϵ_* bound given in Eq. (4.24).

been shown that for an ideal quantum absorption refrigerator based on an elementary three-level system, the efficiency at maximum cooling power has an upper bound given by [132]

$$\epsilon_* \leq \frac{d_c}{d_c + 1}\epsilon_c, \tag{4.24}$$

here d_c being the dimensionality of the cold bath. Contrary to the previous proposal [132, 123], we show that our proposed refrigerator based on coupled qubits can surpass this established bound.

Fig. 4.7 shows the normalized coefficient of performance (efficiency) as a function of the cooling power for several values of the coupling strength g. The shaded region in the figure denotes the efficiency at maximum power bound ϵ_*. The ϵ_* shows a monotonic increase with the increase in the coupling strength g, and for larger values of the coupling strength, the established bound (Eq. (4.24)) for previously proposed models of QARs can be surpassed. Remarkably, the efficiency at maximum cooling power can approach the Carnot limit $\epsilon_* \to \epsilon_c$. However, the cooling power vanishes at this limit as enforced by the second law of thermodynamics.

The breakdown of the bound ϵ_* can be explained by noting that it depends on the cold bath's spatial dimensionality; if we increase the dimensions of the cold bath, the ϵ_* becomes larger. For d-dimensional cold bath, the power spectrum has the form $G(\omega_c) \propto \omega_c^d$. In our model, due to the asymmetric coupling between the qubits, $c = \omega_B/\omega_c$ dependent terms in the master equation (4.18) effectively increase the dimensionality of the cold bath. We note that if the coupling strength between the qubits is $g = N\omega_c$ with N being a real number, the coefficient c in the master equation (4.18) becomes independent of ω_c. In this case, it is impossible to surpass the bound given in Eq. (4.24) for any value of coupling strength g.

4.5.4 Non ideal QAR: Heat leaks

Typically thermal operations are characterized by the power versus efficiency curves. In the case of an ideal quantum absorption refrigerator, these curves are open as shown in Fig. 4.5, which describes that in the Carnot limit, the QAR achieves unit efficiency at the cost of vanishing power. On the contrary, more practical models of QARs schemes should incorporate the internal dissipation and heat leak in the efficiency and power quantification [133]. For these non-ideal models of QARs, the efficiency versus power curves are closed.

Here we consider a case of a non-ideal quantum absorption refrigerator in our model by allowing more than one thermal bath to induce the same energy transition. The overlapping spectral of the thermal baths results in the direct energy transfer between the thermal baths and is referred to as "heat leaks," which affect the performance of the QAR. If the filtered bath spectra are not spectrally separated, these can result in heat leaks. For instance, if the work-like and the hot bath induce the same

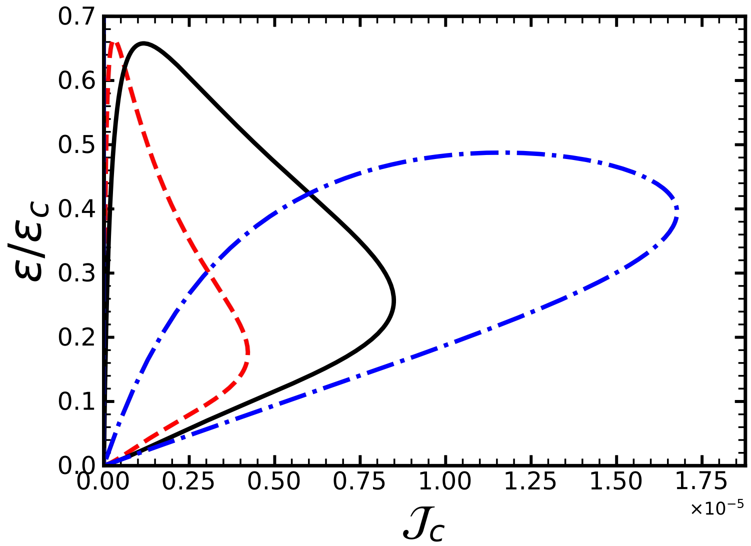

Figure 4.8: The parametric plot of normalized coefficient of performance ϵ/ϵ_c as a function of normalized cooling power $\mathcal{J}_c/\mathcal{J}_0$ for different values of the coupling strength g in case of overlapping bath spectra of the work-like and hot thermal baths. Dashed, solid, and dash-dotted curves are for coupling strength $g = 0.005, 0.01, 0.05$, respectively.

energy transition, say $|2\rangle \leftrightarrow |3\rangle$ in Fig. 4.4, this can result in the direct energy transfer between the hot and work-like baths and decreases the efficiency of the QAR. Fig. 4.8 confirms this analysis where we plot efficiency versus cooling power for different values of coupling strength g. We obtain close curves of efficiency versus cooling power, and the irreversibility increases with the increase in the coupling strength. The overlap of the work-like and hot bath is parasitic, which produces irreversibility due to the introduction of heat leaks in the model.

4.6 Summary

We have proposed a quantum absorption refrigerator based on two-coupled qubits contrary to widely employed three-body interaction schemes. We considered an asymmetric interaction between the qubits and investigated the heat transfer through the qubits by employing a global master equation consistent with the laws of thermodynamics. The mechanism behind the cooling process was explained by considering energy cycles consisting of transitions between the dressed states of the qubits, which are induced by the thermal baths.We showed that heat could be removed from the cold by employing the bath spectrum filtering and selecting the system parameters within the cooling window.

The reservoir engineering helped to attain the Carnot limit by not allowing the overlapping bath spectra; however, the cooling power at the Carnot limit vanishes as required by the second law of thermodynamics. In addition, we investigated a more practical bound, namely efficiency at maximum cooling power. In the strong coupling regime of the coupled qubits, we showed that our model could surpass the bound established on the efficiency at cooling power for previous QAR schemes. Finally, we allowed overlapping bath spectra, which results in the direct energy transfer between the thermal baths, and deteriorates the efficiency of the quantum absorption refrigerator.

We note that our proposal of the quantum absorption refrigerator can be realized using versatile experimental platforms; for instance, circuit QED can be used for its implementation, for coupled qubits [24], for the optomechanical system [1], for the atom-cavity model as working medium [128]. Unlike previously proposed models of the quantum absorption refrigerators in bosonic systems, which require a trilinear interaction between the harmonic oscillators [124], our model can be implemented using only two harmonic oscillator. In our model, by employing bath spectrum filtering, both the efficiency and efficiency at maximum power can be made very close to the Carnot limit, which is impossible in the previous two-body QARs proposals [123].

Chapter 5

SIMULTANEOUS COOLING OF RESONATORS BY THERMAL RESERVOIR

5.1 Introduction: Ground-state cooling of resonators

One of the crucial steps toward quantum technologies based on the mechanical resonators is effective and energy-efficient cooling of the mechanical resonators to their ground-states. For example, cooling the mechanical resonators is an essential prerequisite in ultrasensitive precision measurement [134] and gravitational wave detection [135]. In addition, the ground-state cooling of mechanical resonators is also required for the experiments designed for the investigation of fundamentals of quantum physics at macroscopic scale [42]. The applications are based on the optomechanical systems in the field of quantum computation and quantum information processing; the ground-state cooling of the resonators plays a vital role [1]. Over the last two decades, extensive efforts have been made to achieve ground-state cooling of the resonators; some of these include feedback-assisted cooling [136, 2, 137, 138, 139, 140, 141], and laser sideband cooling [142, 143, 144, 145, 146, 147, 148, 3, 7, 149, 150].

In recent years, systems with multiple mechanical resonators have caught much attention [151, 152, 153, 154, 155]. For example, in Ref. [63, 156] heat modulation is proposed based on multiple mechanical resonators coupled to a single cavity mode; in addition, entanglement between distant mechanical resonators has been demonstrated recently [157]. In the case of multiple resonators of similar frequencies, the ground-state cooling becomes impossible due to the dark mode, which is not involved in the system's dynamics, hence decoupled from the common cooling agent. The existence of dark mode obstructs the cooling process unless the mechanical resonators of distinct frequencies are not considered [158, 159, 160]. There are few recent attempts to overcome this challenge; for example, a dark mode breaking scheme is proposed, which is based on a phase-dependent coupling between the mechanical resonators [161, 162]. The other possibility can be using cold-damping feedbkack [140, 141]; however, for the identical mechanical resonators, this scheme fails to cool the resonators to the ground-state.

A complementary approach removes thermal energy from the mechanical resonators by driving the cooling agent with a very hot thermal bath [163, 164]. This scheme requires no external control drive or work source to cool the mechanical resonator. It is proposed in a multimode optomechanical system, in which two cavity modes are coupled to a single mechanical resonator. A tri-linear interaction between the two-cavity modes and the mechanical resonator is required [163]. The cooling scheme is valid in a very weak-optomechanical coupling regime, and the investigation involved a mean-field approach; as a result, the correlations between the cooling agent and the mechanical resonators are entirely ignored. In the weak-coupling regime, it may not be possible to cool the mechanical resonator to its ground state considering realistic experimental system parameters. Here we propose a scheme of cooling multiple mechanical resonators of the same or different frequencies using a thermal environment. We show that the mechanical resonators can be cooled to their ground states using realistic system parameters. The bath spectrum filtering plays a vital role in the realization of our scheme. Finally, we propose several setups for the possible experimental realization of the proposed cooling scheme.

5.2 The microscopic model and master equation

Our scheme is based on a typical optomechanical system in which a single optical resonator of frequency ω_a is coupled to N independent mechanical resonators of frequency ω_i ($i = 1, 2...N$), as shown in Fig. 5.1. The Hamiltonian of this system is

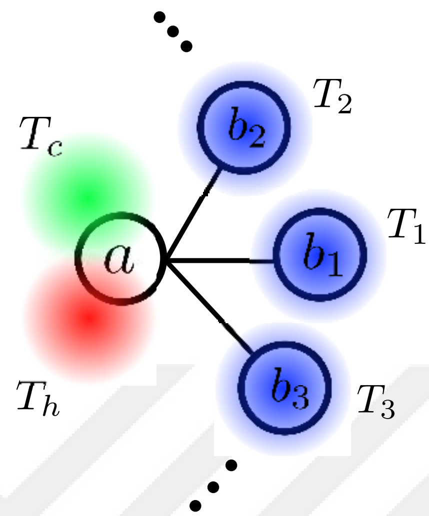

Figure 5.1: Schematic depiction of a multimode optomechanical system in which a single optical mode a is coupled with N mechanical modes b_i or independent mechanical resonators. Each mechanical resonator b_i is unavoidably coupled to an independent thermal bath of temperature T_i. In addition, the optical resonator is coupled to two independent thermal baths of temperatures T_h, and T_c. The optical resonator baths are spectrally filtered to cool the mechanical resonators. All thermal baths are independent and can attain any non-negative temperature.

given by

$$\hat{H}_s = \omega_a \hat{a}^\dagger \hat{a} + \sum_{i=1}^{N} \left[\omega_i \hat{b}_i^\dagger \hat{b}_i - g_i \hat{a}^\dagger \hat{a}(\hat{b}_i + \hat{b}_i^\dagger)\right], \tag{5.1}$$

here g being the single-photon optomechanical coupling strength. In addition, the creation (annihilation) bosonic operators of the mechanical and optical resonators are given by $\hat{b}_i$ ($\hat{b}_i^\dagger$), and $\hat{a}$ ($\hat{a}^\dagger$), respectively. Each mechanical resonator is unavoidably coupled to an independent thermal bath of temperature T_i, and the optical resonator is coupled to two thermal baths of temperatures T_h and T_c. The optomechanical system with multiple mechanical resonators can be implemented using a circuit electromechanical system [165, 7] or photonic crystal optomechanical system [166].

5.2.1 The master equation

The Hamiltonian of the thermal baths is given by

$$\hat{H}_{Bx} = \sum_{k,x} \omega_{k,x} \hat{a}^{\dagger}_{k,x} \hat{a}_{k,x}, \tag{5.2}$$

here, $x = c, h, i$ represents the cold, hot, and baths coupled to mechanical resonators, respectively. The sum is taken over the infinite number of bath modes indicated by k. In our cooling scheme, we require two baths to couple with the optical resonator; the hot bath assists in removing the thermal energy from the mechanical resonator's baths and dump into the cold bath. Following the second law of thermodynamics, it is impossible to cool the mechanical resonators to the ground state using only a single bath attached to the optical resonator. The interaction between the thermal baths and the optomechanical system is given by

$$\hat{H}_{SB} = \sum_{k} g_{k,j}(\hat{a} + \hat{a}^{\dagger}) \otimes (\hat{a}_{k,j} + \hat{a}^{\dagger}_{k,j}) + \sum_{k,i} g_{k,i}(\hat{b}_i + \hat{b}^{\dagger}_i) \otimes (\hat{a}_{k,i} + \hat{a}^{\dagger}_{k,i}), \tag{5.3}$$

here, $j = h, c$ indicates the hot and cold baths, respectively. The first term in Eq. (5.3) gives the interaction of the hot and cold baths with the optical resonator, and the second term in the Hamiltonian describes the interaction between the mechanical resonator i with its bath maintained at temperature T_i. The eigenenergies of the optomechanical system is given by

$$E_{n_a,m_i} = n_a\omega_a + m_i\omega_i - n_a^2 \frac{g_i^2}{\omega_i}, \tag{5.4}$$

here n_a and m_i indicates the number of photons and phonons in the optical and mechanical resonator, respectively.

We follow the derivation of the master equation given for a standard optomechanical system in Sec. 3.7.1, and the derived master equation has the form

$$\frac{d}{dt}\tilde{\rho} = \mathcal{L}_h + \mathcal{L}_c + \mathcal{L}_i, \tag{5.5}$$

here, the Liouville superoperators of the optical and mechanial resonators are given by

$$\begin{aligned}\mathcal{L}_j &= G_j(\omega_a)D[\tilde{a}] + G_j(-\omega_a)D[\tilde{a}^\dagger] \\ &+ \sum_i \alpha_i^2 \Big[G_j(\omega_-)D[\tilde{a}\tilde{b}_i^\dagger] + G_\alpha(-\omega_-)D[\tilde{a}^\dagger\tilde{b}_i] + G_j(\omega_+)D[\tilde{a}\tilde{b}_i] + G_j(-\omega_+)D[\tilde{a}^\dagger\tilde{b}_i^\dagger]\Big], \end{aligned} \tag{5.6}$$

$$\mathcal{L}_i = G_i(\omega_i)D[\tilde{b}_i] + G_i(-\omega_i)D[\tilde{b}_i^\dagger], \tag{5.7}$$

here, $\omega_\pm = \omega_a - \omega_i$, $\alpha_i = g/\omega_i$ and $G_\alpha(\omega)$ being the spectral densities of the baths, and we consider Ohmic spectral densities in our results (see Eq. (2.11)). The transformed operators have the form

$$\tilde{a} = \hat{a}e^{-\alpha\sum_i(\hat{b}_i^\dagger - \hat{b}_i)} \quad \text{and} \qquad \tilde{b}_i = \hat{b}_i - \alpha\hat{a}^\dagger\hat{a}. \tag{5.8}$$

In addition, $D[\hat{A}]$ being the Lindblad dissipators and given by Eq. (3.6). We remark that, in the derivation of the master equation, the weak optomechanical coupling regime is considered [56],

$$\alpha_i^2\langle\tilde{b}_i^\dagger\tilde{b}_i\rangle \ll 1, \tag{5.9}$$

and we have neglected all higher order terms $\mathcal{O}(\alpha^3)$.

5.3 Results and discussion

For the analytical and numerical results, the system parameters representative of a typical optomechanical system is considered [1]: $g_i = 2\pi\times100$ kHz, $\omega_i = 2\pi\times10$ MHz, $\kappa_h = \kappa_c = 2\pi\times1$ MHz, $\kappa_i = 2\pi\times100$ Hz. The temperature of the mechanical resonator is $T_i \sim 1.5$ K, and the associated average phonon number is $\bar{n}_i(0) \sim 2\times10^3$. The hot bath temperature is larger by many orders of magnitude, i.e., $4\times10^4 \lesssim T_h \lesssim 4\times10^7$ K. In all the results, the system parameters are scaled with the optical frequency ω_a.

5.3.1 Cooling mechanism

First, we consider a case in which a single mechanical resonator is coupled to the optical cavity to explain the underlying physical mechanism of cooling. This simple model based on a single mechanical resonator helps us to establish a direct link between the typical laser cooling schemes and "cooling by heating" in an optomechanical system. The index i is dropped in the master equation (5.5) for the case of a single mechanical resonator. The dynamics of the mechanical resonator can be obtained by taking a trace over the optical resonator in the master equation (5.5), and the reduced master equation for the mechanical resonator has the form

$$\frac{d\tilde{\rho}}{dt} = (\Gamma^- + \Gamma^-_{\text{th}})D[\tilde{b}_1] + (\Gamma^+ + \Gamma^+_{\text{th}})D[\tilde{b}_1^\dagger], \tag{5.10}$$

here the upward transition rate Γ^+ (Γ^+_{th}), and the downward transition rate Γ^- (Γ^-_{th}) for the mechanical resonator are induced by the optical (mechanical) thermal baths. These rates are given by

$$\begin{aligned}
\Gamma^- &:= \alpha_1^2 \sum_{j=h,c} (G_j(\omega_+)\langle\tilde{n}_a\rangle + G_j(-\omega_-)\langle\tilde{n}_a+1\rangle), \\
\Gamma^+ &:= \alpha_1^2 \sum_{j=h,c} \big(G_j(\omega_-)\langle\tilde{n}_a\rangle + G_j(-\omega_+)\langle\tilde{n}_a+1\rangle\big), \\
\Gamma^-_{\text{th}} &:= G_1(\omega_1), \qquad \Gamma^+_{\text{th}} := G_1(-\omega_1).
\end{aligned} \tag{5.11}$$

In what follows, we only assume the Ohmic spectral densities of the thermal baths (see Eq. (2.11)). The filtered nonoverlapping spectra of the hot and cold optical baths are considered, which can be obtained using [26]

$$\tilde{G}_j := \frac{1}{\pi}\frac{\pi G_j(\omega)}{[(\omega - (\omega(n+1/2) + \Delta_j(\omega))^2 + (\pi G_j(\omega))^2]}, \tag{5.12}$$

here $\Delta_\alpha(\omega)$ being the Lamb-shift due to the thermal bath.

In the case of the laser sideband cooling scheme in a standard optomechanical system, the input coherent drive of frequency ω_L is made resonant with the lower sideband $\omega_{\text{L}} = \omega_- = \omega_a - \omega_1$ [3], which leads to the cooling of the mechanical resonator. As a result, the anti-Stokes (cooling) process becomes more favorable than the Stokes (heating) process, as shown in Fig. 5.2(a). The mechanical resonator can be cool to the ground state by the input laser drive if the upper sideband $\omega_+ = \omega_a + \omega_1$ remains far off-resonant. On the contrary, in our model, the input coherent drive is not present; instead, the cold and hot thermal baths incoherently drive the cavity. We aim to design a cooling scheme based on only system-environment interaction without needing external control drives. Accordingly, we drive the optical mode with incoherent thermal baths, due to which the cavity mode reaches to a thermal state (see Eq. (5.15)). In the case of laser-driven cavity mode, coherence assists in removing energy from the mechanical resonators. In our scheme, we replace laser drives with thermal baths and show that it is still possible to cool the mechanical resonators. Similar to the laser-driven cavity, we obtain both upper and lower phonon sidebands in the case of the incoherently driven cavity. For the cooling process in our model, making an analogy with the laser sideband cooling, we may want to suppress the upper sideband and incoherently drive the cavity at the lower sideband. The upper sideband can be suppressed by employing bath spectrum filtering [128].

For the cooling process, the hot thermal bath only drives the lower sideband of transition frequency ω_-, and all other energy transfer channels are suppressed for the hot thermal bath. Similarly, the cold bath only induces the transition of frequency ω_a, and other heat transfer channels are filtered out for the cold bath. The hot and cold baths spectra that can fulfill these conditions on the energy transitions should be non-overlapping and must satisfy

$$\tilde{G}_c(\omega_a) \gg \tilde{G}_h(\omega_a), \quad \text{and} \quad \tilde{G}_c(\omega_-) \ll \tilde{G}_h(\omega_-). \tag{5.13}$$

The underlying cooling mechanism in our scheme can be understood by directly connecting with the widely employed laser sideband cooling scheme, as shown in Fig. 5.2. The increase in the temperature of the hot bath results in the increase in the number of hot photons in the cavity with "correct frequency" these photons trigger the energy transition of frequency ω_- (lower sideband); as a result, cooling process dominates. The photons follow Plank's distribution, and an increase in the temperature of the hot bath increases the number of photons with the correct frequency in the considered range of system parameters. In a complete refrigeration cycle (Fig. 5.2), the hot bath at temperature T_h completes the transition of frequency ω_- with the

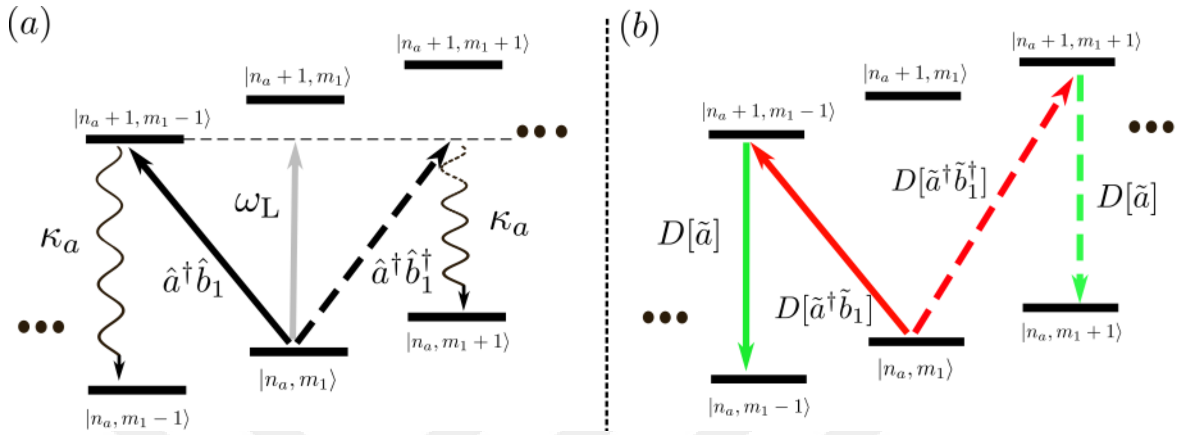

Figure 5.2: The dressed states $|n_a, m_1\rangle$ of a standard optomechanical system having a single mechanical mode, and arrows indicate the energy transitions between the dressed states, which are responsible for energy transfer. The dashed and solid lines describe the heating and cooling process, respectively. **(a)** The heating and cooling processes in case the cavity is driven by an external coherent drive of frequency ω_{L}. In the cooling process, the lower sideband is resonant with the drive, which leads to the destruction of a phonon with a blue-shifted photon leaving the cavity. **(b)** The underlying energy transitions are involved in the heat transfer in our scheme. The hot bath induced the transition of frequency ω_- (lower sideband); this leads to the creation of a higher energy photon (blue-shifted), and this energetic photon is dumped into the cold bath by the transition of frequency ω_a.

destruction of single phonon. This blue-shifted (energetic) photon is dumped into the cold bath at temperature T_c to complete the cooling cycle. We note that the analogy with the sideband cooling is only valid if the hot and cold bath spectra are non-overlapping; in the case of the unfiltered baths, the cooling process is obstructed.

5.3.2 Single resonator cooling

In the case of the filtered hot and cold baths, the master equation (5.5) reduces to

$$\begin{aligned}\mathcal{L}_c &= \tilde{G}_c(\omega_a)D[\tilde{a}] + \tilde{G}_c(-\omega_a)D[\tilde{a}^\dagger],\\ \mathcal{L}_h &= \alpha_1^2\big(\tilde{G}_H(\omega_-)D[\tilde{a}\tilde{b}_1^\dagger] + \tilde{G}_h(-\omega_-)D[\tilde{a}^\dagger\tilde{b}_1]\big),\\ \mathcal{L}_1 &= G_1(\omega_1)D[\tilde{b}_1] + G_1(-\omega_1)D[\tilde{b}_1^\dagger],\end{aligned} \tag{5.14}$$

As a result of the dynamical evolution governed by this master equation the cavity mode becomes an almost thermal steady-state with other terms of the order $\mathcal{O}(\alpha^2)$ [56, 167, 168]. The mean number of photons in cavity is given by

$$\langle\tilde{n}_a\rangle_{\text{ss}} \approx \frac{\tilde{G}_c(-\omega_a) + \tilde{G}_1(-\omega_1)}{\big(\tilde{G}_c(\omega_a) + \tilde{G}_c(-\omega_a)\big) + \big(\tilde{G}_1(\omega_1) + \tilde{G}_1(-\omega_1)\big)}, \tag{5.15}$$

here higher order terms in α are ignored. We have ignored the contribution from the hot bath in the steady-state mean photon number of the cavity mode because the hot bath is only couple to the transition frequency of $\omega_- = \omega_a - \omega_1$ (lower sideband). The hot bath spectrum is assumed to obey $G_h(\omega_a) \approx 0$; accordingly, the contribution from the hot bath in mean photon number can be ignored for $\alpha^2 \ll 1$. To check the validity of this approximation, we plot the mean phonon number of the mechanical resonator by considering the approximated photon number in the cavity and compare the results with the numerical solutions obtained by solving the master equation (5.14). From this master equation, we can evaluate the average phonon number in the mechanical resonator

$$\frac{d\langle\tilde{n}_1\rangle}{dt} = (\Gamma_c^+ + \Gamma_{\text{th}}^+)\langle\tilde{n}_1 + 1\rangle - (\Gamma_c^- + \Gamma_{\text{th}}^-)\langle\tilde{n}_1\rangle, \tag{5.16}$$

where the downward (upward) transition rate induced by cavity filtered baths is given by

$$\Gamma_c^- := \alpha_1^2\tilde{G}_h(-\omega_-)\langle\tilde{n}_a + 1\rangle, \qquad \Gamma_c^+ := \alpha_1^2\tilde{G}_h(\omega_-)\langle\tilde{n}_a\rangle. \tag{5.17}$$

The average number of excitations in the mechanical resonator at steady-state evaluate to

$$\langle\tilde{n}_1\rangle_{\text{ss}} = \frac{\Gamma_c^+ + \kappa_1\bar{n}_1}{\tilde{\Gamma}_c + \kappa_1}, \tag{5.18}$$

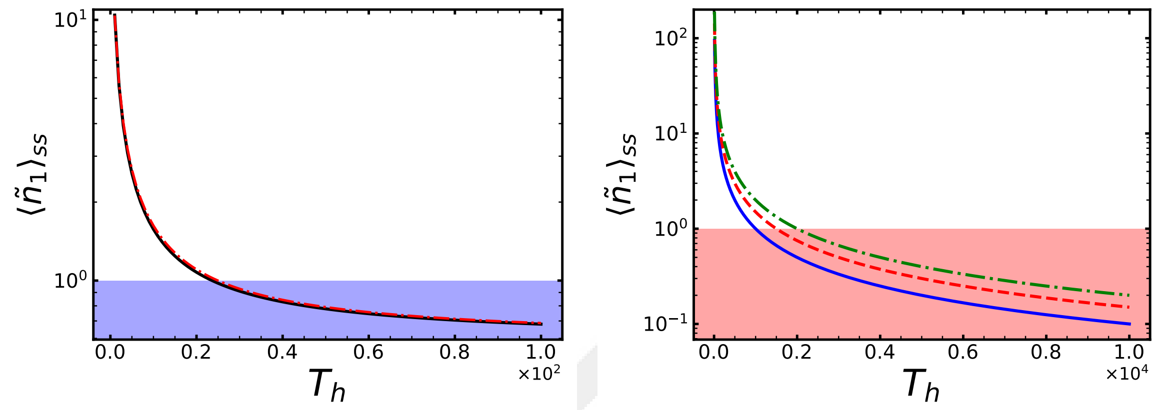

a b

Figure 5.3: (a) Comparison of the steady-state mean phonon number $\langle \tilde{n}_1 \rangle_{ss}$ as a function of the hot bath temperature T_h obtained by the numerical solution of the master equation (5.14) and by using approximated analytical results given in Eq. (5.18). The solid and dashed lines indicate the numerical and approximated analytical results, respectively. (b) The steady-state average excitation number $\langle \tilde{n}_1 \rangle_{ss}$ as a function of the hot bath temperature T_h. The dot-dashed, dashed, and solid lines are for $T_1 = 3 \times 10^{-4}, 2 \times 10^{-4}$ and 1×10^{-4}, respectively. The rest of the system parameters are: $\omega_1 = 1 \times 10^{-7}$, $\omega_a = 1$, $\kappa_1 = 1 \times 10^{-12}$, $\kappa_h = \kappa_c = 1 \times 10^{-8}$, $T_c = 1 \times 10^{-5}$, and $g_1 = 1 \times 10^{-9}$. All the parameters are scaled with the optical frequency $\omega_a = 2\pi \times 10^{14}$ Hz. The bath temperatures in SI units are: $T_1 \approx 1.5, 1$ and 0.5 K for dot-dashed, dashed, and solid lines, respectively. The cold bath has a temperate $T_c \approx 5$ mK, and the hot bath temperature is ultra-hot and it's temperature is approximately $4 \times 10^4 \lesssim T_h \lesssim 4 \times 10^7$ K.

here we define the net damping rate due to optical baths as $\tilde{\Gamma}_c = \Gamma_c^- - \Gamma_c^+$. The steady-state phonon number equation is very similar to the phonon number equation in the case of laser sideband cooling in a typical optomechanical system [1], which has the form $\langle n_1 \rangle_{ss} = (\Gamma^+ + \kappa_1 \bar{n}_1)/(\Gamma_{\text{opt}} + \kappa_1)$. The total optomechanical damping rate is given by $\Gamma_{\text{opt}} = \Gamma^- - \Gamma^+$. In addition, Γ^- and Γ^+ indicate the cooling (anti-

Stokes) and heating (Stokes) scattering process, respectively. We note that the mean phonon number $\langle\tilde{n}_1\rangle_{\rm ss}$ of the mechanical resonator depends on the $\bar{n}_1$, representing the number of excitations associated with the mechanical thermal bath T_1. It should be the case because for the same system parameters; the final mean phonon number $\langle\tilde{n}_1\rangle_{\rm ss}$ should be greater for the higher temperatures mechanical bath T_1 compared to a mechanical bath of a lower temperature. In equation (5.18), Γ_c represents the net damping rate of both hot and the cold baths (see Eq. 5.17).

In the case of laser, sideband resolved cooling, the following conditions should be fulfilled to achieve ground-state cooling of the mechanical resonator; (i) the Stokes scattering should be largely or entirely suppressed, (ii) the mechanical dissipation κ_1 due to its environment must be much smaller than the net optical damping $\Gamma_{\rm opt}$ in the system, (iii) The quality factor of the mechanical resonator must be very large compared to the initial mean phonon number $\bar{n}_1 \ll \omega_1/\kappa_1$ [148]. The ground-state cooling in our scheme can be possible with similar conditions given for laser sideband cooling; (i) the hot bath spectrum is filtered so that it can not induce the transition at frequency ω_+ (upper sideband), so the heating (Stokes) process is suppressed, (ii) The optical dissipation rate induced by the optical baths must be larger than the mechanical dissipation rate $\tilde{\Gamma}_c \gg \kappa_1$, (iii) The quality factor of the mechanical resonator is much larger than the initial mean phonon number $\bar{n}_1 \ll \omega_1/\kappa_1$. These conditions are satisfied for the filtered non-overlapping hot and cold bath spectra and in the temperature limit $T_h \gg T_1 > T_c$. To analyze the performance of our cooling scheme, we plot the steady-state mean phonon number $\langle\tilde{n}_1\rangle_{ss}$ as a function of the hot bath temperature T_h in Fig. 5.3. The results show that it is possible to cool the mechanical resonator to its ground state in the case of very high hot bath temperatures. We note that the mechanical resonator is not coupled to the ultra-hot bath; it is directly coupled to the optical resonator, which reaches a thermal steady-state at a much lower temperature.

5.3.3 Multiple resonator cooling

Here we investigate the simultaneous cooling of two mechanical resonators of identical and different frequencies which are coupled to the same optical resonator. Extending these results to an arbitrary number of N mechanical resonators is straightforward. In the case of two mechanical resonators and filtered spectra of the hot and cold bath, the reduced master equation for the mechanical resonators is given by

$$\frac{d\tilde{\rho}}{dt} = (\Gamma_i^- + \Gamma_{\text{th},i}^-)D[\tilde{b}_i] + (\Gamma_i^+ + \Gamma_{\text{th},i}^+)D[\tilde{b}_i^\dagger], \tag{5.19}$$

here the optical bath transition rates are defined as

$$\Gamma_i^- \quad := \quad \alpha_i^2\tilde{G}_h(-\omega_{-,i})\langle\tilde{n}_a + 1\rangle, \quad \Gamma_i^+ := \alpha_i^2\tilde{G}_h(\omega_{-,i})\langle\tilde{n}_a\rangle, \tag{5.20}$$

and $\omega_{-,i} = \omega_a - \omega_i$. The steady-state mean phonon number in indvidual resonator is given by

$$\langle\tilde{n}_i\rangle_{\text{ss}} = \frac{\Gamma_i^+ + \kappa_i\bar{n}_i}{\tilde{\Gamma}_i + \kappa_i}, \tag{5.21}$$

here $\tilde{\Gamma}_i = \Gamma_i^- - \Gamma_i^+$. The mean phonon number of each resonator depends on the dissipation rates of other resonators with the thermal baths.

It is possible to cool the degenerate or non-degenerate mechanical resonators to their ground state, provided the dissipation rates are sufficiently low. On the contrary, in the laser sideband cooling in a standard optomechanical system, the dark mode hinders the cooling process for the degenerate mechanical resonators [140, 141]. Further, for the mechanical resonators of nearby frequencies, it may not be possible to cool any of these resonators [159]. Compared to the standard laser cooling scheme, our advantageous cooling scheme allows simultaneous cooling of the degenerate or non-degenerate mechanical resonators. In Fig. 5.4, we plot the steady-state mean phonon number as a function of the hot bath temperature, which confirms the prediction of simultaneous cooling of multiple mechanical resonators in our scheme.

In the case of identical resonators of the same frequency and dissipation rates and coupled to baths of the same temperature, the mean phonon number curves are

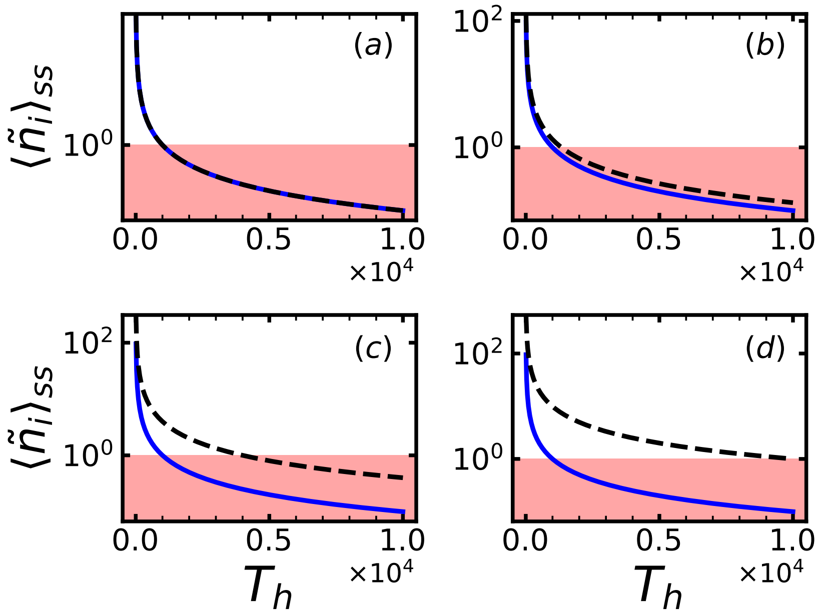

Figure 5.4: The steady-state average excitation number $\langle \tilde{n}_i \rangle_{ss}$ as a function of the hot bath temperature T_h. The blue Solid, and black dashed lines are associated with the first and second mechanical resonator, respectively. Parameters: $\omega_a = 1$, $\omega_1 = 1 \times 10^{-7}$, $T_1 = T_2 = 2 \times 10^{-4}$, $\kappa_1 = 1 \times 10^{-12}$, $T_c = 1 \times 10^{-5}$, $\kappa_h = \kappa_c = 1 \times 10^{-8}$, , and $g_1 = 1 \times 10^{-9}$. The system parameters are scaled with the cavity frequency $\omega_a = 2\pi \times 10^{14}$ Hz. (a) $g_1 = g_2$, $\omega_1 = \omega_2$, (b) $g_1 = g_2$, $\omega_2 = 0.75\ \omega_1$, (c) $\omega_1 = \omega_2$, $g_2 = 0.5\ g_1$ and (d) $\omega_1 = \omega_2$, $\kappa_2 = 10\ \kappa_1$, $g_1 = g_2$.

identical, as shown in Fig. 5.4(a). The cooling rates are not identical for different mechanical resonators, and the mean phonon number curves are different for both resonators, as shown in Fig. 5.4(b). Here, the more significant cooling in the first resonator is because the hot bath spectrum is filtered with a peak at $\omega_a - \omega_1$, which means the first resonator has a larger cooling rate than the second resonator. The optomechanical coupling strength effect on the cooling of the mechanical resonator is shown in Fig. 5.4(c), the strongly coupled mechanical resonator with the optical cavity has a more significant optical dissipation rate ($\tilde{\Gamma}_2 < \tilde{\Gamma}_1$), which leads to more cooling of the strongly coupled mechanical resonator. Finally, we show that the mechanical resonator with more considerable coupling strength with the mechanical thermal bath has lesser cooling (Fig. 5.4(d)). Extending our cooling scheme to an arbitrary number of mechanical resonators coupled to the same optical resonator is straightforward. This is because Eqs. (5.19) and (5.21) has the same mathematical structure for any number of mechanical resonators.

5.3.4 Cooling by a non-thermal bath

In the optomechanical system driven by an external coherent drive, the heating (Stokes) and cooling (anti-Stokes) processes compete with each other. In the cooling process, the anti-Stokes process dominates the Stokes scattering, which results in the cooling of the mechanical resonator. However, it is impossible to completely suppress the Stokes scattering process with the coherent drive due to vacuum fluctuations. Consequently, a limit exists on the cooling of the mechanical resonator, which prevents us from cooling the resonator to its true ground state [144]. This limit is referred to as the "quantum back-action limit", which can be saturated for the optimal system parameters [144]. We note that unlike limits set by the basic physical laws, this is not a fundamental limit. Several strategies have been proposed to go beyond this limit on cooling the resonator [169, 170, 171]. One promising direction is cooling the mechanical resonator with the squeezed light, which can remove this limit [172], and experimental demonstration of this proposal showed a significant enhancement in the cooling beyond the quantum back-action limit [173]. Similarly, in the quantum absorption refrigerators, squeezed thermal baths show significant enhancement in performance by increasing both the cooling power and efficiency simultaneously [132].

In the previous section, we showed that it is possible to cool the mechanical resonator to its ground state using an ultra-high temperature thermal bath. However, it can be experimentally challenging to realize such a bath with this high temperature. Here we propose to use the squeezed thermal bath to cool the mechanical resonator to overcome the challenge of achieving an ultra-high temperature of the thermal bath.

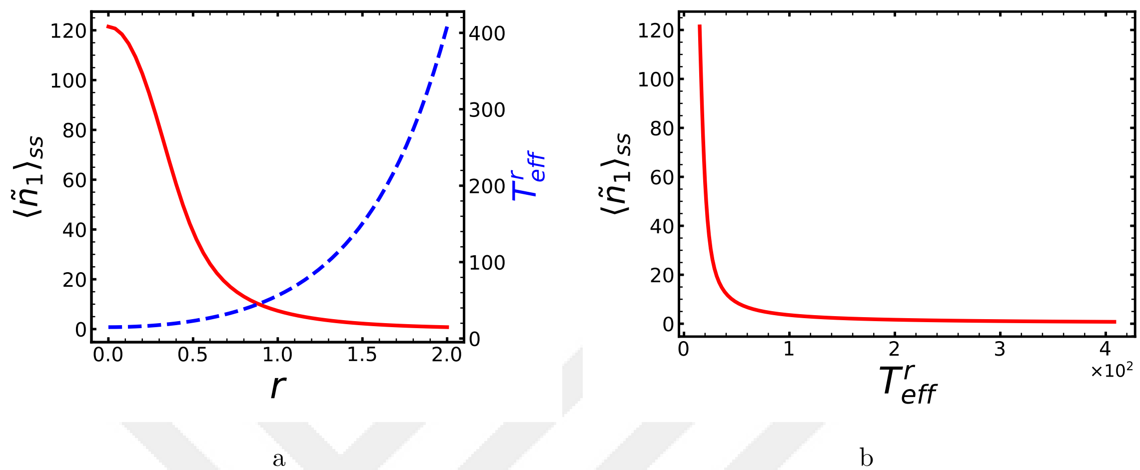

Figure 5.5: (a) The steady-state average number of phonons $\langle\tilde{n}_1\rangle_{ss}$, and effective temperature T^r_{eff} as a function of the squeezing parameter r. Blue dashed and red solid lines are for the effective temperature T_{eff} and average phonon number $\langle\tilde{n}_1\rangle_{ss}$, respectively. (b) The steady-state mean phonon number $\langle\tilde{n}_1\rangle_{ss}$ as a function of the effective temperature T^r_{eff} of the squeezed bath. Parameters: $\omega_1 = 2\pi \times 10$ MHz, $\omega_a = 2\pi \times 7$ GHz, $g_1 = 2\pi \times 100$ kHz, $\tilde{\kappa}_h = 2\pi \times 1.5$ MHz, $\kappa_1 = 2\pi \times 32$ Hz, $\kappa_c = 2\pi \times 1$ MHz, and $T_1 = T_c \approx 65$ mK. For $\langle\tilde{n}_1\rangle_{ss}$, all the parameters are scaled with the microwave resonator frequency $\omega_a = 2\pi \times 7$ GHz. The effective temperature T^r_{eff} of squeezed thermal bath is calculated in SI units for $\bar{n}_h = 0$.

For the demonstration, we consider an electro-mechanical system [3, 6, 4] having one mechanical resonator because of the constraints on numerical computation for very large Hilbert space sizes. The master equation with the squeezed thermal bath is given by

$$\mathcal{L}^r_h = \tilde{\kappa}_h\alpha_1^2\big((N+1)D[\tilde{w}] + ND[\tilde{w}^\dagger]\big) - \tilde{\kappa}_h\alpha_1^2 MD[\tilde{w},\tilde{w}] - \tilde{\kappa}_h\zeta_1^2 MD[\tilde{w}^\dagger,\tilde{w}^\dagger], \tag{5.22}$$

here $\tilde{w} = \tilde{a}\tilde{b}^\dagger$, $D[A,B] := 2A\tilde{\rho}B - BA\tilde{\rho} - AB\tilde{\rho}$, and $\tilde{\kappa}_h$ is the effective system-bath coupling [8]. Note that the mechanical and cold baths dissipative terms remain the same as given in Eq. (5.14); we only consider squeezed hot bath to enhance cooling. In the master equation with the squeezed thermal bath, we assume that the squeeze bath can only induce the transition of frequency $\pm\omega_-$, and the bath spectrum filtering process suppresses all other transition frequencies. The mechanical and cold bath dissipators do not change in this case. The coefficients N and M, which depend on the squeezing parameter r are given by

$$N := \bar{n}_h(\cosh^2 r + \sinh^2 r) + \sinh^2 r, \quad M := -\sinh r \cosh r\,(2\bar{n}_h + 1), \tag{5.23}$$

here we consider real squeezing parameter r. The dissipators in Eq. (5.22) can always be transformed into the standard Lindbald form by an appropriate unitary transformation. The Lindbald form ensures that the the reduced state of the system remains trace-perserving and completely positive in the presence of a squeezed thermal drive [174].

Fig. 5.5a shows the steady-state average excitation in the mechanical resonator as a function of the squeezed bath temperature. The average phonon number is obtained using numerical solution of Eq. (5.14) by replacing $\mathcal{L}_h$ with the squeezed dissipators given in Eq. (5.22). We consider Hilbert space with four hundred phonon and four-photon states in the numerical results, and the robustness of the solutions against change in Hilbert space size is confirmed. The effective temperature of a squeezed thermal bath which depends on squeezing parameters, is given by [175]

$$T^r_{\text{eff}} = \frac{\omega_-}{\log[\frac{\tanh^2 r + e^{\omega_-/T_h}}{1+\tanh^2 r e^{\omega_-/T_h}}]} \geq T_h. \tag{5.24}$$

In Fig. 5.5b we plot the steady-state mean phonon number as a function of the effective temperature T^r_{eff} of the squeezed bath. The mean phonon number shows similar behavior as in the case of the hot thermal bath shown in Fig. 5.3b. Fig. 5.5 results show that it is possible to cool the mechanical resonator to its ground state by considering reasonable hot bath temperature and other system parameters which are experimentally realizable, which include squeezing parameter $r \sim 1.2$ [176]. In addition, if required, a very large squeezing parameter can be obtained by employing a non-thermal coherent atomic reservoir [177].

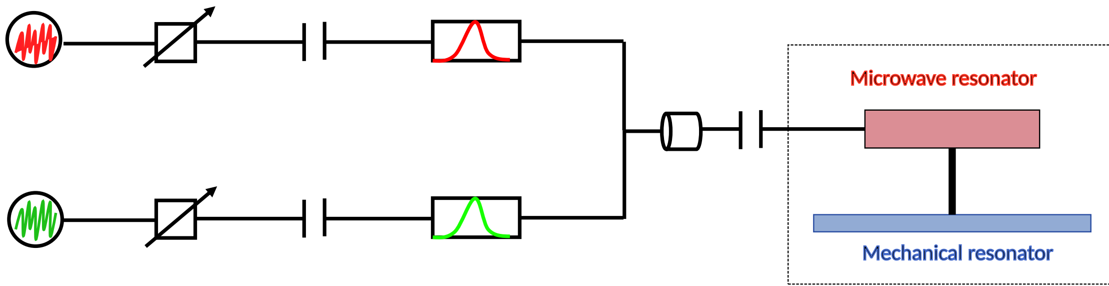

Figure 5.6: The experimental feasibility of our scheme is based on an electromechanical system analogous to the typical optomechanical system. In the setup, a qubit [2] or a microwave circuit [3, 4, 5] or superconducting microwave resonator [6] of frequency ω_a is interacting with a mechanical resonator of frequency ω_1 via optomechanical-like coupling. The dotted black box indicates the isolated system is placed inside a dilution refrigerator [3, 4]. In this setup, it is possible to consider multiple mechanical resonators coupled to the same qubit or microwave resonator [7]. This superconducting microwave resonator is coupled to spectrally filtered hot and cold sources of white noise. The attenuators can be used to control the amplitude of these white noise drives. Two resistive circuits can be used to implement the hot and cold thermal baths [8]. The microwave resonators designed at frequencies ω_a, and ω_- coupled to the white noise source act as thermal bandpass filters for the cold and hot, respectively [8, 9].

5.4 Experimental feasibility

Our scheme of cooling multiple mechanical resonators to the ground state is enabled by quantum reservoir engineering and based on the cooling by heating mechanism. The proposal can be realized by various experimental setups based on optomechanical-like interaction between the cooling mode and mechanical resonators.

5.4.1 Electromechanical system

In Sec. 5.3, we showed that it is possible to cool multiple mechanical resonators simultaneously to the ground state by employing bath spectrum filtering. However, the cooling of resonators requires very high temperatures of the hot bath, and it can be challenging to realize ultra-high temperatures in the experimental setups. Here we suggest an alternative setup for the realization of our proposal, which requires an electro-mechanical system [3, 4, 5] as shown in Fig. 5.6. A superconducting microwave resonator designed at frequency ω_a is coupled to a mechanical resonator of frequency ω_1 via an optomechanical-like coupling [1]. The superconducting microwave resonators are driven by the spectrally filtered cold and hot leads, and the whole setup, excluding thermal baths, is placed inside a dilution refrigerator. In addition, two microwave resonators of frequencies ω_-, and ω_a are coupled to the superconducting resonator for the purpose of bandpass filters. Each of these microwave resonators interacts with the resistive circuit, which plays the role of thermal baths in this scheme [8]. This model of a single mechanical resonator can also be extended to multiple mechanical resonators coupled to the same superconducting microwave resonator, which is the cooling agent in the setup [7].

For this electro-mechanical system and heat baths, the master equation (5.14) can be used for the dynamics of the system and the steady-state average phonon number is given by Eq. (5.21). Fig. 5.7 shows that for experimentally realizable system parameters, the mean phonon number of the mechanical resonator can reach the ground state of the resonator without requiring an ultra-high temperature of the thermal baths. In the case of the ground state cooling of the mechanical resonator initially, at a higher temperature, single-photon strong optomechanical coupling strength is required. Recently, the single-photon strong coupling can be realized by a flux-mediated interaction between the mechanical resonator and superconducting microwave resonator [178].

If initially the mechanical resonator is at room temperature, an ultra-high temperature hot bath $T_h \sim 10^9 - 10^{10}$ K along with single-photon strong coupling

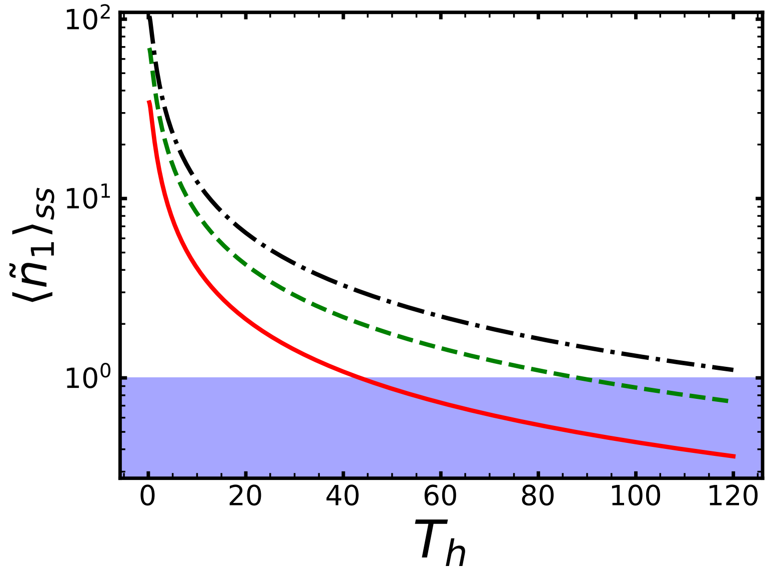

Figure 5.7: The steady-state average excitation number $\langle \tilde{n}_1 \rangle_{ss}$ as a function of the hot bath temperature T_h. The dot-dashed, dashed, and solid lines are for $T_1 = 3\times10^{-4}, 2\times 10^{-4}$ and 1×10^{-4}, respectively. The rest of the system parameters are: $\omega_1 = 1\times10^{-7}$, $\omega_a = 1$, $\kappa_1 = 1 \times 10^{-12}$, $\kappa_h = \kappa_c = 1 \times 10^{-8}$, $T_c = 1 \times 10^{-5}$, and $g_1 = 1 \times 10^{-9}$. All the parameters are scaled with the optical frequency $\omega_a = 2\pi \times 10^{14}$ Hz. The bath temperatures in SI units are: $T_1 \approx 1.5, 1$ and 0.5 K for dot-dashed, dashed, and solid lines, respectively. The cold bath has a temperate $T_c \approx 5$ mK, and the hot bath temperature is ultra-hot, and it's temperature is approximate $1 \lesssim T_h \lesssim 400$ K.

$g \sim (\omega_1, \kappa_x)$ [179] may lead to the ground state cooling in our scheme. It is challenging to achieve both the ultra-high temperature of a thermal bath and a single-photon strong coupling regime; however, it is possible to significantly reduce the effective temperature of the mechanical resonator by considering experimentally realizable system parameters. We note that it is possible to consider a hot bath with a very high temperature in the electromechanical system, as the superconducting microwave resonator does not reach a thermal state with an effective temperature near to hot bath temperature. Instead, the cold bath is resonantly coupled with the superconducting resonator; as a result, it reaches a steady state with a much lower temperature than that of a hot bath. In addition, it is possible to design a significantly hot bath with a very high temperature $T_h \sim 9500$ K in the superconducting circuits [180].

5.4.2 Qubit-resonator coupling

Our advantageous scheme of cooling multiple resonators can be implemented based on a qubit coupled to mechanical resonators via *energy-field* interaction [2, 181]. In this case, two microwave resonators designed at frequencies ω_a, and ω_- couple to the qubit for the realization of bath spectral filtering of the cold and hot bath, respectively. The filtered spectra of the baths have Lorentzian form [9], whose width and center can be controlled by the microwave resonator frequencies. In this setup, the master equation (5.14) remains the same with a difference that the optical resonator bosonic operators are replaced by the respective Pauli operators [27].

5.4.3 Optomechanical system

Our cooling scheme can be implemented in the optical regime using a toroid optical microresonator coupled to the mechanical resonators via optomechanical interaction [1]. In this case, the electromagnetic vacuum coupled to the optical mode acts as the cold bath and has a Lorentzian bath spectrum which can be tuned with the optical cavity linewidth [56]. A state-dependent quantum heat engine was proposed based on the same setup [56]. The ground state cooling of multiple resonators may be challenging in the optical regime, as it requires an ultra-high temperature of the hot bath. However, the mechanical resonators can be significantly cool by using experimentally realizable system parameters. Alternatively, this setup can employ spectrally filtered squeezed hot thermal bath with significant squeezing to attain ground state cooling.

5.4.4 Cooling with squeezed-thermal bath

An appealing possibility of realizing our scheme of cooling based on a squeezed thermal reservoir in the optical regime can be a merger of the micromaser heating scheme [182] with the standard optomechanical system. In this case, an electromagnetic vacuum can serve as a cold bath which typically has Lorentzian spectrum [1], and the width of this spectrum can be controlled by the cavity linewidth [56]. The squeezed thermal hot bath can be conceived by preparing atoms in a quantum coherent superposition and letting them interact with the optical resonator by the Tavis-Cummings model [177]. In this setup, it is possible to realize a very large squeezing parameter $r \sim 3.5$ [177]. This scheme based on the micromaser can also be extended to more practical on-chip systems, where the interaction between the resonator and two-level system can be turned on and off [183]. This also allows for more efficient non-thermal baths for the thermalizing effect by preparing the atoms in different initial coherent superposition states [177]. It is also possible to have a similar thermalizing effect from non-thermal baths by periodically driving the optical resonator and applying the Floquet method to analyze the evolution of the system [101].

5.5 Summary

We have proposed a simultaneous ground state cooling scheme of multiple degenerate or non-degenerate resonators in an optomechanical system. Unlike typical cooling schemes, which rely on an external coherent drive or work input for cooling, we employ only thermal baths to cool the mechanical resonators. In our scheme, bath spectrum filtering allowed us to cool identical multiple resonators simultaneously, which is not possible with typical cooling schemes due to dark mode obstructing the cooling process. We showed that an ultra-high temperature of the hot bath is required to cool the resonators to the quantum ground state. However, realizing such a bath with a very high temperature may be challenging. To overcome this challenge, we suggested an electromechanical system-based realization of our proposal in which it is possible to achieve ground state cooling with the experimentally realizable system parameters. Alternatively, we proposed to employ a spectrally filtered hot squeezed thermal bath with significant squeezing to cool the mechanical resonators. Our advantageous scheme of cooling enabled by bath spectrum filtering can be realized using various setups based on the optomechanical-like interaction between the cooling agent and the mechanical resonators.

Chapter 6

ENGINEERING ENTANGLEMENT BETWEEN RESONATORS VIA HOT ENVIRONMENT

Entanglement generation and its protection is a crucial step toward building quantum technologies; in particular, it is vital in quantum communication and quantum information processing [184]. However, the generally unavoidable and uncontrolled interaction between the environment and the quantum systems degrades or completely destroys the entanglement between the quantum systems. Many efforts have been devoted in the past few decades to overcome the challenge of environment-caused decoherence in quantum systems [185, 186, 187, 188]. One of the promising directions is based on exploiting the non-unitary dynamics itself caused by system-environment interaction for the generation of entanglement [187, 188]. This led to so-called "reservoir engineering" protocols in which the desired dynamics of the system are engineered by work inputs classical external control drives [189, 190, 191, 10, 192, 193, 194, 12]. The quantum system evolves under the engineered dissipative dynamics, and deterministic entanglement is achieved at a steady state. The entanglement generation between different quantum systems based on reservoir engineering protocol has been proposed using several physical systems [189, 190, 191, 10, 192, 193, 194, 12], and it has experimentally demonstrated in atomic systems [195, 196, 197, 198]. The idea of steady-state entanglement generation by controlling the dissipative dynamics of the system has been extended to the multimode optomechanical system in which entanglement is created between two mechanical or optical resonators [152, 154, 199, 200].

Entanglement between the interacting systems can also be created by investigating them at thermal equilibrium, and cooling these systems close to the ground state may result in an entangled state of the system [201, 202]. In the presence of a temperature gradient, the heat or particle flow between the environments can generate entanglement between the systems [203, 13, 204, 205, 206, 207, 208, 209, 210, 211, 212, 213, 214, 215, 216, 217, 218]. It has been shown that a critical heat flow through the coupled qubits sandwiched between two thermal baths is required for the entanglement generation [215]. In entanglement generation schemes based on heat or particle, flow requires additional feedback or filtering operation for signification entanglement creation [212, 215], with some exceptions in qubits-based models [219]. Alternatively, a hot non-thermal bath with an effective negative temperature can boost the entanglement generation [220]. These proposals on entanglement generation are based on two-level systems with few exceptions on atomic and optical resonators [13, 221]. This chapter discusses the entanglement generation between two distant mechanical resonators interacting to a common two-level system or optical resonator via optomechanical-like coupling. We show that it is possible to create significantly large entanglement with the need for filtering or additional feedback control.

6.1 Introduction: Environment assisted entanglement

Here we set out to ask these questions: Is it possible to engineer an entanglement generation protocol based on reservoir engineering but does not require work output or external control? If yes, can we apply this protocol to generate significantly large entanglement between distant mechanical resonators without the need for filtering operation or feedback control? Our answer is yes; such a scheme can be engineered by employing the bath spectrum filtering method, which allows us to suppress unwanted dissipative interaction between the quantum systems. Our scheme combine the advantages of reservoir engineering with autonomous quantum thermal machines.

We consider two distant microwave or mechanical resonators interacting to a common two-level system or a harmonic oscillator via optomechanical-like interaction [1, 222, 66]. We employ bath spectrum filtering, which suppresses the unwanted incoherent interactions and leads to desired dissipative evolution of the joint system that results in the entangled state of the mechanical resonators. In the typical reservoir engineering schemes, work input or external coherent control drives are required [212, 215]; on the contrary, bath spectrum filtering does not rely on external control or work input, hence can be considered an autonomous scheme for entanglement generation. Bath spectrum filtering has been previously proposed for boosting various thermal tasks such as power output [167], efficiency at maximum power [27], heat amplification [26], cooling of the mechanical resonators [28], and quantum state preparation of a phonon field [127].

Our advantageous scheme of entanglement creation has several key features which are different from previous proposals; (i) We employ a simple autonomous thermal bath filtering scheme to engineer desired dissipative dynamics of the mechanical resonators. A two-mode squeezing interaction between the mechanical resonators guarantees entanglement between them, provided these are kept at sufficiently low temeprature [200]. Our scheme of entanglement creation is completely different compared to coherent two-mode squeezing interaction-based schemes [152, 154, 200], which are based on work input or coherent control drives to engineer an effective two-mode interaction. Instead, we rely only on thermal baths and an ancilla system to engineer an effective two-mode squeezing-like coupling between distant uncoupled mechanical resonators. (ii) The entanglement between the distant resonators increases monotonically with the thermal gradient increase, allowing us to have nonzero entanglement at high environment temperatures. (iii) Our autonomous thermal entanglement generation machine can create significantly large entanglement between the resonators without the filtering or feedback control [212]. In out-of-equilibrium entanglement generation studies, typically, entanglement is very weak [212]. The entanglement can be enhanced via non-thermal baths [220], feedback, or filtering operation [13, 212]. Here the filtering operation refers to the system's projection onto a subspace of total Hilbert space [223]. For instance, it is shown that a $(d+1)$-dimensional system can be driven to an entangled state using thermal baths alone, which is then projected onto a d-dimensional system to enhance the entanglement [223]. However, this local filtering operation is not deterministic. On the contrary, our scheme does

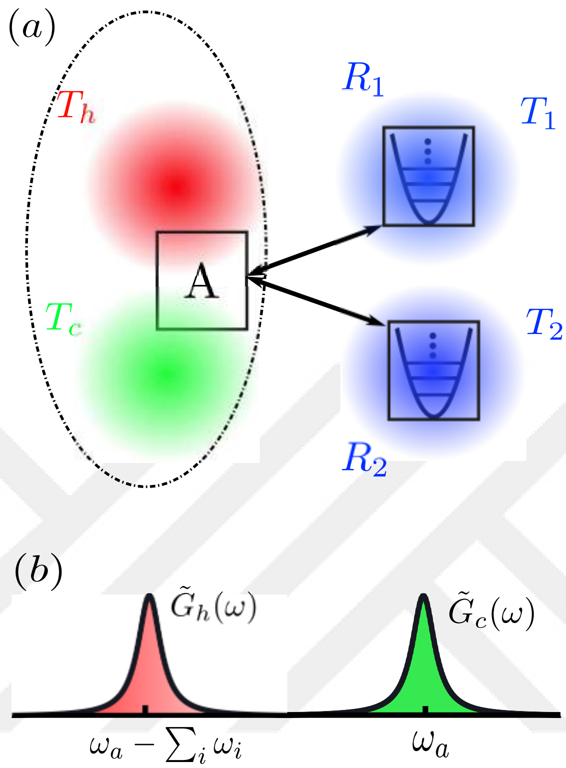

Figure 6.1: (a) Schematic description of the model based on two uncoupled microwave resonators or mechanical resonators R_i interacting to the same ancilla system A that can be a two-level system or a harmonic oscillator. We assume an *energy-field* or optomechanical-like interaction between the ancilla and mechanical resonators [1]. The ancilla A is coupled to two thermal baths, and the resonators R_i are unavoidably interacting with their own environments of temperature T. All the thermal baths are independent and can attain any non-negative temperature provided $T_h > T_i > T_c$. The dash-dotted oval represents an effective environment for the resonators, which is obtained after taking a trace over the ancilla system. This effective common bath can create quantum correlations between the mechanical resonators. (b) The spectrally filtered bath spectra of the hot and cold bath are indicated by $\tilde{G}_h$ and $\tilde{G}_c$, respectively.

not rely on such filtering of the entangled state of the resonators. Our filtering operation refers to suppressing unwanted bath-induced transitions, which can be realized by simple band-pass filters. (iv) Remarkably, entanglement creation and cooling of the mechanical resonators can occur with the same system parameters, which is impossible with previous proposals.

6.2 The model and master equation

6.2.1 The microscopic model

Our autonomous entanglement generation quantum thermal machine is based on two microwave resonators or mechanical resonators R_1 and R_2 interacting with a common two-level system or a harmonic oscillator via optomechanical-like interaction , as shown in Fig. 6.1. The Hamiltonian of this isolated system is given by [1]

$$\hat{H}_S = \omega_a \hat{n}_a + \sum_{i=1,2} \omega_i \hat{b}_i^\dagger \hat{b}_i + \sum_{i=1,2} g_i \hat{n}_a (\hat{b}_i + \hat{b}_i^\dagger), \tag{6.1}$$

here ω_i (ω_a) being the frequency of the resonator R_i (subsystem A), and g_i is the optomechanical-like coupling stregth between the resonators R_i and ancilla system A. The creation (destruction) bsonic operator of the resonator R_i is indicated by $\hat{b}_i$ ($\hat{b}_i^\dagger$). The number operator of the resonator A is represented by $\hat{n}_a = \hat{a}^\dagger \hat{a}$, with $\hat{a}_i^\dagger$ and $\hat{a}_i$ being creation and annihilation operators, respectively. In the case of a two-level system, the number operator $\hat{n}_a$ is replaced by respective Pauli spin matrix $\hat{\sigma}_z$, and ω_a is divided by 2 in Eq. (6.1).

In addition to the coupling with mechanical resonators, the ancilla system A is coupled to two thermal baths maintained at temperature T_h, and T_c. The resonators R_i are unavoidably coupled to a thermal environment of temperature T_i. All the thermal baths are independent and can attain any non-negative temperature, and in this work, we assume $T_c < T_i \ll T_h$. We assume that the initial state of the mechanical resonators is the ground state; this requires simultaneous cooling of the resonators. Two thermal baths of different temperatures coupled to the ancilla assists this cooling process at the start of the entanglement generation protocol. The cooling of the resonators needs a very hot bath which can remove energy from the resonators and dump it into another bath at a much lower temperature [28]. In addition, we employ bath spectrum filtering, which results in the non-overlapping spectra of the hot and cold baths [Fig. 6.1(b)]; this imposes a condition that more than one bath can not induce a single energy transition. Accordingly, the heat transfer between the baths can only be possible if the ancilla A is coupled with more than one thermal baths [28].

The self Hamiltonian of the thermal baths in the system is given by

$$\hat{H}_B = \sum_{k,B} \omega_{k,B} \hat{c}^{\dagger}_{k,B} \hat{c}_{k,B}, \tag{6.2}$$

here $B = h, c, i$, and $\omega_{k,B}$ being the frequency of kth mode and $\hat{c}^{\dagger}_{k,B}$ ($\hat{c}_{k,B}$) is corresponding bosonic creation (annihilation) operator. The coupling of the isolated system with the thermal baths is given by

$$\hat{H}_{S-B} = \sum_{k,l=h,c} g_{k,l}(\hat{a} + \hat{a}^{\dagger})(\hat{c}_{k,l} + \hat{c}^{\dagger}_{k,l}) + \sum_{k,i} g_{k,i}(\hat{b}_i + \hat{b}^{\dagger}_i)(\hat{c}_{k,i} + \hat{c}^{\dagger}_{k,i}), \tag{6.3}$$

here $g_{k,i}$ ($g_{k,l}$) being the interaction strength between the resonators R_i (A) with the kth mode of the thermal bath. In the case of a two-level ancilla system, the bosonic operators $\hat{a}^{\dagger}$ and $\hat{a}$ are exchanged with $\hat{\sigma}_+$ and $\hat{\sigma}_-$ spin matrices.

6.2.2 *The master eqution*

We follow the microscopic derivation of the master equation given in Sec. 1.3, and the resulting master equation has the form [29]

$$\frac{d\tilde{\rho}}{dt} = \mathcal{L}_l \tilde{\rho} + \sum_i \mathcal{L}_i \tilde{\rho}. \tag{6.4}$$

Here the Liouville super-operators for the resonators R_i and the ancilla system A are described by $\tilde{\mathcal{L}}_i$ and $\tilde{\mathcal{L}}_l$, respectively. These are given by

$$
\begin{aligned}
\mathcal{L}_l\tilde{\rho} \;=\;& G_l(\omega_a)\{D[\tilde{a}] + \alpha^3\sum_i D[\tilde{a}\tilde{b}_i^\dagger\tilde{b}_i]\} + G_l(-\omega_a)\{D[\tilde{a}^\dagger] + \sum_i \alpha^3 D[\tilde{a}^\dagger\tilde{b}_i^\dagger\tilde{b}_i]\} \\
+& \sum_{i,n=1,2}\alpha^{n+1}\{G_l(\omega_a - n\omega_i)D[\tilde{a}\tilde{b}_i^{\dagger n}] + G_l(-\omega_a + n\omega_i)D[\tilde{a}^\dagger\tilde{b}_i^n] + G_l(\omega_a + n\omega_i)D[\tilde{a}\tilde{b}_i^n] \\
+& G_l(-\omega_a - n\omega_i)D[\tilde{a}^\dagger\tilde{b}_i^{\dagger n}]\}, +\alpha^3\Big\{G_l(\omega_a - \sum_i\omega_i)D[\tilde{a}\tilde{b}_1^\dagger\tilde{b}_2^\dagger] + G_l(-\omega_a + \sum_i\omega_i)D[\tilde{a}^\dagger\tilde{b}_1\tilde{b}_2] \\
+& G_l(\omega_a + \sum_i\omega_i)D[\tilde{a}\tilde{b}_1\tilde{b}_2] + G_l(-\omega_a - \sum_i\omega_i)D[\tilde{a}^\dagger\tilde{b}_1^\dagger\tilde{b}_2^\dagger] + G_l(\omega_a - \omega_1 + \omega_2)D[\tilde{a}\tilde{b}_1^\dagger\tilde{b}_2] \\
+& G_l(-\omega_a + \omega_1 - \omega_2)D[\tilde{a}^\dagger\tilde{b}_1\tilde{b}_2^\dagger] + G_l(\omega_a + \omega_1 - \omega_2)D[\tilde{a}\tilde{b}_1\tilde{b}_2^\dagger] \\
+& G_l(-\omega_a - \omega_1 + \omega_2)D[\tilde{a}^\dagger\tilde{b}_1^\dagger\tilde{b}_2]\Big\}, \\
\mathcal{L}_i\tilde{\rho} \;=\;& G_i(\omega_i)D[\tilde{b}_i] + G_i(-\omega_i)D[\tilde{b}_i^\dagger].
\end{aligned}
\tag{6.5}
$$

Here $\alpha_i = g/\omega_i$, and we have ignored all higher-order terms $\mathcal{O}(\alpha^4)$ in the derivation of the master equation, and without the loss of generality assume $\alpha = \alpha_i$. The transformed operators are given by

$$
\tilde{a} = \hat{a}e^{-\alpha\sum_i(\hat{b}_i^\dagger - \hat{b}_i)} \text{ and } \qquad \tilde{b}_i = \hat{b}_i - \alpha\hat{a}^\dagger\hat{a}. \tag{6.6}
$$

6.3 Physical mechanism of entanglement generation

In what follows, we consider a two-level ancilla system A to demonstrate our proposed scheme of entanglement generation between uncoupled mechanical resonators. In the case of a *energy-field* interaction between ancilla and a harmonic oscillator, sideband transitions of the order n can be induced by a coherent drive of frequency $\omega_c = |\omega_a \pm n\omega_i|$. For example, a coherent external drive of frequency $\omega_c = |\omega_a - \omega_i|$ leads to anti-Stokes scattering processes, which results in the cooling of the mechanical resonators [3]. Similarly, if the lower second-order sideband is resonant with the external coherent drive, it can lead to two-photon (phonon) processes which may yield antibunching of the photo (phonon) field [224, 225]. In a complementary approach, if a spectrally filtered hot thermal is coupled to the ancilla A and its spectrum peaks at the lower first-order sideband, this results in the cooling of the resonators, referred to as "cooling by heating". The dissipative dynamics of the system is dominated by $D[\tilde{a}^\dagger \tilde{b}_i]$ in this case [28]. In both cases of coherent and incoherent drives, the equation for steady-state mean phonon number is similar [28].

The preceeding analysis may lead to the direction that if we consider incoherent interaction couterpart of the two-mode squeezing interaction , i.e., $D[\tilde{a}\tilde{b}_1^\dagger \tilde{b}_2^\dagger]$ $(D[\tilde{a}^\dagger \tilde{b}_1 \tilde{b}_2])$, it may leads to entanglement between the uncoupled resonators R_i. However, our goal is to entagle the modes $\hat{b}_i$ and not the diagnolized modes $\tilde{b}_i$. Accordingly, for entanglement analysis in the local basis, we transform $D[\tilde{a}^\dagger \tilde{b}_1 \tilde{b}_2]$ into the local basis of the resonators and by taking trace over the ancilla system

$$D_{\text{ent}} = \text{Tr}_A[\hat{u}^\dagger D[\tilde{a}^\dagger \tilde{b}_1 \tilde{b}_2]\hat{u}] = \langle \hat{n}_a + 1 \rangle D[e^{\hat{c}-\hat{c}^\dagger}(\hat{d} - \hat{c})], \tag{6.7}$$

here

$$\hat{c} \;=\; \alpha(\hat{b}_1 + \hat{b}_2), \quad \text{and} \quad \hat{d} = \hat{b}_1 \hat{b}_2 + \alpha^2. \tag{6.8}$$

It was shown in a previous study that a nonclassical state of two optical cavity modes can be engineered by a repeated interaction scheme [10]. The initial states of three-level atoms carefully prepared with the help of coherent control drives are allowed to interact randomly with the cavity fields, which results in the dissipative dynamics governed by the Liouville super-operator [10]

$$\mathcal{L}_{\text{eff}}\hat{\rho} = \kappa_c D[\hat{c}_-] + \kappa_d D[\hat{d}_-]. \tag{6.9}$$

Here, the effective dissipation rates of the cavity modes are given by $\kappa_{c,d}$, and $\hat{d}_-$ and $\hat{c}_-$ are the global jump operators for the cavity fields and given by [10]

$$\hat{c}_- \;=\; \frac{1}{\sqrt{2}}(\hat{b}_1 - \hat{b}_2), \quad \text{and} \quad \hat{d}_- = \frac{1}{2}\hat{b}_1 \hat{b}_2 - \beta^2, \tag{6.10}$$

here β is the complex amplitude of cavities' coherent states. We note that Eq. (6.9) reflects that it may be possible to create an entangled state of the resonators R_i under the dynamics governed by D_{ent}. However, additional terms are present in D_{ent} as compared with Eq. (6.9). To analyze the effect of additional terms on the creation and stabilization of entanglement, we assume a hypothetical case in which two uncoupled resonator dynamics are investigated under the influence of only D_{ent}. We compare the results of entanglement generation of this hypothetical case with that of Eq. (6.9).

The resonators are considered in a separable ground-state, $\hat{\rho}(0) = \hat{\rho}_1 \otimes \hat{\rho}_2 = |0_1\rangle\langle 0_1| \otimes |0_2\rangle\langle 0_2|$ initially. We consider other initial state of the resonators as well, such as thermal state at different temperatures, and note that the entanglement is maximum in case of initial ground state of the resonators. We employ logarithmic negativity to quntify the entanglement between the resonators R_i [226]

$$E_N(\hat{\rho}) = \log_2 \|\hat{\rho}^{\Gamma_2}\|. \tag{6.11}$$

Here, $\|.\|$ indicates the trace norm of $\hat{\rho}^{\Gamma_2}$, and the partial transpose operation of the density matrix is described by $\hat{\rho}^{\Gamma_2}$.

Fig. 6.2 shows a comparison of entanglement generation between the resonators which are evolved under the dynamics governed by Eq. (6.7) and Eq. (6.9). For a fair comparison, we assume identical system parameters, including the dissipation rates. In the numerical simulations, we considered a Hilbert space with ten photon states for each resonator and checked the robustness of the results against the change in the Hilbert space size. The results in Fig. 6.2 shows that entanglement do not vanish instead becomes significant in the case of D_{ent}. The populations $\langle \hat{b}_1^\dagger \hat{b}_1 \rangle$ and entanglement $E_N(\hat{\rho})$ show identical oscillatory behavior with a period $T = 2\pi/\sum_i \omega_i$ in the transient regime, and these oscillations disappear in the steady-state. As a result, the mean photon number governs the dynamics of the entanglement between the resonators. The maxima and minima of both entanglement and mean photon number co-occur in these results. A previous study of coupled resonators undergoing nonlinear dissipation [227] reported similar oscillatory behavior of entanglement and mean photon number.

Now we show that D_{ent} is the dominant source of dissipation in our model given in Eq. (6.1). To this end, we consider bath spectrum filtering, which can suppress the unwanted incoherent interaction that may destroy the entanglement between the

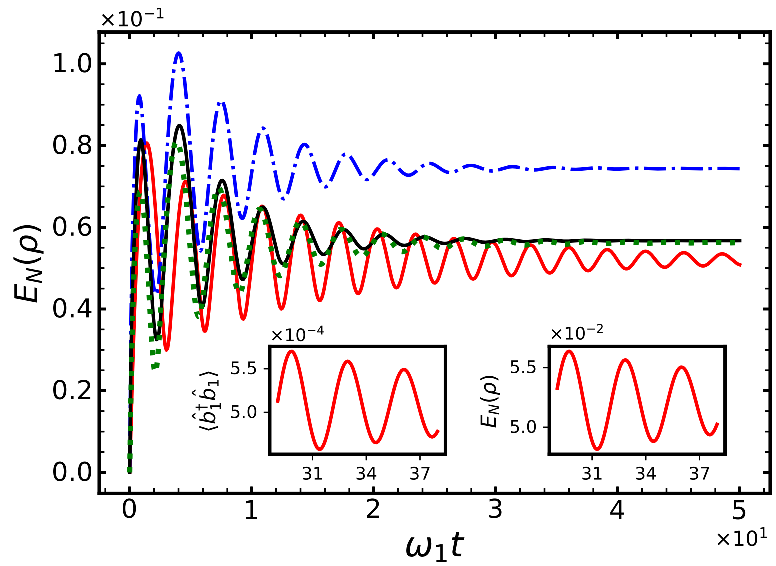

Figure 6.2: The underlying physical mechanism of entanglement creation. The logarithmic negativity $E_N(\rho)$ as a function of time $\omega_1 t$. The solid red line indicates the entanglement in the case of optical resonators undergoing dissipative dynamics governed by Eq. (6.9); this scheme was proposed in [10]. The green dotted line represents logarithmic negativity $E_N(\rho)$ for a hypothetical case of two uncoupled mechanical resonators evolving under Eq. (6.7). The blue dash-dotted and black solid curves are associated with the entanglement by keeping first and second-order correction terms in α given in Eq. (6.7), respectively. The left and right inset show mean phonon number $\langle \hat{b}_1^\dagger \hat{b}_1 \rangle$ and logarithmic negativity $E_N(\rho)$, respectively, as a function of scaled time $\omega_1 t$. In the transient regime, all these results show an oscillatory behavior with a a period $T \approx 2\pi/\sum_i \omega_i$. The resonators are taken in the initialseparable groundstate; $\hat{\rho}(0) = \hat{\rho}_1 \otimes \hat{\rho}_2 = |0_1\rangle \langle 0_1| \otimes |0_2\rangle \langle 0_2|$. We considered Hilbert space size with ten phonons (photon) states for each mechanical (optical) resonator and verified the results do not change with the change in the Hilbert space size.

resonators. We assume the filtered spectra of the hot and cold bath, which is given by [126, 128]

$$\tilde{G}_l(\omega) = \frac{\kappa_l}{\pi}\frac{(\pi G_l(\omega))^2}{(\omega-(\omega_l^r+\Delta_l(\omega))^2+(\pi G_l(\omega))^2}. \tag{6.12}$$

Here κ_l being the interaction strength between the ancilla A and the bath filter, and ω_l^r is the resonance frequency. The Lamb shift induced by the environement is given by

$$\Delta_l(\omega) = P\int_o^\infty d\omega' \frac{G_l(\omega')}{\omega-\omega'}, \tag{6.13}$$

here P being the principal value. The bath modes which are closer to the resonance frequency ω_l^r are coupled more strongly to the ancilla.

6.4 Results

Here, we shall analyze the entanglement generation between the uncoupled mechanical resonators in our scheme shown in Fig. 6.1. For the numerical simulations, we assume the system parameters of an electro-mechanical system [2, 7], unless otherwise mentioned: $\omega_i = 2\pi\times 10$ MHz, $\omega_a = 2\pi\times 10$ GHz, $\gamma_i = 2\pi\times 100$ Hz, $\gamma_h = \gamma_c = 2\pi\times 5$ MHz, and $g_i = 2\pi\times 500$ KHz.

6.4.1 Non-degenerate resonators

First, we investigate the case in which we assume two mechanical resonators with different frequencies but the same dissipation rates and the thermal baths of the same temperatures. If we assume the cold and hot bath resonance frequencies $\omega_c^r = \omega_a$, and $\omega_h^r = \omega_a - \sum_i \omega_i$ in Eq. (6.12), respectively, the Liouville super-operators of the cold and hot baths take the form

$$\begin{aligned}
\mathcal{L}_c^d\tilde{\rho} &= \tilde{G}_c(\omega_a)\{D[\tilde{a}]+\alpha^3\sum_i D[\tilde{a}\tilde{b}_i^\dagger\tilde{b}_i]\}+\tilde{G}_c(-\omega_a)\{D[\tilde{a}^\dagger]+\sum_i\alpha^3 D[\tilde{a}^\dagger\tilde{b}_i^\dagger\tilde{b}_i]\},\\
\mathcal{L}_h^d\tilde{\rho} &= \alpha^3\big\{\tilde{G}_h(\omega_-)D[\tilde{a}\tilde{b}_1^\dagger\tilde{b}_2^\dagger]+\tilde{G}_h(-\omega_-)D[\tilde{a}^\dagger\tilde{b}_1\tilde{b}_2]\big\},\\
\mathcal{L}_i\tilde{\rho} &= G_i(\omega_i)D[\tilde{b}_i]+G_i(-\omega_i)D[\tilde{b}_i^\dagger],
\end{aligned} \tag{6.14}$$

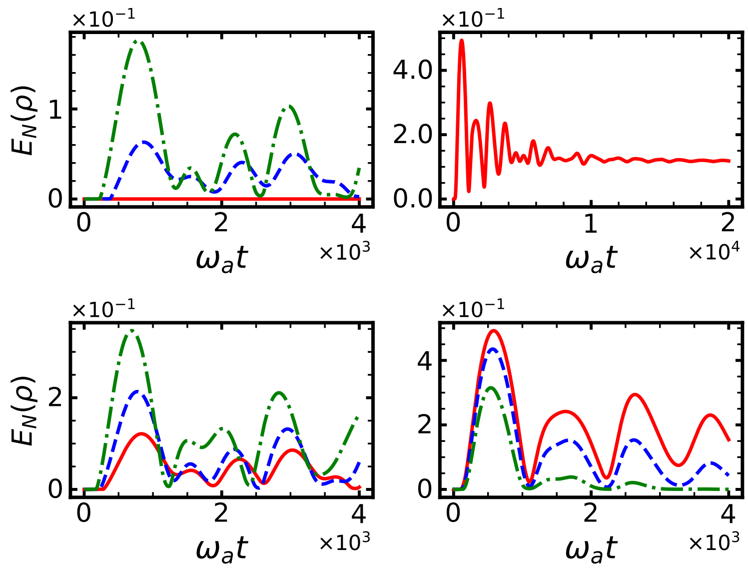

Figure 6.3: Entanglement in the case of non-degenerate resonators. The entanglement quantified by logarithmic negativity $E_N(\rho)$ as a function of scaled time $\omega_a t$. The entanglement is quantified by first solving Eq. (6.14) by numerical integration and then take the inverse tranformation [Eq. (3.10)] of the density matrix to get transformed $\hat{\rho}$ in the basis of the resonators, followed by computing $E_N(\rho)$ by using the definiation of logarithmic negativity given in Eq. (6.11). The initial state of the joint system is considered separable ground state; $\hat{\rho}(o) = \hat{\rho}_a \otimes \hat{\rho}_1 \otimes \hat{\rho}_2 = |g_a\rangle \langle g_a| \otimes |0_1\rangle \langle 0_1| \otimes |0_2\rangle \langle 0_2|$, here $|g_a\rangle$ indicates the ground state of the two-level ancilla. Parameters: $\omega_1 = 2\omega_2 = 2\pi \times 5$ MHz, $\omega_a = 2\pi \times 10$ GHz, $\gamma_i = 2\pi \times 100$ Hz, $\gamma_h = \gamma_c = 2\pi \times 500$ KHz, and $T_c = 65$ mK. All the parameters are scaled with the ancilla frequency ω_a. **(a)** red solid, blue dashed, and green dot-dashed curves are for $T_h = 1, 70, 300$ K, respectively. Here, $\alpha_i = 0.1$ and $T_i = 0.1$ K. **(b)** Long time entanglement $E_N(\rho)$ for $T_h = 300$ K, $\alpha_i = 0.2$ and $T_i = 0.05$ K. **(c)** Red solid, blue dashed, and green dot-dashed lines are associated with $\alpha_i = 0.05, 0.1, 0.2$, respectively. $T_i = 0.1$ K, $T_h = 300$ K. **(d)** Red solid, blue dashed, and green dot-dashed lines are for $T_i = 0.1, 0.15, 0.2$ K, respectively. $\alpha_i = 0.2$ and $T_h = 300$ K.

here $\mathcal{L}_i$ Liouville super-operators of the mechanical resonators remain unchanged and we define $\omega_- = \omega_a - \sum_i \omega_i$ and. We consider $\gamma_i \bar{n}_i \ll \alpha^3 \tilde{f}_h(\omega_-)$ and $T_h \gg T_i > T_c$ which makes $D_{\rm ent}$ the dominant over other dissipation channels in the system. According to our analysis in Sec. 6.3, the evolution of the mechanical resonators with $D_{\rm ent}$ as the dominant source may lead to entanglement between the resonators. Here we assume that the mechanical resonators are prepared in their ground states, and the initial state of the joint system is a separable ground state. The initial ground state of the resonators can be prepared in our scheme without the need for external control or work input by tuning the resonance frequencies of the hot and cold bath to the first lower sideband, which leads to simultaneous cooling of the mechanical resonators[see Eq. (6.12)] [28].

Fig. 6.3 shows the logarithmic negativity $E_N(\hat{\rho})$ as a function of the scaled time. For the case $T_h \sim T_i > T_c$, we observe no entanglement between the mechanical resonators because the mechanical dissipation rates dominate in this range of temperatures which destroys the quantum correlations between the resonators. However, for $T_c < T_i \ll T_h$, the entanglement between the mechanical resonators becomes non-zero and it increases significantly with the increase in the hot bath temperature T_h, as shown in Fig. 6.3(a). The long-time limit entanglement $E_N(\hat{\rho})$ quantified by logarithmic negativity is shown in Fig. 6.3(b). In comparision with Fig. 6.2, entanglement does not show periodicity in time for the case considered in Fig. 6.3. This is due to the fact that in Fig. 6.3 we consider two different resonators, which yield non-synchronized dynamical evolution of the mean phonon number $\hat{n}_i = \langle \hat{b}_i^\dagger \hat{b}_i \rangle$. In addition, Fig. 6.2 results indiacate that the mean phonon number $\hat{n}_i$ governs the dynamics of $E_N(\hat{\rho})$, as a result, non-synchronized dynamics of $\hat{n}_i$ results in the aperiodic behavior of entanglement $E_N(\hat{\rho})$. The entanglement increases monotonically with the increase in the coupling strength between the two-level ancilla and mechanical resonators, as shown in Fig. 6.3(c). Finally, we analyze the robustness of entanglement between the resonators against thermal dissipation induced by the mechanical baths in Fig. 6.3(d).

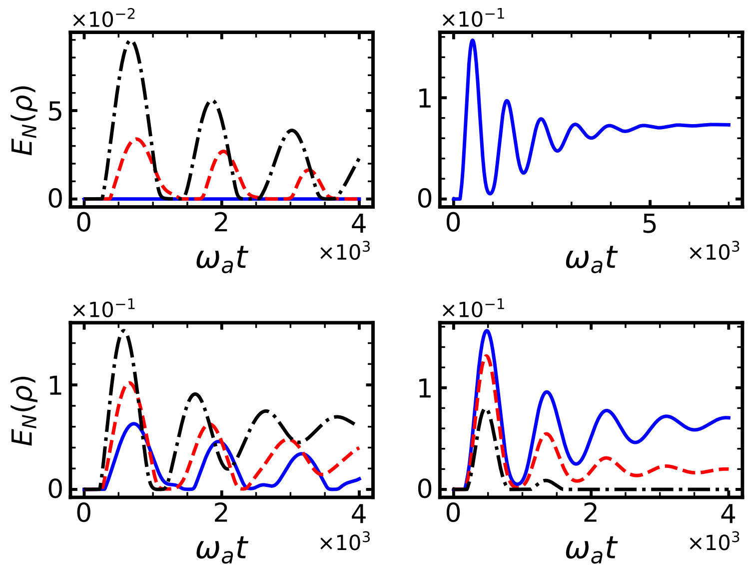

Figure 6.4: Entanglement in the case of degenerate resonators. The entanglement quantified by logarithmic negativity $E_N(\rho)$ as a function of scaled time $\omega_a t$. The entanglement is quantified by first solving Eq. (6.15) by numerical integration and then take the inverse tranformation [Eq. (3.10)] of the density matrix to get transformed $\hat{\rho}$ in the basis of the resonators, followed by computing $E_N(\rho)$ by using the definiation of logarithmic negativity given in Eq. (6.11). The initial state of the joint system is considered separable ground state; $\hat{\rho}(o) = \hat{\rho}_a \otimes \hat{\rho}_1 \otimes \hat{\rho}_2 = |g_a\rangle \langle g_a| \otimes |0_1\rangle \langle 0_1| \otimes |0_2\rangle \langle 0_2|$, here $|g_a\rangle$ indicates the ground state of the two-level ancilla. Parameters: $\omega_a = 2\pi \times 10$ GHz, $\omega_1 = \omega_2 = 2\pi \times 5$ MHz, $\gamma_h = \gamma_c = 2\pi \times 500$ KHz, $\gamma_i = 2\pi \times 100$ Hz, and $T_c = 65$ mK. **(a)** Blue solid, red dashed, and black dot-dashed curves are for $T_h = 1, 70, 300$ K, respectively. Here, $T_i = 0.1$ K and $\alpha_i = 0.1$. **(b)** Long time entanglement $E_N(\rho)$ for $\alpha_i = 0.2$, $T_h = 300$ K and $T_i = 0.05$ K. **(c)** Blue solid, red dashed, and black dot-dashed curves are for $\alpha_i = 0.05, 0.1, 0.2$, respectively. $T_h = 300$ K and $T_i = 0.1$. **(d)** Blue solid, red dashed, and black dot-dashed curves are for $T_i = 0.1, 0.15, 0.2$ K, respectively. $T_h = 300$ K and $\alpha_i = 0.2$.

6.4.2 Degenerate resonators

In the case of identical resonators $\omega_1 = \omega_2 = \Omega$, if we assume the resonance frequencies of the cold and hot bath as $\omega_c^r = \omega_a$ and $\omega_h^r = \omega_a - 2\Omega$, respectively, then the master equation (5.6) reduces to

$$
\begin{aligned}
\mathcal{L}_c^s\tilde{\rho} &= \mathcal{L}_c^d\tilde{\rho} + \alpha^3\tilde{G}_c(\omega_a)D[\tilde{a}\tilde{b}_1^\dagger\tilde{b}_2] + D[\tilde{a}\tilde{b}_1\tilde{b}_2^\dagger]\} + \alpha^3\tilde{G}_c(-\omega_a)\{D[\tilde{a}^\dagger\tilde{b}_1\tilde{b}_2^\dagger] + D[\tilde{a}^\dagger\tilde{b}_1^\dagger\tilde{b}_2]\},\\
\mathcal{L}_h^s\tilde{\rho} &= \mathcal{L}_h^d\tilde{\rho} + \alpha^3\{\tilde{G}_h(\omega_a - 2\Omega)\sum_i D[\tilde{a}\tilde{b}_i^{\dagger 2}] + \tilde{G}_h(-\omega_a + 2\Omega)\sum_i D[\tilde{a}^\dagger\tilde{b}_i^2]\},\\
\tilde{\mathcal{L}}_i\tilde{\rho} &= G_i(\Omega)D[\tilde{b}_i] + G_i(-\Omega)D[\tilde{b}_i^\dagger].
\end{aligned}
\tag{6.15}
$$

We note that as compared to Eq. (6.14), there are some additional terms in Eq. (6.15). The effect of additional terms in $\tilde{\mathcal{L}}_c^s\tilde{\rho}$ on entanglement is not significant because we consider $T_c \ll 1$ K in our results. However, the second and third terms of $\tilde{\mathcal{L}}_h^s\tilde{\rho}$ dissipation rates depends on T_h, consequently, have non-negligible negative effect on the entanglement. The results in Fig. 6.4 confirms the decrease in the entanglement for the degenerate resonators due to the presence of additional terms in Eq. (6.15).

6.5 Simultaneous entanglement and cooling of the resonators

In a typical optomechanical system, simultaneous entanglement and cooling of the resonators are not possible. The reason is that cooling of the resonators requires beam splitter interaction, and entanglement generation between the resonators is possible with two-mode squeezing interaction. Depending on the input laser drive frequency choice, one of these two interactions can be made resonant. Accordingly, entanglement and cooling occur in two separate sets of system parameters [1]. On the contrary, in our scheme, both entanglement and cooling of the resonators can co-occur. This is one of the key features of our scheme, and to the best of our knowledge, it is not reported in the bosonic out-of-equilibrium entanglement generation schemes too.

To investigate the entanglement and cooling of the resonators, after tracing the ancilla system A, Eq. (6.14) is given by

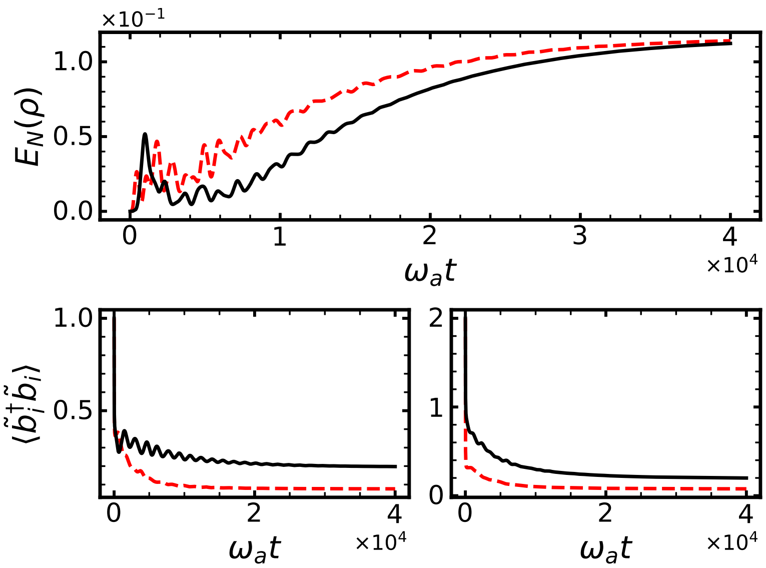

Figure 6.5: **(a)** Entanglement quantified by logarithmic negativity $E_N(\rho)$ between the mechanical resonators for different initial states as a function of scaled time $\omega_a t$. The dashed and solid lines indicate the initial thermal state with the mean phonon number $\bar{n}_i = 1, 2$, respectively. The entanglement is quantified by first solving Eq. (6.14) by numerical integration and then take the inverse transformation [Eq. (3.10)] of the density matrix to get transformed $\hat{\rho}$ in the basis of the resonators, followed by computing $E_N(\rho)$ by using the definition of logarithmic negativity given in Eq. (6.11). **(b)**, and **(c)** show the average excitation number $\langle \tilde{b}_i^\dagger \tilde{b}_i \rangle$ for the initial mean phonon number $\bar{n}_i = 1, 2$, as a function of scaled time $\omega_a t$, respectively. The dashed and solid curves are associated with the resonators R_1 and R_2, respectively. Parameters: $\omega_1 = 2\omega_2 = 2\pi \times 5$ MHz, $\omega_a = 2\pi \times 10$ GHz, $\gamma_h = \gamma_c = 2\pi \times 500$ KHz, $\alpha_i = 0.2$, $T_h = 300$ K, $\gamma_i = 2\pi \times 100$ Hz, $T_c = 65$ mK and $T_i = 0.05$ K.

$$\frac{d\tilde{\rho}}{dt} = \sum_i (\gamma_{i,\downarrow} D[\tilde{b}_i] + \gamma_{i,\uparrow} D[\tilde{b}_i^\dagger] + \gamma_d D[\tilde{b}_i^\dagger \tilde{b}_i]) + \Gamma_\downarrow D[\tilde{b}_1 \tilde{b}_2] + \Gamma_\uparrow D[\tilde{b}_1^\dagger \tilde{b}_2^\dagger], \quad (6.16)$$

here, we define

$$\begin{aligned}
\gamma_{i,\downarrow} &= G_i(\omega_i), \qquad \gamma_{i,\uparrow} = G_i(-\omega_i), \\
\Gamma_{\downarrow} &= \alpha^3 \tilde{G}(-\omega_-)\langle \tilde{n}_a + 1\rangle, \qquad \Gamma_{\uparrow} = \alpha^3 \tilde{G}(\omega_-)\langle \tilde{n}_a\rangle, \\
\gamma_d &= \alpha^3(\tilde{G}(\omega_a)\langle \tilde{n}_a\rangle + \tilde{G}(-\omega_a)\langle \tilde{n}_a + 1\rangle).
\end{aligned} \tag{6.17}$$

For sufficiently low excitations $\bar{n}_i$ in the resonators and $T_h \gg T_i > T_c$, the simultaneous cooling rate $\Gamma_{\downarrow}$ becomes larger than the simultaneous $\Gamma_{\uparrow}$ and the individual heating rates $\gamma_{i,\uparrow}$ of the resonators [28]. Accordingly, the cooling of the mechanical resonators is accompanied by entanglement generation (see Sec. 6.4.1). This analysis is confirmed by the numerical results presented in Fig. 6.5, which show that the cooling and entanglement co-occur in our scheme. Due to the different frequencies of the resonators, cooling rates are different [159, 28]. For the optimal performance of our scheme, the resonators should be considered in their ground states. However, this is not a requirement, as Fig. 6.5 shows that the thermal state with sufficiently low excitations $\bar{n}_i$ can also lead to entanglement between the resonators.

6.6 Summary

We proposed and analyzed an autonomous quantum thermal machine to generate transient and steady-state entanglement of two uncoupled macroscopic mechanical resonators. Unlike previous proposals on reservoir engineering, our quantum entanglement engine does not rely on external control or work input to generate entanglement between uncoupled macroscopic mechanical resonators. Entanglement between two uncoupled resonators is created by coupling them to a common incoherently driven two-level system or a harmonic oscillator. We proposed bath spectrum filtering to engineer desirable incoherent interaction with the thermal baths to create entanglement, which is a critical step in our scheme. Our numerical results showed a significantly large amount of entanglement established between the resonators in the absence of thermal equilibrium and even in the presence of the local dissipation of the resonators. In addition, the amount of early time entanglement showed a monotonic increase with the increase in a temperature gradient. To the best of our knowledge, there are no reported results of steady-state entanglement generation between uncoupled mechanical resonators using temperature gradient. If we consider circuit QED implementation of our scheme, then entanglement generation may be compared with Ref. [13] in which entanglement between two optical cavities is investigated in a similar setting. In our system, entanglement is almost two orders of magnitude larger than reported in Ref. [13].

The periodic oscillations in the entanglement are reported for the resonators of the same frequency. For the non-degenerate case, the periodicity breaks down due to the non-synchronized dynamics of the resonators. For the experimental realizations, several physical systems are conceivable such as optomechanical system [1], circuit QED [66, 228], and electro-mechanical systems [2].

Chapter 7

CONCLUSIONS

In Ch. 2 we have investigated a typical optomechanical system in which the optical and the mechanical resonators are each coupled to a thermal bath. We focused our analysis on the thermodynamic consistency of the master equations in the local and global approaches. At thermal equilibrium, the local and semi-global master equations predicted nonzero heat current through the system, violating the second law of thermodynamics. Upon describing the system dynamics with the global master equation, in which the jump operators become nonlocal, the heat currents vanish at thermal equilibrium. Hence, the global approach predicts the dynamics accurately compared to the local description of the system. In addition, in the presence of temperature bias, the local approaches predict the wrong direction of the heat flow, violating the second law of thermodynamics again. The addition of the phonon sideband in the global master equation recovers the validity of the second law in this regime. Our results show that the global approach is superior and consistent with the laws of thermodynamics in predicting the evolution of the optomechanical system in both weak and strong coupling regimes. Our analysis shows that the widely used assumption of the validity of the local master equation in the weak optomechanical coupling is incorrect. Significant qualitative and quantitative differences in the local and global approaches to predicting the heat current in both weak and strong coupling can facilitate testing our predictions in the current optomechanical systems.

We presented the discussion of heat management based on a two-qubit and typical optomechanical system in Ch. 3. We investigated the thermal management between independent thermal baths based on either two coupled qubits or two nonlinearly coupled harmonic oscillators. In particular, it was shown that two qubits coupled via asymmetric spin-spin interaction support the heat flow asymmetry between two thermal baths. In previous proposals, the heat rectification based on spins required either unequal bath dissipation rates or frequency difference of the coupled spins. In the case of equal dissipation and resonant spins, it was not possible to have thermal diode operation in the previous schemes. We showed that by considering asymmetric spin-spin interaction, a high-quality diode could be designed with equal dissipation rates with the baths and the same frequencies of the spins. Our advantageous proposal of the heat diode, contrary to the previous proposals, showed no trade-off between the heat flow and rectification factor. We explained the rectification by the preferential direction of the energy cycles induced by the thermal baths between the dressed states of the qubits. Some of the heat transport channels between the qubits were obstructed due to the asymmetry of the coupling strengths between the energy levels under the exchange of the temperature gradient.

We showed that it is possible to construct a quantum thermal transistor based on two nonlinearly coupled harmonic oscillators. The control of the base bath temperature showed the modulation of the heat current between the collector and emitter baths. It is possible to obtain substantial amplification factors by tuning either the coupling strength between the resonators or the relative magnitude of the frequencies of the resonators. The origin of the heat amplification is explained by the negative differential resistance, which appeared in our system due to the presence of the anharmonicity induced by the nonlinear coupling between the resonators. The control base heat current was associated with the lowest energy transition in the system, and the output heat currents were associated with the most significant energy transition. Accordingly, a slight change in the base heat current could control the large magnitudes of the collector and emitter heat currents.

In Ch. 4, we have proposed a quantum absorption refrigerator based on two-coupled qubits contrary to widely employed three-body interaction schemes. We considered an asymmetric interaction between the qubits and investigated the heat transfer through the qubits by employing a global master equation consistent with the laws of thermodynamics. The mechanism behind the cooling process was explained by considering energy cycles consisting of transitions between the dressed states of the qubits, which are induced by the thermal baths.We showed that heat could be removed from the cold by employing the bath spectrum filtering and selecting the system parameters within the cooling window. The reservoir engineering helped to attain the Carnot limit by not allowing the overlapping bath spectra; however, the cooling power at the Carnot limit vanishes as required by the second law of thermodynamics. In addition, we investigated a more practical bound, namely efficiency at maximum cooling power. In the strong coupling regime of the coupled qubits, we showed that our model could surpass the bound established on the efficiency at cooling power for previous QAR schemes. Finally, we allowed overlapping bath spectra, which results in the direct energy transfer between the thermal baths, and deteriorates the efficiency of the quantum absorption refrigerator.

We discussed the possibility of cooling multiple resonators via incoherent thermal baths in Ch. 5. We have proposed a simultaneous ground state cooling scheme of multiple degenerate or non-degenerate resonators in an optomechanical system. Unlike typical cooling schemes, which rely on an external coherent drive or work input for cooling, we employ only thermal baths to cool the mechanical resonators. In our scheme, bath spectrum filtering allowed us to cool identical multiple resonators simultaneously, which is not possible with typical cooling schemes due to dark mode obstructing the cooling process. We showed that an ultra-high temperature of the hot bath is required to cool the resonators to the quantum ground state. However, realizing such a bath with a very high temperature may be challenging. To overcome this challenge, we suggested an electromechanical system-based realization of our proposal in which it is possible to achieve ground state cooling with the experimentally realizable system parameters. Alternatively, we proposed to employ a spectrally filtered hot squeezed thermal bath with significant squeezing to cool the mechanical resonators. Our advantageous scheme of cooling enabled by bath spectrum filtering can be realized using various setups based on the optomechanical-like interaction between the cooling agent and the mechanical resonators.

Finally, Ch. 6 presents a scheme to engineer entanglement between two uncoupled resonators using a common ancilla driven by spectrally filtered hot and a cold bath. We showed that by suppressing unwanted energy transitions induced by the thermal bath, a significantly large entanglement between distant mechanical resonators becomes possible. A critical step towards realizing this scheme is bath spectrum filtering, which leads to effective two-mode squeezing-like interaction between the resonators. In addition, in our quantum thermal entanglement machine, both entanglement and cooling can co-occur, which is in variance with existing proposals on entanglement generation via reservoir engineering.

Quantum thermodynamics is a happy union between quantum mechanics and classical thermodynamics. Quantum mechanics introduces dynamics to classical thermodynamics. Following conventional learning by example approach of classical thermodynamics, the relationship between heat, work, and entropy production is investigated using thermal machines in quantum thermodynamics. Now the field has grown to the stage where proof-of-principal experiments have become possible such as the realization of a single-atom heat engine [229], superradiant quantum heat engine [230, 231], quantum absorption refrigerator [122], quantum heat valve [79], and quantum thermal diode [8] are some examples among many. Following this, the bulk of this thesis is devoted to investigating and designing efficient models for more practical self-contained quantum thermal machines. Often we restrict ourselves to linear interaction between quantum systems in these thermal machines. Here, we focus our efforts on nonlinear (optomechanical) interaction and show that introducing nonlinearity can improve a thermal machine's performance and allow it to perform thermal tasks in the parameters regime, which is otherwise impossible.

Most of the studies in quantum thermodynamics assume a linear system-environment interaction; moving forward, it would be interesting to consider nonlinear system-environment interaction in the designs of quantum thermal machines. Based on our current analysis, going beyond linear interaction can be fruitful. It would also be interesting to use non-thermal baths for the purpose of heat management. For instance, revisiting the model of the quantum thermal transistor by replacing the control bath with a squeezed thermal bath may enhance heat amplification. Another possible direction can be considering the nonlinear optomechanical system as a quantum thermometer. Our analysis shows that in the case of optomechanical coupling, sidebands appear in the master equation, and the generation of these sidebands may enhance the thermometer's sensitivity [232].

.1 Appendix A: System dynamics governed by LME or the DSME

The rate equations for the relevant dynamical observables of the optomechanical system considered in Fig. 2.1 determined from the DSME, Eq. (2.21), are given by

$$
\begin{aligned}
\frac{d}{dt}\langle\hat{n}_{\mathrm{a}}\rangle &= \kappa_{\mathrm{a}}(\bar{n}_{\mathrm{a}} - \langle\hat{n}_{\mathrm{a}}\rangle), \\
\frac{d}{dt}\langle\hat{p}\rangle &= -\omega_{\mathrm{b}}\langle\hat{q}\rangle - \frac{\kappa_{\mathrm{b}}}{2}\langle\hat{p}\rangle + 2g\langle\hat{n}_{\mathrm{a}}\rangle, \\
\frac{d}{dt}\langle\hat{q}\rangle &= \omega_{\mathrm{b}}\langle\hat{p}\rangle - \frac{\kappa_{\mathrm{b}}}{2}\langle\hat{q}\rangle + \kappa_{\mathrm{b}}\alpha\langle\hat{n}_{\mathrm{a}}\rangle, \\
\frac{d}{dt}\langle(\Delta\hat{n}_{\mathrm{a}})^2\rangle &= \kappa_{\mathrm{a}}\bar{n}_{\mathrm{a}} + (2\kappa_{\mathrm{a}}\bar{n}_{\mathrm{a}} + \kappa_{\mathrm{a}})\langle\hat{n}_{\mathrm{a}}\rangle - 2\kappa_{\mathrm{a}}\langle(\Delta\hat{n}_{\mathrm{a}})^2\rangle, \\
\frac{d}{dt}\langle\hat{n}_{\mathrm{a}},\hat{p}\rangle &= -\kappa\langle\hat{n}_{\mathrm{a}},\hat{p}\rangle - \omega_{\mathrm{b}}\langle\hat{n}_{\mathrm{a}},\hat{q}\rangle + 2g\langle(\Delta\hat{n}_{\mathrm{a}})^2\rangle, \\
\frac{d}{dt}\langle\hat{n}_{\mathrm{a}},\hat{q}\rangle &= -\kappa\langle\hat{n}_{\mathrm{a}},\hat{q}\rangle + \omega_{\mathrm{b}}\langle\hat{n}_{\mathrm{a}},\hat{p}\rangle + \kappa_{\mathrm{b}}\alpha\langle(\Delta\hat{n}_{\mathrm{a}})^2\rangle, \\
\frac{d}{dt}\langle\hat{n}_{\mathrm{b}}\rangle &= -\kappa_{\mathrm{b}}(\langle\hat{n}_{\mathrm{b}}\rangle - \bar{n}_{\mathrm{b}}) + g(\langle\hat{n}_{\mathrm{a}},\hat{p}\rangle + \langle\hat{n}_{\mathrm{a}}\rangle\langle\hat{p}\rangle) + \frac{\kappa_{\mathrm{b}}}{2}\alpha(\langle\hat{n}_{\mathrm{a}},\hat{q}\rangle + \langle\hat{n}_{\mathrm{a}}\rangle\langle\hat{q}\rangle), \\
\frac{d}{dt}\langle\hat{n}_{\mathrm{a}}\hat{p}\rangle &= -\kappa\langle\hat{n}_{\mathrm{a}}\hat{p}\rangle - \omega_{\mathrm{b}}\langle\hat{n}_{\mathrm{a}}\hat{q}\rangle + 2g\langle\hat{n}_{\mathrm{a}}^2\rangle + \kappa_{\mathrm{a}}\bar{n}_{\mathrm{a}}\langle\hat{p}\rangle, \\
\frac{d}{dt}\langle\hat{n}_{\mathrm{a}}\hat{q}\rangle &= -\kappa\langle\hat{n}_{\mathrm{a}}q\rangle + \alpha\kappa_{\mathrm{b}}\langle\hat{n}_{\mathrm{a}}^2\rangle + \kappa_{\mathrm{a}}\bar{n}_{\mathrm{a}}\langle q\rangle + \omega_{\mathrm{b}}\langle\hat{n}_{\mathrm{a}}\hat{p}\rangle, \text{ and} \\
\frac{d}{dt}\langle\hat{n}_{\mathrm{a}}^2\rangle &= \kappa_{\mathrm{a}}\bar{n}_{\mathrm{a}} - 2\kappa_{\mathrm{a}}\langle\hat{n}_{\mathrm{a}}^2\rangle + \kappa_{\mathrm{a}}(4\bar{n}_{\mathrm{a}} + 1)\langle\hat{n}_{\mathrm{a}}\rangle,
\end{aligned}
$$

here $\hat{q} = \hat{b}+\hat{b}^\dagger$, $\hat{p} = i(\hat{b}-\hat{b}^\dagger)$, and $\kappa = \kappa_{\mathrm{a}}+\kappa_{\mathrm{b}}/2$. The correlation functions between any two operators $\hat{o}_1$ and $\hat{o}_2$ are denoted by $\langle\hat{o}_1,\hat{o}_2\rangle := \langle\hat{o}_1\hat{o}_2\rangle - \langle\hat{o}_1\rangle\langle\hat{o}_2\rangle$. In the long time limit, the steady-state solutions of the dynamical equations are obtained as follows:

$$
\begin{aligned}
\langle \hat{n}_{\mathrm{a}} \rangle^{\mathrm{ss}} &= \bar{n}_{\mathrm{a}}, \\
\langle \hat{q} \rangle^{\mathrm{ss}} &= \left(\frac{8g\omega_{\mathrm{b}} + 2\alpha\kappa_{\mathrm{b}}^2}{4\omega_{\mathrm{b}}^2 + \kappa_{\mathrm{b}}^2} \right) \langle \hat{n}_{\mathrm{a}} \rangle^{\mathrm{ss}}, \\
\langle \hat{p} \rangle^{\mathrm{ss}} &= \left(\frac{4g\kappa_{\mathrm{b}} - 4\alpha\omega_{\mathrm{b}}\kappa_{\mathrm{b}}}{4\omega_{\mathrm{b}}^2 + \kappa_{\mathrm{b}}^2} \right) \langle \hat{n}_{\mathrm{a}} \rangle^{\mathrm{ss}}, \\
\langle (\Delta \hat{n}_{\mathrm{a}})^2 \rangle^{\mathrm{ss}} &= \bar{n}_{\mathrm{a}}(\bar{n}_{\mathrm{a}} + 1), \\
\langle \hat{n}_{\mathrm{a}}, \hat{p} \rangle^{\mathrm{ss}} &= \frac{2g\kappa_{\mathrm{a}}}{\omega_{\mathrm{b}}^2 + \kappa^2} \langle (\Delta \hat{n}_{\mathrm{a}})^2 \rangle^{\mathrm{ss}}, \\
\langle \hat{n}_{\mathrm{a}}, \hat{q} \rangle^{\mathrm{ss}} &= \left(\frac{2g\omega_{\mathrm{b}} + \alpha\kappa_{\mathrm{b}}\kappa}{\omega_{\mathrm{b}}^2 + \kappa^2} \right) \langle (\Delta \hat{n}_{\mathrm{a}})^2 \rangle^{\mathrm{ss}}, \\
\langle \hat{n}_{\mathrm{b}} \rangle^{\mathrm{ss}} &= \bar{n}_{\mathrm{b}} + \frac{g}{\kappa_{\mathrm{b}}} (\langle \hat{n}_{\mathrm{a}}, \hat{p} \rangle^{\mathrm{ss}} + \langle \hat{n}_{\mathrm{a}} \rangle^{\mathrm{ss}} \langle \hat{p} \rangle^{\mathrm{ss}}) + \frac{\alpha}{2} (\langle \hat{n}_{\mathrm{a}}, \hat{q} \rangle^{\mathrm{ss}} + \langle \hat{n}_{\mathrm{a}} \rangle^{\mathrm{ss}} \langle \hat{q} \rangle^{\mathrm{ss}}), \\
\langle \hat{n}_{\mathrm{a}} \hat{q} \rangle^{\mathrm{ss}} &= A \Big[\kappa_{\mathrm{a}} \bar{n}_{\mathrm{a}} (\kappa \langle q \rangle^{\mathrm{ss}} + \omega_{\mathrm{b}} \langle p \rangle^{\mathrm{ss}}) + (\kappa\alpha\kappa_{\mathrm{b}} + 2g\omega_{\mathrm{b}}) \langle \hat{n}_{\mathrm{a}}^2 \rangle^{\mathrm{ss}} \Big], \\
\langle \hat{n}_{\mathrm{a}} \hat{p} \rangle^{\mathrm{ss}} &= A \Big[\kappa_{\mathrm{a}} \bar{n}_{\mathrm{a}} (\kappa \langle p \rangle^{\mathrm{ss}} - \omega_{\mathrm{b}} \langle q \rangle^{\mathrm{ss}}) + (2\kappa g - \alpha\kappa_{\mathrm{b}}\omega_{\mathrm{b}}) \langle \hat{n}_{\mathrm{a}}^2 \rangle \Big], \text{ and} \\
\langle \hat{n}_{\mathrm{a}}^2 \rangle^{\mathrm{ss}} &= \bar{n}_{\mathrm{a}}(2\bar{n}_{\mathrm{a}} + 1),
\end{aligned}
$$

where $A = 1/\left(\kappa^2 + \omega_{\mathrm{m}}^2\right)$ and $\bar{n}_{\mathrm{a}} := \bar{n}_{\mathrm{a}}(\omega_{\mathrm{a}})$. By setting $\alpha = 0$, the corresponding equations can be found for the LME.

.2 *Appendix B: Heat currents using the LME or the DSME*

The heat currents from the optical and the mechanical resonator baths are given by

$$
\begin{aligned}
\mathcal{J}_{\mathrm{a}} &= \kappa_{\mathrm{a}}(\omega_{\mathrm{a}} - g\langle \hat{q} \rangle)(\bar{n}_{\mathrm{a}} - \langle \hat{n}_{\mathrm{c}} \rangle) + g\kappa_{\mathrm{a}} \langle \hat{n}_{\mathrm{a}}, \hat{q} \rangle, \text{ and} \\
\mathcal{J}_{\mathrm{b}} &= \omega_{\mathrm{b}}\kappa_{\mathrm{b}}(\bar{n}_{\mathrm{b}} - \langle \hat{n}_{\mathrm{b}} \rangle) + g\kappa_{\mathrm{b}}(\langle \hat{n}_{\mathrm{b}}, \hat{q} \rangle + \langle \hat{n}_{\mathrm{a}} \rangle \langle \hat{q} \rangle) - g\alpha\kappa_{\mathrm{b}}(\langle (\Delta \hat{n}_{\mathrm{a}})^2 \rangle + \langle \hat{n}_{\mathrm{a}} \rangle^2).
\end{aligned}
$$

At steady-state, the heat currents evaluate to

$$
\begin{aligned}
\mathcal{J}_{\mathrm{a}}^{\mathrm{ss}} &= g\kappa_{\mathrm{a}} \langle \hat{n}_{\mathrm{a}}, \hat{q} \rangle^{\mathrm{ss}} \text{ and} \\
\mathcal{J}_{\mathrm{b}}^{\mathrm{ss}} &= -g\kappa_{\mathrm{a}} \langle \hat{n}_{\mathrm{a}}, \hat{q} \rangle^{\mathrm{ss}}.
\end{aligned}
$$

For the case of the LME, the heat flows can be obtained by setting $\alpha = 0$.

.3 Appendix C: The steady-state heat currents

The steady-state heat currents can be evaluated by writing the equations of motion for the relevant dynamical observables from the master equation (4.13), and given by

$$\begin{aligned}
\frac{d}{dt}\langle\tilde{\sigma}^z_{\mathrm{L}}\rangle &= \cos^2\theta[G_{\mathrm{L}}(-\omega_{\mathrm{L}})\langle\mathbb{A}\rangle - G_{\mathrm{L}}(\omega_{\mathrm{L}})\langle\mathbb{B}\rangle] \quad (1)\\
&+\frac{1}{2}\sin^2\theta[G_{\mathrm{L}}(\omega_-)\langle\mathbb{A}\mathbb{D}\rangle - G_{\mathrm{L}}(-\omega_-)\langle\mathbb{B}\mathbb{C}\rangle + G_{\mathrm{L}}(-\omega_+)\langle\mathbb{A}\mathbb{C}\rangle - G_{\mathrm{L}}(\omega_+)\langle\mathbb{B}\mathbb{D}\rangle]\\
\frac{d}{dt}\langle\hat{\tilde{\sigma}}^z_{\mathrm{R}}\rangle &= \cos^2\theta[G_{\mathrm{R}}(-\Omega)\langle\mathbb{C}\rangle - G_{\mathrm{R}}(\Omega)\langle\mathbb{D}\rangle] \quad (2)\\
&+\frac{1}{2}\sin^2\theta[-G_{\mathrm{L}}(\omega_-)\langle\mathbb{A}\mathbb{D}\rangle + G_{\mathrm{L}}(-\omega_-)\langle\mathbb{B}\mathbb{C}\rangle + G_{\mathrm{L}}(-\omega_+)\langle\mathbb{A}\mathbb{C}\rangle - G_{\mathrm{L}}(\omega_+)\langle\mathbb{B}\mathbb{D}\rangle]\\
\frac{d}{dt}\langle\tilde{\sigma}^z_{\mathrm{L}}\tilde{\sigma}^z_{\mathrm{R}}\rangle &= \cos^2\theta[G_{\mathrm{L}}(-\omega_{\mathrm{L}})\langle\mathbb{A}\tilde{\sigma}^z_{\mathrm{R}}\rangle - G_{\mathrm{L}}(\omega_{\mathrm{L}})\langle\mathbb{B}\tilde{\sigma}^z_{\mathrm{R}}\rangle + G_{\mathrm{R}}(-\Omega)\langle\mathbb{D}\tilde{\sigma}^z_{\mathrm{L}}\rangle - G_{\mathrm{R}}(\Omega)\langle\mathbb{C}\tilde{\sigma}^z_{\mathrm{L}}\rangle] \quad (3)
\end{aligned}$$

here we have defined $\mathbb{A} = (\mathbb{1} - \tilde{\sigma}^z_{\mathrm{L}})$, $\mathbb{B} = (\mathbb{1} + \tilde{\sigma}^z_{\mathrm{L}})$, $\mathbb{C} = (\mathbb{1} - \tilde{\sigma}^z_{\mathrm{R}})$, and $\mathbb{D} = (\mathbb{1} + \tilde{\sigma}^z_{\mathrm{R}})$. Accordingly, the heat currents are given by

$$\begin{aligned}
\mathcal{J}_{\mathrm{L}} &= \frac{1}{2}\omega_{\mathrm{L}}\cos^2\theta[G_{\mathrm{L}}(-\omega_{\mathrm{L}})\langle\mathbb{A}\rangle - G_{\mathrm{L}}(\omega_{\mathrm{L}})\langle\mathbb{B}\rangle] \quad (4)\\
&+ \frac{1}{4}\sin^2\theta[\omega_1 G_{\mathrm{L}}(-\omega_1)\langle\mathbb{B}\mathbb{C}\rangle - \omega_1 G_{\mathrm{L}}(\omega_1)\langle\mathbb{A}\mathbb{D}\rangle\\
&- \omega_2 G_{\mathrm{L}}(\omega_2)\langle\mathbb{B}\mathbb{D}\rangle + \omega_2 G_{\mathrm{L}}(-\omega_2)\langle\mathbb{A}\mathbb{C}\rangle],\\
\mathcal{J}_{\mathrm{R}} &= \frac{1}{2}\Omega\cos^2\theta[G_{\mathrm{R}}(-\Omega)\langle\mathbb{C}\rangle - G_{\mathrm{R}}(\Omega)\langle\mathbb{D}\rangle]. \quad (5)
\end{aligned}$$

The analytical expressions for the heat currents are too cumbersome to report here.

.4 Appendix D: Heat Currents for coupled qubits

In case of filtered bath spectra, the steady-state heat currents can be determined by calculating the rate equations from the master equation (4.18), and given by

$$\begin{aligned}
\frac{d}{dt}\langle\tilde{\sigma}^+_A\tilde{\sigma}^-_A\rangle &= -c^2\Gamma_h(1+e^{-\frac{\omega_h}{T_h}})\langle\tilde{\sigma}^+_A\tilde{\sigma}^-_A\rangle + c^2\Gamma_h e^{-\frac{\omega_h}{T_h}}\\
&+ s^2\Gamma_w(\langle\tilde{\sigma}^+_B\tilde{\sigma}^-_B\rangle - \langle\tilde{\sigma}^+_A\tilde{\sigma}^-_A\rangle), \quad (6)\\
\frac{d}{dt}\langle\tilde{\sigma}^+_B\tilde{\sigma}^-_B\rangle &= -c^2\Gamma_c(1+e^{-\frac{\omega_c}{T_c}})\langle\tilde{\sigma}^+_B\tilde{\sigma}^-_B\rangle + c^2\Gamma_c e^{-\frac{\omega_c}{T_c}}\\
&+ s^2\Gamma_w(\langle\tilde{\sigma}^+_A\tilde{\sigma}^-_A\rangle - \langle\tilde{\sigma}^+_B\tilde{\sigma}^-_B\rangle), \quad (7)
\end{aligned}$$

here we have considered $T_w \to \infty$. As a result, the higher order correlations $\langle \tilde{\sigma}_A^+ \tilde{\sigma}_A^- \tilde{\sigma}_B^+ \tilde{\sigma}_B^- \rangle$ become zero. In addition, $s = \sin\theta$, $c = \cos\theta$ and

$$\Gamma_\alpha = \omega_\alpha \kappa_\alpha \bar{n}(\omega_\alpha), \tag{8}$$

In the high temperature limint of the work-like bath, the heat currents are given by

$$\mathcal{J}_\alpha = C\omega_\alpha, \tag{9}$$

and

$$C = \frac{c^2 s^2 \Gamma_w \Gamma_h \Gamma_c (e^{\frac{\omega_c}{T_c}} - e^{\frac{\omega_c}{T_h}})}{c^2 \Gamma_w \Gamma_c (1 + e^{\frac{\omega_c}{T_c}})(1 + e^{\frac{\omega_h}{T_h}}) + s^2 \Gamma_w [e^{\frac{\omega_h}{T_h}} \Gamma_c + e^{\frac{\omega_c}{T_c}} (\Gamma_w + e^{\frac{\omega_h}{T_h}} (\Gamma_w + \Gamma_c))]}. \tag{10}$$

.5 *Appendix E: Dynamics of the system*

If we consider the spectrally filtered bath spectra of the hot and cold baths coupled to the optical mode of the optomechanical system, then the master equation governing the dynamics is given by

$$\begin{aligned}
\mathcal{L}_c &= \gamma_c (D[\tilde{a}] + e^{-\beta_c \omega_a} D[\tilde{a}^\dagger]), && (11)\\
\mathcal{L}_h &= \gamma_h \alpha_1^2 \big(D[\tilde{a}\tilde{b}_1^\dagger] + e^{-\beta_h \omega_+} D[\tilde{a}^\dagger \tilde{b}_1]\big), && (12)\\
\mathcal{L}_1 &= \gamma_1 (D[\tilde{b}_1] + e^{-\beta_1 \omega_1} D[\tilde{b}_1^\dagger]). && (13)
\end{aligned}$$

Here γ_c, γ_h, and γ_1 are the relaxation rates, which depend on the choice of the spectral density of the bath. In addition, β_1, β_h, and β_c indicates the inverse temperatures of the mechanical, hot and cold baths, respectively. In the limit, $T_h \to \infty$, the rate equations for the average excitation number read

$$\begin{aligned}
\frac{d}{dt}\langle \tilde{n}_a \rangle = &- \gamma_c (1 - e^{-\beta_c \omega_a}) \langle \tilde{n}_a \rangle + \gamma_c e^{-\beta_c \omega_a} \\
&+ \gamma_h (\langle \tilde{n}_1 \rangle - \langle \tilde{n}_a \rangle), && (14)\\
\frac{d}{dt}\langle \tilde{n}_1 \rangle = &- \gamma_1 (1 - e^{-\beta_1 \omega_1}) \langle \tilde{n}_1 \rangle + \gamma_1 e^{-\beta_1 \omega_1} \\
&+ \gamma_h (\langle \tilde{n}_a \rangle - \langle \tilde{n}_1 \rangle), && (15)
\end{aligned}$$

and the steady-state average excitation number of mechanical resonator evaluate to

$$\langle\tilde{n}_1\rangle_{\rm ss} = \frac{\gamma_c e^{-\beta_c\omega_a} + \gamma_1 e^{-\beta_1\omega_1}}{-\gamma_c e^{-\beta_c\omega_a} - \gamma_1 e^{-\beta_1\omega_1} + \gamma_c + \gamma_1}. \tag{16}$$

In the case of the Ohmic spectral densities of the thermal baths, Eq. (16) takes the form

$$\langle\tilde{n}_1\rangle_{\rm ss} = \frac{\omega_a\kappa_c\bar{n}_c + \omega_1\kappa_1\bar{n}_1}{\omega_a\kappa_c + \omega_1\kappa_1}, \tag{17}$$

this equation shows that it is possible to cool the mechanical resonator to its ground state by considering appropriate system parameters.

BIBLIOGRAPHY

[1] Markus Aspelmeyer, Tobias J. Kippenberg, and Florian Marquardt. Cavity optomechanics. *Rev. Mod. Phys.*, 86:1391–1452, Dec 2014.

[2] M. D. LaHaye, J. Suh, P. M. Echternach, K. C. Schwab, and M. L. Roukes. Nanomechanical measurements of a superconducting qubit. *Nature*, 459(7249):960–964, Jun 2009.

[3] J. D. Teufel, T. Donner, Dale Li, J. W. Harlow, M. S. Allman, K. Cicak, A. J. Sirois, J. D. Whittaker, K. W. Lehnert, and R. W. Simmonds. Sideband cooling of micromechanical motion to the quantum ground state. *Nature*, 475(7356):359–363, Jul 2011.

[4] J. D. Teufel, Dale Li, M. S. Allman, K. Cicak, A. J. Sirois, J. D. Whittaker, and R. W. Simmonds. Circuit cavity electromechanics in the strong-coupling regime. *Nature*, 471(7337):204–208, Mar 2011.

[5] I. C. Rodrigues, D. Bothner, and G. A. Steele. Coupling microwave photons to a mechanical resonator using quantum interference. *Nat. Commun.*, 10(1):5359, Nov 2019.

[6] T. Rocheleau, T. Ndukum, C. Macklin, J. B. Hertzberg, A. A. Clerk, and K. C. Schwab. Preparation and detection of a mechanical resonator near the ground state of motion. *Nature*, 463(7277):72–75, Jan 2010.

[7] Francesco Massel, Sung Un Cho, Juha-Matti Pirkkalainen, Pertti J. Hakonen, Tero T. Heikkilä, and Mika A. Sillanpää. Multimode circuit optomechanics near the quantum limit. *Nat. Commun.*, 3(1):987, Aug 2012.

[8] Jorden Senior, Azat Gubaydullin, Bayan Karimi, Joonas T. Peltonen, Joachim Ankerhold, and Jukka P. Pekola. Heat rectification via a superconducting artificial atom. *Commun. Phys.*, 3(1):40, Feb 2020.

[9] Jake Iles-Smith, Neill Lambert, and Ahsan Nazir. Environmental dynamics, correlations, and the emergence of noncanonical equilibrium states in open quantum systems. *Phys. Rev. A*, 90:032114, Sep 2014.

[10] Christian Arenz, Cecilia Cormick, David Vitali, and Giovanna Morigi. Generation of two-mode entangled states by quantum reservoir engineering. *J. Phys. B: At. Mol. Opt. Phys.*, 46(22):224001, nov 2013.

[11] Hendrik Weimer, Markus Müller, Igor Lesanovsky, Peter Zoller, and Hans Peter Büchler. A rydberg quantum simulator. *Nat. Phys.*, 6(5):382–388, May 2010.

[12] Susanne Pielawa, Giovanna Morigi, David Vitali, and Luiz Davidovich. Generation of einstein-podolsky-rosen-entangled radiation through an atomic reservoir. *Phys. Rev. Lett.*, 98:240401, Jun 2007.

[13] M. B. Plenio and S. F. Huelga. Entangled light from white noise. *Phys. Rev. Lett.*, 88:197901, Apr 2002.

[14] H. P. Breuer and F. Petruccione. *The theory of open quantum systems*. Oxford university press, 2002.

[15] Amikam Levy and Ronnie Kosloff. The local approach to quantum transport may violate the second law of thermodynamics. *Europhys. Lett.*, 107(2):20004, jul 2014.

[16] P. P. Hofer, M. P. Llobet, D. M. Miranda, G. Haack, R. Silva, J. B. Brask, and N. Brunner. Markovian master equations for quantum thermal machines: local versus global approach. *New. J. Phys.*, 19(123037):123037, 2017.

[17] P. D. Manrique, F. Rodríguez, L. Quiroga, and N. F. Johnson. Nonequilibrium quantum systems: Divergence between global and local descriptions. *Adv. Condens. Matter Phys.*, 19(615727):615727, 2015.

[18] J. O. González, L. A. Correa, G. Nocerino, J. P. Palao, D. Alonso, and G. Adesso. Testing the validity of the 'local' and 'global' gkls master equations on an exactly solvable model. *Open Syst. Inf. Dyn.*, 24(1740010):1740010, 2017.

[19] J. Cohen-Tannoudji, C. Dupont-Roc and G. Grynberg. *Atom–photon interactions*. Wiley, 2002.

[20] H. Breuer and F. Petruccione. *The Theory of Open Quantum Systems*. Oxford University Press, 2002.

[21] S. Kryszewski and C. K. Justyna. Markovian master equations: a critical study. *arXiv:0801.1757*, 2008.

[22] Ángel Rivas, A Douglas K Plato, Susana F Huelga, and Martin B Plenio. Markovian master equations: a critical study. *New J. Phys.*, 12(11):113032, 2010.

[23] M. Tahir Naseem, André Xuereb, and Özgür E. Müstecaplıoğlu. Thermodynamic consistency of the optomechanical master equation. *Phys. Rev. A*, 98:052123, Nov 2018.

[24] Cahit Karg ı, M. Tahir Naseem, Tomá š Opatrný, Özgür E. Müstecaplıoğlu, and Gershon Kurizki. Quantum optical two-atom thermal diode. *Phys. Rev. E*, 99:042121, Apr 2019.

[25] Vipul Upadhyay, M. Tahir Naseem, Rahul Marathe, and Özgür E. Müstecaplıoğlu. Heat rectification by two qubits coupled with dzyaloshinskii-moriya interaction. *Phys. Rev. E*, 104:054137, Nov 2021.

[26] M. Tahir Naseem, Avijit Misra, Özgür E. Müstecaplioğlu, and Gershon Kurizki. Minimal quantum heat manager boosted by bath spectral filtering. *Phys. Rev. Research*, 2:033285, Aug 2020.

[27] M Tahir Naseem, Avijit Misra, and Özgür E Müstecaplıoğlu. Two-body quantum absorption refrigerators with optomechanical-like interactions. *Quantum Sci. Technol.*, 5(3):035006, jun 2020.

[28] Muhammad Tahir Naseem and Özgür E. Müstecaplıoğlu. Ground-state cooling of mechanical resonators by quantum reservoir engineering. *Commun. Phys.*, 4(1):95, May 2021.

[29] M Tahir Naseem and Özgür E Müstecaplıoğlu. Engineering entanglement between resonators by hot environment. *Quantum Sci. Technol.*, 7(4):045012, jul 2022.

[30] K. Hornberger. *Introduction to Decoherence Theory*, pages 221–276. Springer Berlin Heidelberg, Berlin, Heidelberg, 2009.

[31] Gershon Kurizki, Patrice Bertet, Yuimaru Kubo, Klaus Mølmer, David Petrosyan, Peter Rabl, and Jörg Schmiedmayer. Quantum technologies with hybrid systems. *Proc. Nat.l Acad. Sci.*, 112(13):3866–3873, 2015.

[32] H. J. Carmichael. *Statistical Methods in Quantum Optics 1*, pages 361–361. Springer Berlin Heidelberg, Berlin, Heidelberg, 1999.

[33] P. Rabl. Photon blockade effect in optomechanical systems. *Phys. Rev. Lett.*, 107:063601, Aug 2011.

[34] A. Nunnenkamp, K. Børkje, and S. M. Girvin. Single-photon optomechanics. *Phys. Rev. Lett.*, 107:063602, Aug 2011.

[35] Ting Hong, Huan Yang, Haixing Miao, and Yanbei Chen. Open quantum dynamics of single-photon optomechanical devices. *Phys. Rev. A*, 88:023812, Aug 2013.

[36] Jie-Qiao Liao, H. K. Cheung, and C. K. Law. Spectrum of single-photon emission and scattering in cavity optomechanics. *Phys. Rev. A*, 85:025803, Feb 2012.

[37] Bing He. Quantum optomechanics beyond linearization. *Phys. Rev. A*, 85:063820, Jun 2012.

[38] Xun-Wei Xu, Yuan-Jie Li, and Yu-xi Liu. Photon-induced tunneling in optomechanical systems. *Phys. Rev. A*, 87:025803, Feb 2013.

[39] Andreas Kronwald, Max Ludwig, and Florian Marquardt. Full photon statistics of a light beam transmitted through an optomechanical system. *Phys. Rev. A*, 87:013847, Jan 2013.

[40] Jie-Qiao Liao and C. K. Law. Correlated two-photon scattering in cavity optomechanics. *Phys. Rev. A*, 87:043809, Apr 2013.

[41] Gao-Feng Xu and C. K. Law. Dark states of a moving mirror in the single-photon strong-coupling regime. *Phys. Rev. A*, 87:053849, May 2013.

[42] William Marshall, Christoph Simon, Roger Penrose, and Dik Bouwmeester. Towards quantum superpositions of a mirror. *Phys. Rev. Lett.*, 91:130401, Sep 2003.

[43] S. Mancini, V. I. Man'ko, and P. Tombesi. Ponderomotive control of quantum macroscopic coherence. *Phys. Rev. A*, 55:3042–3050, Apr 1997.

[44] C. K. Law. Interaction between a moving mirror and radiation pressure: A hamiltonian formulation. *Phys. Rev. A*, 51:2537–2541, Mar 1995.

[45] Subhadeep Gupta, Kevin L. Moore, Kater W. Murch, and Dan M. Stamper-Kurn. Cavity nonlinear optics at low photon numbers from collective atomic motion. *Phys. Rev. Lett.*, 99:213601, Nov 2007.

[46] Matt Eichenfield, Jasper Chan, Ryan M. Camacho, Kerry J. Vahala, and Oskar Painter. Optomechanical crystals. *Nature*, 462(7269):78–82, Nov 2009.

[47] Ying-Dan Wang and Aashish A. Clerk. Using interference for high fidelity quantum state transfer in optomechanics. *Phys. Rev. Lett.*, 108:153603, Apr 2012.

[48] K. Stannigel, P. Rabl, A. S. Sørensen, P. Zoller, and M. D. Lukin. Optomechanical transducers for long-distance quantum communication. *Phys. Rev. Lett.*, 105:220501, Nov 2010.

[49] K. Stannigel, P. Komar, S. J. M. Habraken, S. D. Bennett, M. D. Lukin, P. Zoller, and P. Rabl. Optomechanical quantum information processing with photons and phonons. *Phys. Rev. Lett.*, 109:013603, Jul 2012.

[50] K. Stannigel, P. Rabl, A. S. Sørensen, M. D. Lukin, and P. Zoller. Optomechanical transducers for quantum-information processing. *Phys. Rev. A*, 84:042341, Oct 2011.

[51] Keye Zhang, Francesco Bariani, and Pierre Meystre. Theory of an optomechanical quantum heat engine. *Phys. Rev. A*, 90:023819, Aug 2014.

[52] Ying Dong, F. Bariani, and P. Meystre. Phonon cooling by an optomechanical heat pump. *Phys. Rev. Lett.*, 115:223602, Nov 2015.

[53] Ying Dong, Keye Zhang, Francesco Bariani, and Pierre Meystre. Work measurement in an optomechanical quantum heat engine. *Phys. Rev. A*, 92:033854, Sep 2015.

[54] M Brunelli, A Xuereb, A Ferraro, G De Chiara, N Kiesel, and M Paternostro. Out-of-equilibrium thermodynamics of quantum optomechanical systems. *New J. Phys.*, 17(3):035016, mar 2015.

[55] A Mari, A Farace, and V Giovannetti. Quantum optomechanical piston engines powered by heat. *J. Phys. B: At. Mol. Opt. Phys.*, 48(17):175501, jul 2015.

[56] D. Gelbwaser-Klimovsky and G. Kurizki. Work extraction from heat-powered quantized optomechanical setups. *Sci. Rep.*, 5(1):7809, Jan 2015.

[57] M. Bathaee and A. R. Bahrampour. Optimal control of the power adiabatic stroke of an optomechanical heat engine. *Phys. Rev. E*, 94:022141, Aug 2016.

[58] Keye Zhang and Weiping Zhang. Quantum optomechanical straight-twin engine. *Phys. Rev. A*, 95:053870, May 2017.

[59] Keye Zhang, Francesco Bariani, and Pierre Meystre. Quantum optomechanical heat engine. *Phys. Rev. Lett.*, 112:150602, Apr 2014.

[60] Ali Ü. C. Hardal, Nur Aslan, C. M. Wilson, and Özgür E. Müstecaplıoğlu. Quantum heat engine with coupled superconducting resonators. *Phys. Rev. E*, 96:062120, Dec 2017.

[61] M. Tahir Naseem and Özgür E. Müstecaplioğlu. Quantum heat engine with a quadratically coupled optomechanical system. *J. Opt. Soc. Am. B*, 36(11):3000–3008, Nov 2019.

[62] Najmeh Etehadi Abari, Giulia Vittoria De Angelis, Stefano Zippilli, and David Vitali. An optomechanical heat engine with feedback-controlled in-loop light. *New J. Phys.*, 21(9):093051, sep 2019.

[63] André Xuereb, Alberto Imparato, and Aurélien Dantan. Heat transport in harmonic oscillator systems with thermal baths: application to optomechanical arrays. *New J. Phys.*, 17(5):055013, may 2015.

[64] Anton Frisk Kockum, Adam Miranowicz, Simone De Liberato, Salvatore Savasta, and Franco Nori. Ultrastrong coupling between light and matter. *Nature Reviews Physics*, 1(1):19–40, Jan 2019.

[65] J. R. Johansson, G. Johansson, and Franco Nori. Optomechanical-like coupling between superconducting resonators. *Phys. Rev. A*, 90:053833, Nov 2014.

[66] C. Eichler and J. R. Petta. Realizing a circuit analog of an optomechanical system with longitudinally coupled superconducting resonators. *Phys. Rev. Lett.*, 120:227702, May 2018.

[67] Dan Hu, Shang-Yu Huang, Jie-Qiao Liao, Lin Tian, and Hsi-Sheng Goan. Quantum coherence in ultrastrong optomechanics. *Phys. Rev. A*, 91:013812, Jan 2015.

[68] Ronnie Kosloff. Quantum thermodynamics: A dynamical viewpoint. *Entropy*, 15(6):2100–2128, 2013.

[69] Dvira Segal and Abraham Nitzan. Spin-boson thermal rectifier. *Phys. Rev. Lett.*, 94:034301, Jan 2005.

[70] Olli-Pentti Saira, Matthias Meschke, Francesco Giazotto, Alexander M. Savin, Mikko Möttönen, and Jukka P. Pekola. Heat transistor: Demonstration of gate-controlled electronic refrigeration. *Phys. Rev. Lett.*, 99:027203, Jul 2007.

[71] Dvira Segal. Single mode heat rectifier: Controlling energy flow between electronic conductors. *Phys. Rev. Lett.*, 100:105901, Mar 2008.

[72] Yuecheng Shen, Matthew Bradford, and Jung-Tsung Shen. Single-photon diode by exploiting the photon polarization in a waveguide. *Phys. Rev. Lett.*, 107:173902, Oct 2011.

[73] T. Werlang, M. A. Marchiori, M. F. Cornelio, and D. Valente. Optimal rectification in the ultrastrong coupling regime. *Phys. Rev. E*, 89:062109, Jun 2014.

[74] Maria José Martínez-Pérez, Antonio Fornieri, and Francesco Giazotto. Rectification of electronic heat current by a hybrid thermal diode. *Nat. Nanotechnol.*, 10(4):303–307, Apr 2015.

[75] Zhong-Xiao Man, Nguyen Ba An, and Yun-Jie Xia. Controlling heat flows among three reservoirs asymmetrically coupled to two two-level systems. *Phys. Rev. E*, 94:042135, Oct 2016.

[76] Karl Joulain, Jérémie Drevillon, Younès Ezzahri, and Jose Ordonez-Miranda. Quantum thermal transistor. *Phys. Rev. Lett.*, 116:200601, May 2016.

[77] Jose Ordonez-Miranda, Younès Ezzahri, and Karl Joulain. Quantum thermal diode based on two interacting spinlike systems under different excitations. *Phys. Rev. E*, 95:022128, Feb 2017.

[78] B Karimi, J P Pekola, M Campisi, and R Fazio. Coupled qubits as a quantum heat switch. *Quantum Sci. Technol.*, 2(4):044007, aug 2017.

[79] Alberto Ronzani, Bayan Karimi, Jorden Senior, Yu-Cheng Chang, Joonas T. Peltonen, ChiiDong Chen, and Jukka P. Pekola. Tunable photonic heat transport in a quantum heat valve. *Nature Physics*, 14(10):991–995, Oct 2018.

[80] Yanchao Zhang, Zhimin Yang, Xin Zhang, Bihong Lin, Guoxing Lin, and Jincan Chen. Coulomb-coupled quantum-dot thermal transistors. *Europhys. Lett.*, 122(1):17002, apr 2018.

[81] Chen Wang, Xu-Min Chen, Ke-Wei Sun, and Jie Ren. Heat amplification and negative differential thermal conductance in a strongly coupled nonequilibrium spin-boson system. *Phys. Rev. A*, 97:052112, May 2018.

[82] Huan Liu, Chen Wang, Lu-Qing Wang, and Jie Ren. Strong system-bath coupling induces negative differential thermal conductance and heat amplification in nonequilibrium two-qubit systems. *Phys. Rev. E*, 99:032114, Mar 2019.

[83] Chen Wang, Dazhi Xu, Huan Liu, and Xianlong Gao. Thermal rectification and heat amplification in a nonequilibrium v-type three-level system. *Phys. Rev. E*, 99:042102, Apr 2019.

[84] Jianying Du, Wei Shen, Shanhe Su, and Jincan Chen. Quantum thermal management devices based on strong coupling qubits. *Phys. Rev. E*, 99:062123, Jun 2019.

[85] T Motz, M Wiedmann, J T Stockburger, and J Ankerhold. Rectification of heat currents across nonlinear quantum chains: a versatile approach beyond weak thermal contact. *New J. Phys.*, 20(11):113020, nov 2018.

[86] T. Werlang and D. Valente. Heat transport between two pure-dephasing reservoirs. *Phys. Rev. E*, 91:012143, Jan 2015.

[87] Tôru Moriya. Anisotropic superexchange interaction and weak ferromagnetism. *Phys. Rev.*, 120:91–98, Oct 1960.

[88] I. S. Tupitsyn, N. V. Prokof'ev, and P. C. E. Stamp. Effective hamiltonian in the problem of a "central spin" coupled to a spin environment. *International Journal of Modern Physics B*, 11(24):2901–2926, 1997.

[89] Michael Martin Nieto and D. Rodney Truax. Holstein-primakoff/bogoliubov transformations and the multiboson system. *Fortschritte der Physik/Progress of Physics*, 45(2):145–156, 1997.

[90] Alexandre Blais, Ren-Shou Huang, Andreas Wallraff, S. M. Girvin, and R. J. Schoelkopf. Cavity quantum electrodynamics for superconducting electrical circuits: An architecture for quantum computation. *Phys. Rev. A*, 69:062320, Jun 2004.

[91] Alexandre Blais, Jay Gambetta, A. Wallraff, D. I. Schuster, S. M. Girvin, M. H. Devoret, and R. J. Schoelkopf. Quantum-information processing with circuit quantum electrodynamics. *Phys. Rev. A*, 75:032329, Mar 2007.

[92] S. J. D. Phoenix and P. L. Knight. Periodicity, phase, and entropy in models of two-photonresonance. *J. Opt. Soc. Am. B*, 7(1):116–124, Jan 1990.

[93] P L Knight. Quantum fluctuations and squeezing in the interaction of an atom with a single field mode. *Phys. Scr.*, T12:51–55, jan 1986.

[94] Ronnie Kosloff and Amikam Levy. Quantum heat engines and refrigerators: Continuous devices. *Annual Review of Physical Chemistry*, 65(1):365–393, 2014. PMID: 24689798.

[95] Johannes Roßnagel, Samuel T. Dawkins, Karl N. Tolazzi, Obinna Abah, Eric Lutz, Ferdinand Schmidt-Kaler, and Kilian Singer. A single-atom heat engine. *Science*, 352(6283):325–329, 2016.

[96] B. Karimi and J. P. Pekola. Otto refrigerator based on a superconducting qubit: Classical and quantum performance. *Phys. Rev. B*, 94:184503, Nov 2016.

[97] Sreenath K. Manikandan, Francesco Giazotto, and Andrew N. Jordan. Superconducting quantum refrigerator: Breaking and rejoining cooper pairs with magnetic field cycles. *Phys. Rev. Applied*, 11:054034, May 2019.

[98] José P. Palao, Ronnie Kosloff, and Jeffrey M. Gordon. Quantum thermodynamic cooling cycle. *Phys. Rev. E*, 64:056130, Oct 2001.

[99] Noah Linden, Sandu Popescu, and Paul Skrzypczyk. How small can thermal machines be? the smallest possible refrigerator. *Phys. Rev. Lett.*, 105:130401, Sep 2010.

[100] Amikam Levy and Ronnie Kosloff. Quantum absorption refrigerator. *Phys. Rev. Lett.*, 108:070604, Feb 2012.

[101] Amikam Levy, Robert Alicki, and Ronnie Kosloff. Quantum refrigerators and the third law of thermodynamics. *Phys. Rev. E*, 85:061126, Jun 2012.

[102] Luis A. Correa, José P. Palao, Gerardo Adesso, and Daniel Alonso. Performance bound for quantum absorption refrigerators. *Phys. Rev. E*, 87:042131, Apr 2013.

[103] Davide Venturelli, Rosario Fazio, and Vittorio Giovannetti. Minimal self-contained quantum refrigeration machine based on four quantum dots. *Phys. Rev. Lett.*, 110:256801, Jun 2013.

[104] Luis A. Correa. Multistage quantum absorption heat pumps. *Phys. Rev. E*, 89:042128, Apr 2014.

[105] Bruno Leggio, Bruno Bellomo, and Mauro Antezza. Quantum thermal machines with single nonequilibrium environments. *Phys. Rev. A*, 91:012117, Jan 2015.

[106] Ralph Silva, Paul Skrzypczyk, and Nicolas Brunner. Small quantum absorption refrigerator with reversed couplings. *Phys. Rev. E*, 92:012136, Jul 2015.

[107] Ralph Silva, Gonzalo Manzano, Paul Skrzypczyk, and Nicolas Brunner. Performance of autonomous quantum thermal machines: Hilbert space dimension as a thermodynamical resource. *Phys. Rev. E*, 94:032120, Sep 2016.

[108] Patrick P. Hofer, Martí Perarnau-Llobet, Jonatan Bohr Brask, Ralph Silva, Marcus Huber, and Nicolas Brunner. Autonomous quantum refrigerator in a

circuit qed architecture based on a josephson junction. *Phys. Rev. B*, 94:235420, Dec 2016.

[109] Pierre Doyeux, Bruno Leggio, Riccardo Messina, and Mauro Antezza. Quantum thermal machine acting on a many-body quantum system: Role of correlations in thermodynamic tasks. *Phys. Rev. E*, 93:022134, Feb 2016.

[110] Alexandre Roulet, Stefan Nimmrichter, Juan Miguel Arrazola, Stella Seah, and Valerio Scarani. Autonomous rotor heat engine. *Phys. Rev. E*, 95:062131, Jun 2017.

[111] Paolo Andrea Erdman, Bibek Bhandari, Rosario Fazio, Jukka P. Pekola, and Fabio Taddei. Absorption refrigerators based on coulomb-coupled single-electron systems. *Phys. Rev. B*, 98:045433, Jul 2018.

[112] R. Härtle, C. Schinabeck, M. Kulkarni, D. Gelbwaser-Klimovsky, M. Thoss, and U. Peskin. Cooling by heating in nonequilibrium nanosystems. *Phys. Rev. B*, 98:081404, Aug 2018.

[113] Dvira Segal. Current fluctuations in quantum absorption refrigerators. *Phys. Rev. E*, 97:052145, May 2018.

[114] Michael Kilgour and Dvira Segal. Coherence and decoherence in quantum absorption refrigerators. *Phys. Rev. E*, 98:012117, Jul 2018.

[115] Stella Seah, Stefan Nimmrichter, and Valerio Scarani. Refrigeration beyond weak internal coupling. *Phys. Rev. E*, 98:012131, Jul 2018.

[116] Mark T Mitchison, Marcus Huber, Javier Prior, Mischa P Woods, and Martin B Plenio. Realising a quantum absorption refrigerator with an atom-cavity system. *Quantum Sci. Technol.*, 1(1):015001, mar 2016.

[117] Yi-Xin Chen and Sheng-Wen Li. Quantum refrigerator driven by current noise. *Europhys. Lett.*, 97(4):40003, feb 2012.

[118] Zi-chen He, Xin-yun Huang, and Chang-shui Yu. Enabling the self-contained refrigerator to work beyond its limits by filtering the reservoirs. *Phys. Rev. E*, 96:052126, Nov 2017.

[119] Chiranjib Mukhopadhyay, Avijit Misra, Samyadeb Bhattacharya, and Arun Kumar Pati. Quantum speed limit constraints on a nanoscale autonomous refrigerator. *Phys. Rev. E*, 97:062116, Jun 2018.

[120] Sreetama Das, Avijit Misra, Amit Kumar Pal, Aditi Sen(De), and Ujjwal Sen. Necessarily transient quantum refrigerator. *Europhys. Lett.*, 125(2):20007, feb 2019.

[121] Adam Hewgill, J. Onam González, José P. Palao, Daniel Alonso, Alessandro Ferraro, and Gabriele De Chiara. Three-qubit refrigerator with two-body interactions. *Phys. Rev. E*, 101:012109, Jan 2020.

[122] Gleb Maslennikov, Shiqian Ding, Roland Hablützel, Jaren Gan, Alexandre Roulet, Stefan Nimmrichter, Jibo Dai, Valerio Scarani, and Dzmitry Matsukevich. Quantum absorption refrigerator with trapped ions. *Nat. Commun.*, 10(1):202, Jan 2019.

[123] Mark T. Mitchison. Quantum thermal absorption machines: refrigerators, engines and clocks. *Contemp. Phys.*, 60(2):164–187, 2019.

[124] Esteban A. Martinez and Juan Pablo Paz. Dynamics and thermodynamics of linear quantum open systems. *Phys. Rev. Lett.*, 110:130406, Mar 2013.

[125] Bibek Bhandari and Andrew N. Jordan. Minimal two-body quantum absorption refrigerator. *Phys. Rev. B*, 104:075442, Aug 2021.

[126] A.G. Kofman, G. Kurizki, and B. Sherman. Spontaneous and induced atomic decay in photonic band structures. *J. Mod. Opt.*, 41(2):353–384, 1994.

[127] M. Tahir Naseem and Özgür E. Müstecaplıoğlu. Antibunching via cooling by heating. *Phys. Rev. A*, 105:012201, Jan 2022.

[128] D. Gelbwaser-Klimovsky and G. Kurizki. Heat-machine control by quantum-state preparation: From quantum engines to refrigerators. *Phys. Rev. E*, 90:022102, Aug 2014.

[129] Asher Peres. Separability criterion for density matrices. *Phys. Rev. Lett.*, 77:1413–1415, Aug 1996.

[130] Harold Ollivier and Wojciech H. Zurek. Quantum discord: A measure of the quantumness of correlations. *Phys. Rev. Lett.*, 88:017901, Dec 2001.

[131] L Henderson and V Vedral. Classical, quantum and total correlations. *J. Phys. A: Math. Gen.*, 34(35):6899–6905, aug 2001.

[132] Luis A. Correa, José P. Palao, Daniel Alonso, and Gerardo Adesso. Quantum-enhanced absorption refrigerators. *Sci. Rep.*, 4(1):3949, Feb 2014.

[133] Hava Meira Friedman and Dvira Segal. Cooling condition for multilevel quantum absorption refrigerators. *Phys. Rev. E*, 100:062112, Dec 2019.

[134] M. D. LaHaye, O. Buu, B. Camarota, and K. C. Schwab. Approaching the quantum limit of a nanomechanical resonator. *Science*, 304(5667):74–77, 2004.

[135] Alex Abramovici, William E. Althouse, Ronald W. P. Drever, Yekta Gürsel, Seiji Kawamura, Frederick J. Raab, David Shoemaker, Lisa Sievers, Robert E. Spero, Kip S. Thorne, Rochus E. Vogt, Rainer Weiss, Stanley E. Whitcomb, and Michael E. Zucker. Ligo: The laser interferometer gravitational-wave observatory. *Science*, 256(5055):325–333, 1992.

[136] P. F. Cohadon, A. Heidmann, and M. Pinard. Cooling of a mirror by radiation pressure. *Phys. Rev. Lett.*, 83:3174–3177, Oct 1999.

[137] Thomas Corbitt, Christopher Wipf, Timothy Bodiya, David Ottaway, Daniel Sigg, Nicolas Smith, Stanley Whitcomb, and Nergis Mavalvala. Optical dilution and feedback cooling of a gram-scale oscillator to 6.9 mk. *Phys. Rev. Lett.*, 99:160801, Oct 2007.

[138] M. Poggio, C. L. Degen, H. J. Mamin, and D. Rugar. Feedback cooling of a cantilever's fundamental mode below 5 mk. *Phys. Rev. Lett.*, 99:017201, Jul 2007.

[139] Massimiliano Rossi, David Mason, Junxin Chen, Yeghishe Tsaturyan, and Albert Schliesser. Measurement-based quantum control of mechanical motion. *Nature*, 563(7729):53–58, Nov 2018.

[140] Christian Sommer and Claudiu Genes. Partial optomechanical refrigeration via multimode cold-damping feedback. *Phys. Rev. Lett.*, 123:203605, Nov 2019.

[141] Christian Sommer, Alekhya Ghosh, and Claudiu Genes. Multimode cold-damping optomechanics with delayed feedback. *Phys. Rev. Research*, 2:033299, Aug 2020.

[142] A. Schliesser, P. Del'Haye, N. Nooshi, K. J. Vahala, and T. J. Kippenberg. Radiation pressure cooling of a micromechanical oscillator using dynamical backaction. *Phys. Rev. Lett.*, 97:243905, Dec 2006.

[143] I. Wilson-Rae, N. Nooshi, W. Zwerger, and T. J. Kippenberg. Theory of ground state cooling of a mechanical oscillator using dynamical backaction. *Phys. Rev. Lett.*, 99:093901, Aug 2007.

[144] Florian Marquardt, Joe P. Chen, A. A. Clerk, and S. M. Girvin. Quantum theory of cavity-assisted sideband cooling of mechanical motion. *Phys. Rev. Lett.*, 99:093902, Aug 2007.

[145] K. R. Brown, J. Britton, R. J. Epstein, J. Chiaverini, D. Leibfried, and D. J. Wineland. Passive cooling of a micromechanical oscillator with a resonant electric circuit. *Phys. Rev. Lett.*, 99:137205, Sep 2007.

[146] C. Genes, D. Vitali, P. Tombesi, S. Gigan, and M. Aspelmeyer. Ground-state cooling of a micromechanical oscillator: Comparing cold damping and cavity-assisted cooling schemes. *Phys. Rev. A*, 77:033804, Mar 2008.

[147] A. Schliesser, R. Rivière, G. Anetsberger, O. Arcizet, and T. J. Kippenberg. Resolved-sideband cooling of a micromechanical oscillator. *Nat. Phys.*, 4(5):415–419, May 2008.

[148] C. Genes, D. Vitali, P. Tombesi, S. Gigan, and M. Aspelmeyer. Erratum: Ground-state cooling of a micromechanical oscillator: Comparing cold damping and cavity-assisted cooling schemes [phys. rev. a 77, 033804 (2008)]. *Phys. Rev. A*, 79:039903, Mar 2009.

[149] R. W. Peterson, T. P. Purdy, N. S. Kampel, R. W. Andrews, P.-L. Yu, K. W. Lehnert, and C. A. Regal. Laser cooling of a micromechanical membrane to the quantum backaction limit. *Phys. Rev. Lett.*, 116:063601, Feb 2016.

[150] Xunnong Xu, Thomas Purdy, and Jacob M. Taylor. Cooling a harmonic oscillator by optomechanical modification of its bath. *Phys. Rev. Lett.*, 118:223602, May 2017.

[151] Juan Pablo Paz and Augusto J. Roncaglia. Dynamics of the entanglement between two oscillators in the same environment. *Phys. Rev. Lett.*, 100:220401, Jun 2008.

[152] Ying-Dan Wang and Aashish A. Clerk. Reservoir-engineered entanglement in optomechanical systems. *Phys. Rev. Lett.*, 110:253601, Jun 2013.

[153] A. Mari, A. Farace, N. Didier, V. Giovannetti, and R. Fazio. Measures of quantum synchronization in continuous variable systems. *Phys. Rev. Lett.*, 111:103605, Sep 2013.

[154] M. J. Woolley and A. A. Clerk. Two-mode squeezed states in cavity optomechanics via engineering of a single reservoir. *Phys. Rev. A*, 89:063805, Jun 2014.

[155] Matthew H. Matheny, Matt Grau, Luis G. Villanueva, Rassul B. Karabalin, M. C. Cross, and Michael L. Roukes. Phase synchronization of two anharmonic nanomechanical oscillators. *Phys. Rev. Lett.*, 112:014101, Jan 2014.

[156] Shabir Barzanjeh, Matteo Aquilina, and André Xuereb. Manipulating the flow of thermal noise in quantum devices. *Phys. Rev. Lett.*, 120:060601, Feb 2018.

[157] C. F. Ockeloen-Korppi, E. Damskägg, J.-M. Pirkkalainen, M. Asjad, A. A. Clerk, F. Massel, M. J. Woolley, and M. A. Sillanpää. Stabilized entanglement of massive mechanical oscillators. *Nature*, 556(7702):478–482, Apr 2018.

[158] A. B. Shkarin, N. E. Flowers-Jacobs, S. W. Hoch, A. D. Kashkanova, C. Deutsch, J. Reichel, and J. G. E. Harris. Optically mediated hybridization between two mechanical modes. *Phys. Rev. Lett.*, 112:013602, Jan 2014.

[159] Claudiu Genes, David Vitali, and Paolo Tombesi. Simultaneous cooling and entanglement of mechanical modes of a micromirror in an optical cavity. *New J. Phys.*, 10(9):095009, sep 2008.

[160] C. F. Ockeloen-Korppi, M. F. Gely, E. Damskägg, M. Jenkins, G. A. Steele, and M. A. Sillanpää. Sideband cooling of nearly degenerate micromechanical oscillators in a multimode optomechanical system. *Phys. Rev. A*, 99:023826, Feb 2019.

[161] Deng-Gao Lai, Fen Zou, Bang-Pin Hou, Yun-Feng Xiao, and Jie-Qiao Liao. Simultaneous cooling of coupled mechanical resonators in cavity optomechanics. *Phys. Rev. A*, 98:023860, Aug 2018.

[162] Deng-Gao Lai, Jin-Feng Huang, Xian-Li Yin, Bang-Pin Hou, Wenlin Li, David Vitali, Franco Nori, and Jie-Qiao Liao. Nonreciprocal ground-state cooling of multiple mechanical resonators. *Phys. Rev. A*, 102:011502, Jul 2020.

[163] A. Mari and J. Eisert. Cooling by heating: Very hot thermal light can significantly cool quantum systems. *Phys. Rev. Lett.*, 108:120602, Mar 2012.

[164] B. Cleuren, B. Rutten, and C. Van den Broeck. Cooling by heating: Refrigeration powered by photons. *Phys. Rev. Lett.*, 108:120603, Mar 2012.

[165] F. Massel, T. T. Heikkilä, J.-M. Pirkkalainen, S. U. Cho, H. Saloniemi, P. J. Hakonen, and M. A. Sillanpää. Microwave amplification with nanomechanical resonators. *Nature*, 480(7377):351–354, Dec 2011.

[166] Kejie Fang, Jie Luo, Anja Metelmann, Matthew H. Matheny, Florian Marquardt, Aashish A. Clerk, and Oskar Painter. Generalized non-reciprocity in an optomechanical circuit via synthetic magnetism and reservoir engineering. *Nature Physics*, 13(5):465–471, May 2017.

[167] A. Ghosh, C. L. Latune, L. Davidovich, and G. Kurizki. Catalysis of heat-to-work conversion in quantum machines. *Proc. Nat.l Acad. Sci.*, 114(46):12156–12161, 2017.

[168] C. L. Latune, I. Sinayskiy, and F. Petruccione. Quantum coherence, many-body correlations, and non-thermal effects for autonomous thermal machines. *Sci. Rep.*, 9(1):3191, Feb 2019.

[169] Florian Elste, S. M. Girvin, and A. A. Clerk. Quantum noise interference and backaction cooling in cavity nanomechanics. *Phys. Rev. Lett.*, 102:207209, May 2009.

[170] S. Machnes, J. Cerrillo, M. Aspelmeyer, W. Wieczorek, M. B. Plenio, and A. Retzker. Pulsed laser cooling for cavity optomechanical resonators. *Phys. Rev. Lett.*, 108:153601, Apr 2012.

[171] Teemu Ojanen and Kjetil Børkje. Ground-state cooling of mechanical motion in the unresolved sideband regime by use of optomechanically induced transparency. *Phys. Rev. A*, 90:013824, Jul 2014.

[172] Muhammad Asjad, Stefano Zippilli, and David Vitali. Suppression of stokes scattering and improved optomechanical cooling with squeezed light. *Phys. Rev. A*, 94:051801, Nov 2016.

[173] Jeremy B. Clark, Florent Lecocq, Raymond W. Simmonds, José Aumentado, and John D. Teufel. Sideband cooling beyond the quantum backaction limit with squeezed light. *Nature*, 541(7636):191–195, Jan 2017.

[174] G. Lindblad. On the generators of quantum dynamical semigroups. *Commun. Math. Phys.*, 48(2):119–130, Jun 1976.

[175] X. L. Huang, Tao Wang, and X. X. Yi. Effects of reservoir squeezing on quantum systems and work extraction. *Phys. Rev. E*, 86:051105, Nov 2012.

[176] Tobias Eberle, Sebastian Steinlechner, Jöran Bauchrowitz, Vitus Händchen, Henning Vahlbruch, Moritz Mehmet, Helge Müller-Ebhardt, and Roman Schnabel. Quantum enhancement of the zero-area sagnac interferometer topology for gravitational wave detection. *Phys. Rev. Lett.*, 104:251102, Jun 2010.

[177] Ceren B. Dağ, Wolfgang Niedenzu, Özgür E. Müstecaplıoğlu, and Gershon Kurizki. Multiatom quantum coherences in micromasers as fuel for thermal and nonthermal machines. *Entropy*, 18(7), 2016.

[178] I. C. Rodrigues, D. Bothner, and G. A. Steele. Coupling microwave photons to a mechanical resonator using quantum interference. *Nat. Commun.*, 10(1):5359, Nov 2019.

[179] G. A. Peterson, S. Kotler, F. Lecocq, K. Cicak, X. Y. Jin, R. W. Simmonds, J. Aumentado, and J. D. Teufel. Ultrastrong parametric coupling between a superconducting cavity and a mechanical resonator. *Phys. Rev. Lett.*, 123:247701, Dec 2019.

[180] Jan Klaers, Stefan Faelt, Atac Imamoglu, and Emre Togan. Squeezed thermal reservoirs as a resource for a nanomechanical engine beyond the carnot limit. *Phys. Rev. X*, 7:031044, Sep 2017.

[181] A. D. O'Connell, M. Hofheinz, M. Ansmann, Radoslaw C. Bialczak, M. Lenander, Erik Lucero, M. Neeley, D. Sank, H. Wang, M. Weides, J. Wenner, John M. Martinis, and A. N. Cleland. Quantum ground state and single-phonon control of a mechanical resonator. *Nature*, 464(7289):697–703, Apr 2010.

[182] Marlan O. Scully and Willis E. Lamb. Quantum theory of an optical maser. i. general theory. *Phys. Rev.*, 159:208–226, Jul 1967.

[183] Jie-Qiao Liao, H. Dong, and C. P. Sun. Single-particle machine for quantum thermalization. *Phys. Rev. A*, 81:052121, May 2010.

[184] Antonio Acín, Immanuel Bloch, Harry Buhrman, Tommaso Calarco, Christopher Eichler, Jens Eisert, Daniel Esteve, Nicolas Gisin, Steffen J Glaser, Fedor Jelezko, Stefan Kuhr, Maciej Lewenstein, Max F Riedel, Piet O Schmidt, Rob Thew, Andreas Wallraff, Ian Walmsley, and Frank K Wilhelm. The

quantum technologies roadmap: a european community view. *New J. Phys.*, 20(8):080201, aug 2018.

[185] Daniel Burgarth and Vittorio Giovannetti. Mediated homogenization. *Phys. Rev. A*, 76:062307, Dec 2007.

[186] B. Kraus, H. P. Büchler, S. Diehl, A. Kantian, A. Micheli, and P. Zoller. Preparation of entangled states by quantum markov processes. *Phys. Rev. A*, 78:042307, Oct 2008.

[187] S. Diehl, A. Micheli, A. Kantian, B. Kraus, H. P. Büchler, and P. Zoller. Quantum states and phases in driven open quantum systems with cold atoms. *Nat. Phys.*, 4(11):878–883, Nov 2008.

[188] Frank Verstraete, Michael M. Wolf, and J. Ignacio Cirac. Quantum computation and quantum-state engineering driven by dissipation. *Nat. Phys.*, 5(9):633–636, Sep 2009.

[189] Susanne Pielawa, Luiz Davidovich, David Vitali, and Giovanna Morigi. Engineering atomic quantum reservoirs for photons. *Phys. Rev. A*, 81:043802, Apr 2010.

[190] Jianming Cai, Sandu Popescu, and Hans J. Briegel. Dynamic entanglement in oscillating molecules and potential biological implications. *Phys. Rev. E*, 82:021921, Aug 2010.

[191] M. J. Kastoryano, F. Reiter, and A. S. Sørensen. Dissipative preparation of entanglement in optical cavities. *Phys. Rev. Lett.*, 106:090502, Feb 2011.

[192] Stefan Walter, Jan Carl Budich, Jens Eisert, and Björn Trauzettel. Entanglement of nanoelectromechanical oscillators by cooper-pair tunneling. *Phys. Rev. B*, 88:035441, Jul 2013.

[193] Florentin Reiter, L. Tornberg, Göran Johansson, and Anders S. Sørensen. Steady-state entanglement of two superconducting qubits engineered by dissipation. *Phys. Rev. A*, 88:032317, Sep 2013.

[194] M. J. A. Schuetz, E. M. Kessler, L. M. K. Vandersypen, J. I. Cirac, and G. Giedke. Steady-state entanglement in the nuclear spin dynamics of a double quantum dot. *Phys. Rev. Lett.*, 111:246802, Dec 2013.

[195] Hanna Krauter, Christine A. Muschik, Kasper Jensen, Wojciech Wasilewski, Jonas M. Petersen, J. Ignacio Cirac, and Eugene S. Polzik. Entanglement generated by dissipation and steady state entanglement of two macroscopic objects. *Phys. Rev. Lett.*, 107:080503, Aug 2011.

[196] Julio T. Barreiro, Markus Müller, Philipp Schindler, Daniel Nigg, Thomas Monz, Michael Chwalla, Markus Hennrich, Christian F. Roos, Peter Zoller, and Rainer Blatt. An open-system quantum simulator with trapped ions. *Nature*, 470(7335):486–491, Feb 2011.

[197] Y. Lin, J. P. Gaebler, F. Reiter, T. R. Tan, R. Bowler, A. S. Sørensen, D. Leibfried, and D. J. Wineland. Dissipative production of a maximally entangled steady state of two quantum bits. *Nature*, 504(7480):415–418, Dec 2013.

[198] S. Shankar, M. Hatridge, Z. Leghtas, K. M. Sliwa, A. Narla, U. Vool, S. M. Girvin, L. Frunzio, M. Mirrahimi, and M. H. Devoret. Autonomously stabilized entanglement between two superconducting quantum bits. *Nature*, 504(7480):419–422, Dec 2013.

[199] Jie-Qiao Liao, Qin-Qin Wu, and Franco Nori. Entangling two macroscopic mechanical mirrors in a two-cavity optomechanical system. *Phys. Rev. A*, 89:014302, Jan 2014.

[200] J Li, I Moaddel Haghighi, N Malossi, S Zippilli, and D Vitali. Generation and detection of large and robust entanglement between two different mechanical resonators in cavity optomechanics. *New J. Phys.*, 17(10):103037, oct 2015.

[201] M. C. Arnesen, S. Bose, and V. Vedral. Natural thermal and magnetic entanglement in the 1d heisenberg model. *Phys. Rev. Lett.*, 87:017901, Jun 2001.

[202] D. Gunlycke, V. M. Kendon, V. Vedral, and S. Bose. Thermal concurrence mixing in a one-dimensional ising model. *Phys. Rev. A*, 64:042302, Sep 2001.

[203] M. B. Plenio, S. F. Huelga, A. Beige, and P. L. Knight. Cavity-loss-induced generation of entangled atoms. *Phys. Rev. A*, 59:2468–2475, Mar 1999.

[204] S. Schneider and G. J. Milburn. Entanglement in the steady state of a collective-angular-momentum (dicke) model. *Phys. Rev. A*, 65:042107, Mar 2002.

[205] M. S. Kim, Jinhyoung Lee, D. Ahn, and P. L. Knight. Entanglement induced by a single-mode heat environment. *Phys. Rev. A*, 65:040101, Apr 2002.

[206] Daniel Braun. Creation of entanglement by interaction with a common heat bath. *Phys. Rev. Lett.*, 89:277901, Dec 2002.

[207] Fabio Benatti, Roberto Floreanini, and Marco Piani. Environment induced entanglement in markovian dissipative dynamics. *Phys. Rev. Lett.*, 91:070402, Aug 2003.

[208] L. Hartmann, W. Dür, and H.-J. Briegel. Steady-state entanglement in open and noisy quantum systems. *Phys. Rev. A*, 74:052304, Nov 2006.

[209] Luis Quiroga, Ferney J. Rodríguez, María E. Ramírez, and Roberto París. Nonequilibrium thermal entanglement. *Phys. Rev. A*, 75:032308, Mar 2007.

[210] Ilya Sinaysky, Francesco Petruccione, and Daniel Burgarth. Dynamics of nonequilibrium thermal entanglement. *Phys. Rev. A*, 78:062301, Dec 2008.

[211] Lian-Ao Wu and Dvira Segal. Quantum effects in thermal conduction: Nonequilibrium quantum discord and entanglement. *Phys. Rev. A*, 84:012319, Jul 2011.

[212] Jonatan Bohr Brask, Géraldine Haack, Nicolas Brunner, and Marcus Huber. Autonomous quantum thermal machine for generating steady-state entanglement. *New J. Phys.*, 17(11):113029, nov 2015.

[213] Karen V Hovhannisyan and Alberto Imparato. Quantum current in dissipative systems. *New J. Phys.*, 21(5):052001, may 2019.

[214] Zhihai Wang, Wei Wu, and Jin Wang. Steady-state entanglement and coherence of two coupled qubits in equilibrium and nonequilibrium environments. *Phys. Rev. A*, 99:042320, Apr 2019.

[215] Shishir Khandelwal, Nicolas Palazzo, Nicolas Brunner, and Géraldine Haack. Critical heat current for operating an entanglement engine. *New J. Phys.*, 22(7):073039, jul 2020.

[216] Armin Tavakoli, Géraldine Haack, Nicolas Brunner, and Jonatan Bohr Brask. Autonomous multipartite entanglement engines. *Phys. Rev. A*, 101:012315, Jan 2020.

[217] Daniel Heineken, Konstantin Beyer, Kimmo Luoma, and Walter T. Strunz. Quantum-memory-enhanced dissipative entanglement creation in nonequilibrium steady states. *Phys. Rev. A*, 104:052426, Nov 2021.

[218] Shishir Khandelwal, Nicolas Brunner, and Géraldine Haack. Signatures of liouvillian exceptional points in a quantum thermal machine. *PRX Quantum*, 2:040346, Dec 2021.

[219] Jonatan Bohr Brask, Fabien Clivaz, Géraldine Haack, and Armin Tavakoli. Operational nonclassicality in minimal autonomous thermal machines. *Quantum*, 6:672, March 2022.

[220] F. Tacchino, A. Auffèves, M. F. Santos, and D. Gerace. Steady state entanglement beyond thermal limits. *Phys. Rev. Lett.*, 120:063604, Feb 2018.

[221] Pradip Laha, Lukáš Slodička, Darren W. Moore, and Radim Filip. Thermally induced entanglement of atomic oscillators. *Opt. Express*, 30(6):8814–8828, Mar 2022.

[222] Ze-Liang Xiang, Sahel Ashhab, J. Q. You, and Franco Nori. Hybrid quantum circuits: Superconducting circuits interacting with other quantum systems. *Rev. Mod. Phys.*, 85:623–653, Apr 2013.

[223] Armin Tavakoli, Géraldine Haack, Marcus Huber, Nicolas Brunner, and Jonatan Bohr Brask. Heralded generation of maximal entanglement in any dimension via incoherent coupling to thermal baths. *Quantum*, 2:73, June 2018.

[224] A. Nunnenkamp, K. Børkje, and S. M. Girvin. Cooling in the single-photon strong-coupling regime of cavity optomechanics. *Phys. Rev. A*, 85:051803, May 2012.

[225] H. Seok and E. M. Wright. Antibunching in an optomechanical oscillator. *Phys. Rev. A*, 95:053844, May 2017.

[226] M. B. Plenio. Logarithmic negativity: A full entanglement monotone that is not convex. *Phys. Rev. Lett.*, 95:090503, Aug 2005.

[227] Aurora Voje, Andreas Isacsson, and Alexander Croy. Nonlinear-dissipation-induced entanglement of coupled nonlinear oscillators. *Phys. Rev. A*, 88:022309, Aug 2013.

[228] D. Bothner, I. C. Rodrigues, and G. A. Steele. Photon-pressure strong coupling between two superconducting circuits. *Nat. Phys.*, 17(1):85–91, Jan 2021.

[229] J. Roßnagel, S. Dawkins, K. Tolazzi, O. Abah, F. Lutz, E.and Kaler, and K. Singer. A single-atom heat engine. *Science*, 352(6283):030602, 2016.

[230] Ali Ü. C. Hardal and Özgür E. Müstecaplıoğlu. Superradiant quantum heat engine. *Sci. Rep.*, 5(1):12953, Aug 2015.

[231] Jinuk Kim, Seung-hoon Oh, Daeho Yang, Junki Kim, Moonjoo Lee, and Kyung-won An. A photonic quantum engine driven by superradiance. *Nat. Photon.*, Jul 2022.

[232] Victor Mukherjee, Analia Zwick, Arnab Ghosh, Xi Chen, and Gershon Kurizki. Enhanced precision bound of low-temperature quantum thermometry via dynamical control. *Commun. Phys.*, 2(1):162, Dec 2019.